Physics – Uspekhi **51** (1) 23 – 56 (2008)

REVIEWS OF TOPICAL PROBLEMS PACS numbers: **71.27.+a**, **71.30.+h**, **74.72.–h**, **75.10.–b**, **75.30.–m**

Materials with strong electron correlations

Yu A Izyumov, E Z Kurmaev

DOI: 10.1070/PU2008v051n01ABEH006388

Contents

Abstract. The electron structure and physical properties of strongly correlated systems containing elements with unfilled 3d, 4d, and 5f shells are analyzed. These systems include several transition metals, rare-earth elements, and actinides, as well as their numerous compounds, such as various oxides exhibiting metal – insulator phase transitions, cuprates, manganites, f systems with heavy fermions, and Kondo insulators. It is shown that the low-energy physics of such systems is described by three basic models: the Hubbard model, the sd-exchange model, and the periodic Anderson model under the condition that the on-site Coulomb repulsion energy U or the sd exchange energy J is of the order of the conduction-band width W. This situation does not involve a small parameter and should be treated nonperturbatively. We describe one such approach, the dynamic mean-field theory (DMFT), in which a system is considered to be only dynamically but not spatially correlated. We show that this approach, which is fully justified in the limit of large spatial dimensions ($d \to \infty$), covers the entire physics of strongly correlated systems and adequately describes the phenomena they exhibit. Extending the DMFT to include spatial correlations enables various d and f systems to be quantitatively described. Being a subject of intense development in recent years, the DMFT is the most effective and universal tool for studying various strongly correlated systems.

Yu A Izyumov, E Z Kurmaev Institute of Metal Physics, Ural Division, Russian Academy of Sciences,
ul. S Kovalevskoi 18, Ekaterinburg 620041, Russian Federation
Tel. +7 (343) 374 41 93; +7 (343) 374 41 83
Fax: +7 (343) 374 52 44
E-mail: yuri.izyumov@imp.uran.ru

Received 10 April 2007; revised 6 September 2007
Uspekhi Fizicheskikh Nauk **178** (1) 25 – 60 (2008)
DOI: 10.3367/UFNr.0178.200801b.0025
Translated by S N Gorin; edited by A M Semikhatov

1. Introduction

In recent decades, the center of gravity of experimental and theoretical studies of the nature of metallic systems has moved into the field of transition and rare-earth elements with incompletely filled 3d, 4f, and 5f shells and the related chemical compounds. In early studies, in the 1960s, the most intriguing problem in this field was that of the metal – insulator (MI) phase transition, which is observed in many oxides of transition metals upon changes in pressure, temperature, or concentration of doping elements. About a decade later, a new class of chemical compounds of rare-earth metals with charge carriers whose effective mass exceeds the

electron mass by one or two orders of magnitude — the so-called heavy-fermion (HF) systems — were discovered. In such systems, a great variety of interesting physical phenomena have been revealed, such as phase transitions with the appearance of magnetically ordered phases and superconductivity, insulating and metallic states, transitions with the appearance and disappearance of localized magnetic moments, and specific transport properties. Such a combination of electric and magnetic properties may be related to the manifestation of strong interactions of the electron and magnetic degrees of freedom in many compounds with 3d and 4f elements. A vivid example of this type of interconnection of various properties is manganites with the colossal magnetoelectric effect, in which a moderate magnetic field is capable of radically changing the electron state of the system, from metallic to insulating. However, the most significant and entirely unexpected phenomenon was the discovery of high-temperature superconductivity (HTSC) in transition-metal oxides. This finally shifted the interest of researchers to the synthesis of new classes of chemical compounds and the study of their physical properties. In the subsequent two decades, numerous new compounds with unique properties have been discovered.

It is clear that the variety of physical phenomena in all these compounds is caused by the existence of incompletely filled 3d, 4f, or 5f electron shells in them; as a result, the atoms of these elements in the solid state retain the fully or partly localized magnetic moments. The strong interaction of these groups of electrons between themselves or with the collectivized electrons of the outer shells is the special feature that determines the unique properties of these compounds. Such systems with strong electron interactions have been called strongly correlated systems (SCSs). All the above-mentioned classes of chemical compounds, and many others with which we deal in this review, refer to SCSs.

With the discovery of new classes of SCSs, difficulties arose in interpreting the physical properties of SCSs from the standpoint of their electron structure. The old band theory of solids, which has long been successfully used for describing the properties of transition metals and semiconductors, proved to be incapable of explaining the properties of SCSs. The point is that the standard band theory ignores electron – electron interactions, which are usually weak in simple metals and semiconductors. But in SCSs, the interactions of electrons are of the same order as the width of the energy band of the active group of electrons (typically belonging to 3d, 4f, or 5f electrons of the basic element atoms), or even substantially exceed this width. In this situation, a completely different quantum-mechanical approach is necessary, which goes beyond the theory based on perturbations in the electron – electron interaction. In the last 40 years, beginning with Hubbard's pioneering works [1, 2], quite numerous approaches have been suggested for describing the electron structure and physical properties of newly discovered SCSs. Usually, the theoretical studies were based on simple models such as the Hubbard, tJ, sd, and Anderson models. Many of these approaches proved to be successful for some classes of SCSs, but they were not universal and frequently did not allow dealing with more complex models close to realistic systems.

It seemed that the theory of SCSs would forever remain motley and semiquantitative because of the difficulties of taking the strong interelectron interaction into account. However, a breakthrough occurred in 1989 after Metzner and Vollhardt [3] proposed formally considering the system of strongly interacting electrons in a space with a large dimension d (or to consider atomic lattices with a large number of nearest neighbors z). It turned out that in the limit as $d \to \infty$ (or $z \to \infty$), the mathematical equations describing electron motion in the lattice simplify dramatically and can be exactly solved at any value of the interelectron interaction; the results of calculations in this limit are very close to those of numerical calculations for real space with the dimension $d = 3$.

The theory simplifies as $d \to \infty$ because it is then possible to neglect spatial fluctuations in the system and examine only dynamic fluctuations. On the basis of this discovery, the dynamic mean-field theory (DMFT) was born, where the frequency (and only frequency) dependence of the mean field acting on a given electron from all other electrons is taken into account but the dependence on the wave vector, which in the usual approaches entails basic difficulties in solving the equations, is ignored. In the DMFT, a computational scheme is suggested that reduces the problem of the structure of the electron spectrum of systems of interacting electrons on a lattice to the problem of a single impurity center located in the effective dynamic field of other electrons. A method of calculation of this field for a given model was proposed. The first to use the new approach for the Hubbard model were Georges and Kotliar in 1992 [4]; they obtained the so-called three-peak structure of the SCS spectrum, which consists of a narrow central peak onto which the Fermi level falls in the case of half filling (one electron per lattice atom), and two wide lateral peaks, which correspond to Hubbard subbands (see also [5]). The spectrum obtained determines whether a metal – insulator phase transition is possible and also determines specific features of the transport properties of the system. Such a structure was soon confirmed experimentally in a number of compounds of 3d and 4d elements.

Subsequently, the DMFT was applied to basic models of SCSs; the results of theoretical studies and their comparison with the experimental data are generalized in review [6]. In recent years, the DMFT has been elaborated for calculating not only simple (in composition, but not from the standpoint of their study!) but also complex chemical compounds. This allows obtaining the electron structure from first principles, i.e., when only the lattice, the chemical elements that compose it, and the electric charges on the atoms are specified. These problems have been considered in reviews [7 – 16], in which the properties of many compounds were considered in detail and a satisfactory agreement with experimental data was noted. In addition, there exist a number of works in which the DMFT is generalized so as to account for spatial correlations ignored in the initial approach. Thus, the DMFT can now be considered a unified theory of SCSs, and the physical properties of these systems following from this theory are frequently in good quantitative agreement with the experimental data. It is therefore not surprising that in 2006, the creators of the DMFT, Georges, Kotliar, Metzner, and Vollhardt, were awarded a special prize (Agilent Technologies Europhysics Prize) [17] for studies in the field of condensed matter physics.

The aim of this review is to consider the basic classes of SCSs from a unified standpoint based on the DMFT; the method itself is not considered in detail because the reader can become acquainted with its various aspects independently using numerous reviews we cite in this paper. It is essential that we consider all the SCSs in totality rather than one of the SCS classes, for each of which there are many detailed surveys. The main task, which is for the first time set in such a way, is to

reveal common features in the electron structure of different compounds and interpret them on the DMFT basis. At the same time, we want to trace those common features that are inherent in different classes of SCSs, such as the structure of phase diagrams in the temperature–electron concentration plane, the development of phase separation, the strong sensitivity of SCSs to the level of doping with other elements, the instability to various types of magnetic ordering, and the degree of localization of magnetic moments, i.e., all those phenomena that are determined by strong electron correlations in the system.

To conclude this introduction, we warn the reader against a possible misinterpretation that there was no understanding of the basic phenomena in the theory of SCSs caused by strong correlations before the development of the DMFT. Beginning with Hubbard's classical works, numerous theoretical approaches based on the decoupling of the equations of motion have been developed, as well as variational methods, the method of auxiliary bosons and fermions, numerical methods, etc., which have allowed qualitatively explaining the basic experimental facts in the physics of SCSs. We simply assert that the DMFT is presently the most universal method of studying different classes of SCSs, which frequently allows obtaining quantitative agreement with experimental data even for complex compounds. The reader can find the description of early theoretical approaches in many reviews of the DMFT given in the references. In particular, various methods of the investigation of SCS models have been described in several reviews published in Russian, e.g., the Hubbard model [18], the tJ model [19], HTSC models [20], and the double-exchange model [21] (see also monograph [22]).

More than thirty years ago, we published two reviews [23, 24] devoted to compounds of transition metals, first and foremost V_3Si and Nb_3Sn, which at that time had record temperatures of the superconducting transition, and then, in cooperation with Vonsovskii, the monograph [25], in which we analyzed the superconductivity of these compounds. However, systems with heavy fermions and superconductivity in copper oxide compounds were not yet known at that time. Nothing then foreshadowed the rapid development in this field, the latest achievements in which we want to discuss in this survey.

2. Electron structure of strongly correlated systems

2.1 Fermi-liquid description

Simple metals and semiconductors, such as silicon, are quite adequately described by the band theory, which considers the motion of a single electron in the periodic field of a lattice. This one-electron approach is well substantiated by the smallness of the interelectron interaction. From the standpoint of the many-body quantum mechanical theory, this approach corresponds to the Landau Fermi-liquid theory. According to this theory, the system of interacting electrons is described by slowly decaying (near the Fermi surface) quasiparticles, which have an energy $\varepsilon_{\mathbf{k}}$ and are characterized by a quasimomentum $\mathbf{k}$. The quasiparticle states (also called coherent states) are determined by the pole of the Green's function (GF) for electrons,

$$G(\mathbf{k},\omega) = \frac{Z_k}{\omega - \varepsilon_k + \mathrm{i}\gamma_k}\,, \tag{2.1}$$

and the spectral density $A(\mathbf{k},\omega)$ is described by the imaginary part of the GF,

$$A(\mathbf{k},\omega) = -\frac{1}{\pi}\,\mathrm{Im}\,G(\mathbf{k},\omega) = Z_k\,\frac{1}{\pi}\,\frac{\gamma_k}{(\omega-\varepsilon_k)^2+\gamma_k^2}\,. \tag{2.2}$$

The quantity Z_k determines the intensity of the quasiparticle peak (for noninteracting electrons, $Z_k = 1$), and γ_k is the quasiparticle damping rate. At the Fermi surface, $\gamma_k = 0$, and hence quasiparticles are nondamping states at this surface.

With a change in the electron concentration, the quantities ε_k and γ_k usually vary monotonically; however, this is certainly not the case for SCSs. Upon band half-filling, as was shown by Mott and Hubbard, a metal–insulator phase transition is possible, and this is a typical experimental fact. Such a situation arises in the case of a strong interelectron interaction. This phenomenon can best be explained within the framework of the simplest SCS model, the Hubbard model, which describes the system of nondegenerate electrons in a lattice with on-site Coulomb repulsion for an electron. This model is described by the Hamiltonian

$$H = \sum_{ij\sigma} t_{ij}\, c^+_{i\sigma}\, c_{j\sigma} + U \sum_i n_{i\uparrow} n_{i\downarrow}\,, \tag{2.3}$$

where i and j label the lattice sites, $\sigma = \uparrow, \downarrow$ are the electron spins, t_{ij} is the matrix element of the electron transition between two sites, and U is the on-site Coulomb repulsion. The Fermi operators $c^+_{i\sigma}$ and $c_{j\sigma}$ respectively describe creation and annihilation of an electron at a given site with a given spin, and $n_{i\sigma} = c^+_{i\sigma} c_{i\sigma}$ is the operator of the number of electrons at a site i with a spin σ.

The terms that correspond to the kinetic and potential energy in (2.3) reflect two opposite tendencies of electrons: toward delocalization (kinetic energy) and toward localization (potential energy). The measure of the kinetic energy is the band width $W = 2zt$ (where t is the matrix element of the electron transition between nearest neighbors), and the measure of the potential energy is the parameter U. For $U \ll W$, a Fermi-liquid description applies, i.e., the system is metallic at any level of the incomplete filling of the band; for at $U \gtrsim W$, the behavior of the system is determined by the competition between both tendencies and, as a result, either a metallic or an insulating state can arise, and a strong dependence of the Fermi states on the electron concentration is observed. As we see below, this competition manifests itself most strongly at the band half-filling, $n = 1$.

In SCSs, exactly the situation where $U \gtrsim W$ is realized, in which case the perturbation theory in the electron interaction becomes inapplicable. In this situation, it is possible to use a small parameter of another nature, namely, $1/d$ (d is the spatial dimension), which leads to the DMFT method.

2.2 Dynamic mean-field approximation

Metzner and Vollhardt showed [3] that as $d \to \infty$, the self-energy part $\Sigma(\mathbf{k},\omega)$ of the electron energy is independent of the quasimomentum: it depends only on frequency. This fact is the basis of the DMFT. We write a general expression for the electron GF with this fact taken into account:

$$G(\mathbf{k},\omega) = \frac{1}{\omega + \mu - \varepsilon_k - \Sigma(\omega)}\,. \tag{2.4}$$

We note that a retarded GF [26] is understood in Eqns (2.1) and (2.4); in the space – time representation for the system described by Hamiltonian (2.3), it is denoted by $G_{ij}(t-t')$ (the spin indices are omitted for simplicity). Expression (2.4) is its Fourier component with respect to time and coordinates. To calculate it, it is convenient to use the formalism of temperature GFs:

$$G_{ij}(\tau-\tau') = -\langle \hat{T} c_i(\tau)\, c_j^+(\tau')\rangle\,, \tag{2.5}$$

where the notation is standard [27], i.e., $c_i(\tau) = \exp\left[(H-\mu N)\,\tau\right] c_i \exp\left[-(H-\mu N)\,\tau\right]$, $\hat{T}$ is the operator of ordering in imaginary time τ, which ranges within the limits $0 \leqslant \tau < \beta = 1/kT$, and $\langle\ldots\rangle$ is the symbol of statistical averaging. The Fourier component $G_{ij}(\mathrm{i}\omega_n)$ of function (2.5) depends on imaginary discrete frequencies $\mathrm{i}\omega_n = \mathrm{i}(2n+1)\,\pi T$. The analytic continuation from the imaginary to the real axis, $\mathrm{i}\omega_n \to \omega + \mathrm{i}\delta$, yields the retarded GF [26].

In the limit $d \to \infty$, the self-energy part of GF (2.5) is also independent of momenta and, instead of relation (2.4), we have an analogous relation for the temperature GF:

$$G(\mathbf{k}, \mathrm{i}\omega_n) = \frac{1}{\mathrm{i}\omega_n + \mu - \varepsilon_k - \Sigma(\mathrm{i}\omega_n)}\,. \tag{2.6}$$

Summing (2.6) over the momenta, we obtain the following expression for $G(\mathrm{i}\omega_n)$:

$$G(\mathrm{i}\omega_n) = \sum_{\mathbf{k}} G(\mathbf{k}, \mathrm{i}\omega_n) = \sum_{\mathbf{k}} \frac{1}{\mathrm{i}\omega_n + \mu - \varepsilon_k - \Sigma(\mathrm{i}\omega_n)}\,, \tag{2.7}$$

which is nothing else but the diagonal matrix element $G_{jj}(\mathrm{i}\omega_n)$ of GF (2.5) (for a spatially uniform system, the site index j can be omitted).

On the other hand, we regard $\Sigma(\mathrm{i}\omega_n)$ as the self-energy part of the GF $G_{\mathrm{loc}}(\mathrm{i}\omega_n)$ of a certain auxiliary problem on the same lattice defined with the help of an action $S[\mathcal{L}_0]$ that is a functional of a certain function $\mathcal{L}_0(\tau-\tau')$:

$$S[\mathcal{L}_0] = -\int_0^\beta \mathrm{d}\tau \int_0^\beta \mathrm{d}\tau' c^+(\tau)\, \mathcal{L}_0^{-1}(\tau-\tau')\, c(\tau') + U\int_0^\beta \mathrm{d}\tau\, n_\uparrow(\tau)\, n_\downarrow(\tau)\,. \tag{2.8}$$

The quantity $S[\mathcal{L}_0]$ should be considered an effective action obtained as a result of integration in the functional integral for the lattice GF over all sites except a preferred one; therefore, $\mathcal{L}_0^{-1}(\tau-\tau')$ contains information about all sites. The function $\mathcal{L}_0^{-1}(\tau-\tau')$ does not coincide with the bare GF for the single-impurity problem, but is essentially a dynamic mean field that acts on the preferred site from all other lattice sites.

Using action (2.8), we can calculate the electron GF of the single-impurity problem. We let it be denoted by $G_{\mathrm{loc}}(\mathrm{i}\omega_n)$. To find $\mathcal{L}_0^{-1}(\tau-\tau')$, we write the self-consistency equation by equating $G_{\mathrm{loc}}(\mathrm{i}\omega_n)$ to the GF $G(\mathrm{i}\omega_n)$. Thus, we obtain the equation

$$G_{\mathrm{loc}}(\mathrm{i}\omega_n) = \sum_{\mathbf{k}} \frac{1}{\mathrm{i}\omega_n + \mu - \varepsilon_k - \Sigma(\mathrm{i}\omega_n)}\,, \tag{2.9}$$

which relates $\mathcal{L}_0^{-1}(\mathrm{i}\omega_n)$ to $\Sigma(\mathrm{i}\omega_n)$. At the same time, all the quantities of the single-impurity problem are related via the Dyson equation

$$\mathcal{L}_0^{-1}(\mathrm{i}\omega_n) = G_{\mathrm{loc}}^{-1}(\mathrm{i}\omega_n) + \Sigma(\mathrm{i}\omega_n)\,. \tag{2.10}$$

Equations (2.9) and (2.10) allow calculating both unknown functions $\mathcal{L}_0^{-1}(\mathrm{i}\omega_n)$ and $\Sigma(\mathrm{i}\omega_n)$. The solution of the equations can be found by of iterations. The iterative procedure consists of the following stages:

(1) using a given initial value of $\mathcal{L}_0^{-1}(\mathrm{i}\omega_n)$, we find the GF $G_{\mathrm{loc}}(\mathrm{i}\omega_n)$ of the single-impurity problem using action (2.8);

(2) from Eqn (2.9), we determine $\Sigma(\mathrm{i}\omega_n)$;

(3) with the value of $\Sigma(\mathrm{i}\omega_n)$ thus obtained, we obtain a refined value of $\mathcal{L}_0^{-1}(\mathrm{i}\omega_n)$ from Eqn (2.10);

(4) the entire cycle is repeated until stable values of $\mathcal{L}_0^{-1}(\mathrm{i}\omega_n)$ and $\Sigma(\mathrm{i}\omega_n)$ are obtained.

From the values of $\Sigma(\mathrm{i}\omega_n)$ thus obtained, the function $\Sigma(\omega)$ is found using analytic continuation, which yields the retarded electron GF (2.4).

Thus, the DMFT reduces the problem of the dynamics of interacting electrons on a lattice to a single-impurity problem, which can be solved numerically; this allows avoiding many difficulties connected with solving the initial lattice problem.

The information about the lattice that corresponds to this model is contained in the right-hand side of Eqn (2.7), where we should pass from summation over the momentum $\mathbf{k}$ to integration over ε with an appropriate density of bare states on the lattice. Thus, in the DMFT, we always deal with the original lattice of crystal, which has a finite dimension ($d = 3$, 2); the passage to the limit $d \to \infty$ manifests itself only in the assumption that the self-energy part of the GF is independent of momentum. A comparison of the results of calculations performed in the DMFT approximation with the results of numerical calculations carried out via the diagonalization of small clusters shows that the dimensions $d = 3$ and even $d = 2$ are sufficiently large for the difference in the results to be unessential. At the same time, the DMFT does not suppose that some of the parameters of the Hamiltonian should be small. Formally, the small parameter is $1/d$.

Georges and Kotliar [4] were the first to apply the general idea of the DMFT to the Hubbard model with Hamiltonian (2.3) and showed that the problem of electron motion over a lattice under conditions of strong interelectron interaction reduces to the problem of a single impurity center placed in the 'sea' of noninteracting electrons, creating a dynamic mean field that acts on the electron located at that 'preferred' center, i.e., reduces to the well-studied single-electron Anderson model (SEAM) [28]. The calculation of the effective parameters of this auxiliary model is the basic difficulty of the DMFT. We do not describe the computational procedure here, but turn directly to the consideration of the results of calculations for the Hubbard model with Hamiltonian (2.3). The basic results are presented in Fig. 1, which displays the local density of states [1]

$$A(\omega) = \sum_{\mathbf{k}} A(\mathbf{k}, \omega)\,. \tag{2.11}$$

Figure 1 moves from one review to another, since it is a classical illustration of the electron structure of SCSs. We see how the system passes from the regime of weak electron correlations to the regime of SCSs with increasing the

[1] The quantity $A(\omega)$, which is defined by Eqn (2.11), is in fact the usual density of states in the electron spectrum [denoted most frequently as $\rho(\omega)$]. In the literature on the DMFT, $A(\omega)$ is usually called the local density of states, because it represents the spectral density of the auxiliary single-impurity problem, which in essence should be calculated. The self-consistency equation leads to the identity $A(\omega) = \rho(\omega)$. In what follows, we use both the $A(\omega)$ and $\rho(\omega)$ notation.

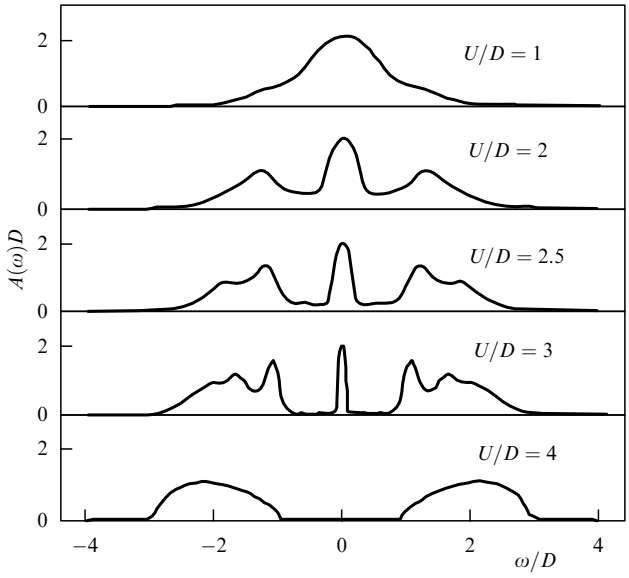

Figure 1. Local spectral density in the Hubbard model at the temperature $T = 0$ and band half-filling ($n = 1$) calculated within the DMFT [4]. D is the half-width of the bare band.

Coulomb parameter U, such that at the band half-filling, when the Fermi level lies at $\omega = 0$, the system passes from the metallic to the insulating state. At intermediate values of U, a three-peak structure occurs, which consists of a central peak and two wide lateral maxima. These maxima correspond to two Hubbard subbands revealed more than 40 years ago with the help of the heuristic approach of decoupling of the electron GF [1, 2]. The Hubbard subbands correspond to the incoherent escape of an electron from the atomic level occupied by two electrons with opposite spins, or to the transition of an electron to an empty atomic level.

The origin of the lateral peaks can be understood by examining Hamiltonian (2.3). The kinetic term becomes diagonal in the momentum representation, whereas the Coulomb term becomes diagonal in the site representation. This means that in the case of weak interelectron interaction, when $U \ll W$, the momentum representation is most convenient for the description, and the spectral density is determined by an expression of type (2.1). On the contrary, in the case where $U \gg W$, the site representation is most convenient, and the spectral density is close to the density characteristic of an isolated atom,

$$A(\omega) = \frac{1/2}{\omega + U/2} + \frac{1/2}{\omega - U/2}\,. \tag{2.12}$$

In the intermediate case, when $U \sim W$, the spectral density must reflect features of both limits, (2.1) and (2.12); therefore, the three-peak structure shown in Fig. 1 appears.

Thus, two energy scales exist in the spectrum of single-particle states of the Hubbard model. One of these is related to the width of the peak of quasiparticle states (let it be called ε_f^*); the other scale is related to the separation of peaks of incoherent states (a value of the order of U). The low-energy scale ε_f^* is defined by an expression $\varepsilon_f^* \sim ZD$, where Z is the statistical weight of the quasiparticle state [see Eqn (2.1)], and D is the band half-width, or the Fermi energy at half-filling. For SCSs, $Z \ll 1$; therefore, $\varepsilon_f^* \ll D$. The integrated intensity of the high-energy excitations that form the incoherent peaks is determined by the factor $1 - Z$. As we see below, such a structure of the quasiparticle spectrum is also characteristic of some other models of SCSs and is observed experimentally in different substances that belong to the class of SCSs.

2.3 Electron spectrum of the Hubbard model calculated in the DMFT approximation

Figure 2 displays the results of calculations of the spectral density in the Hubbard model at a finite temperature [29] that were performed using another DMFT procedure. As we already noted, it is necessary to solve an auxiliary problem of the single-impurity Anderson model, which can be done using various numerical methods. In the above-cited work [4], the authors used the quantum Monte Carlo method (QMC), and in [29], the numerical renormalization group (NRG) method.[2] It is seen from Fig. 2 that the spectrum has a three-peak structure in the range of intermediate values of U. The intensity of the quasiparticle peak sharply decreases (without becoming zero, however) in a vicinity of the critical point, after which it gradually decreases to zero with increasing U. Figure 3a shows the behavior of the $A(0)\,W(U/W)$ dependence with a change in temperature. The hysteresis, which is revealed with increasing and decreasing U, indicates the occurrence of a first-order metal–insulator phase transition (Fig. 4). The critical values U_{c2} and U_{c1} corresponding to the loss of stability of the metallic and insulating phases (whose existence manifests itself in the hysteresis, Fig. 3b), are the initial points of spinodal curves, which intersect at the critical point T_c, where a second-order phase transition occurs. For $T < T_c$, there is a first-order

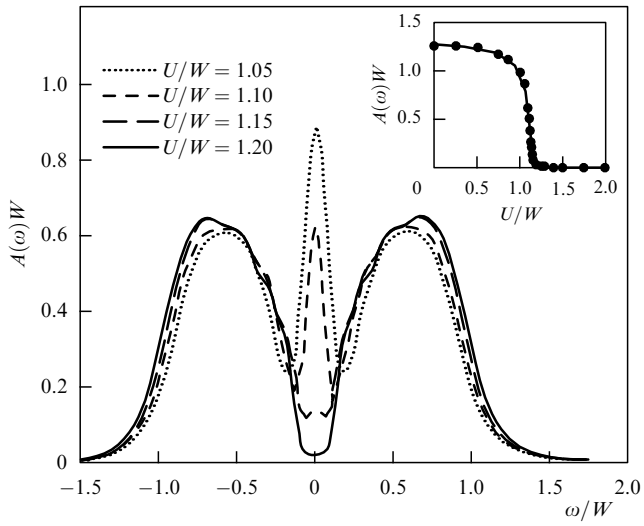

Figure 2. Evolution of the spectral density in the Hubbard model with increasing U at a finite temperature $T = 0.0276W$, where W is the width of the bare band. The inset displays the dependence of the quasiparticle peak on U [29].

[2] In [29], the authors used the Fye–Hirsch algorithm [30] with the QMC method. Recently, an extremely effective generalization of the QMC was suggested, namely, the method of 'continuous-time quantum Monte Carlo expansion' [31], which is free of the disadvantages of the usual QMC method and allows performing calculations at very low temperatures. There already exist first applications of the new method to SCS models [32]. The efficiency of the method is so high that it allows making DMFT calculations for actinides with several orbitals at the impurity center. Using this method, it is likely possible to conduct LDA + DMFT calculations of electron spectra for arbitrarily complex SCSs.

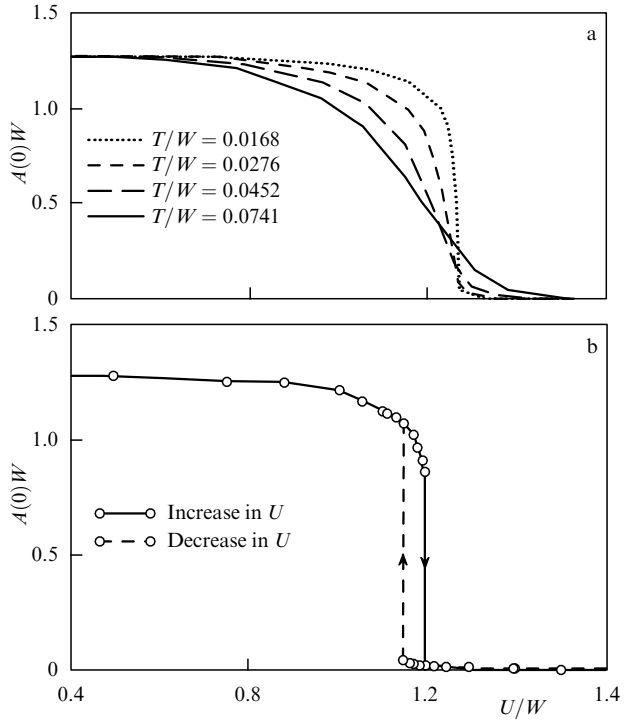

Figure 3. (a) Temperature behavior of the height of the quasiparticle peak and (b) hysteresis observed upon an increase and decrease in U [29].

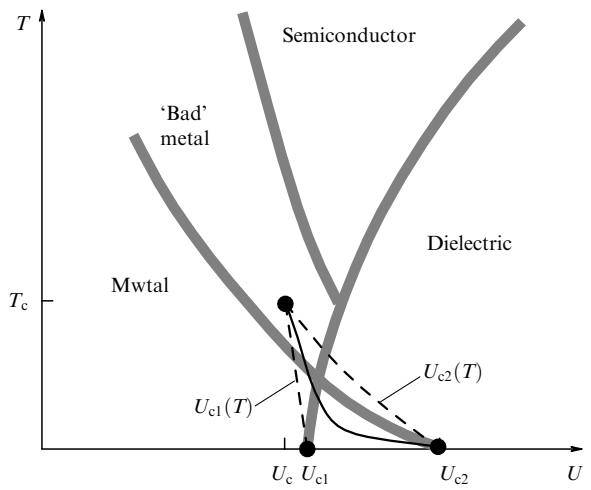

Figure 4. Phase diagram of the Hubbard model in the (T, U) plane (schematic) [9]. Dashed lines show spinodal curves; the solid curve corresponds to a first-order transition; the 'washed' curves correspond to a crossover.

phase transition; for $T > T_c$, no phase transition between the metallic and dielectric phases occurs and only a crossover is observed.

Figure 5 displays the temperature dependence of the electric resistance in the metallic phase of the Hubbard model near the metal – insulator phase transition. This figure was obtained in the DMFT approximation, where the auxiliary problem of the effective single-impurity Anderson model was solved using the method of iterative perturbation theory (IPT) — one more method frequently utilized in the DMFT framework. At low temperatures, $\rho \sim T^2$; this temperature range corresponds to the regime of $T \ll \varepsilon_f^*$. In

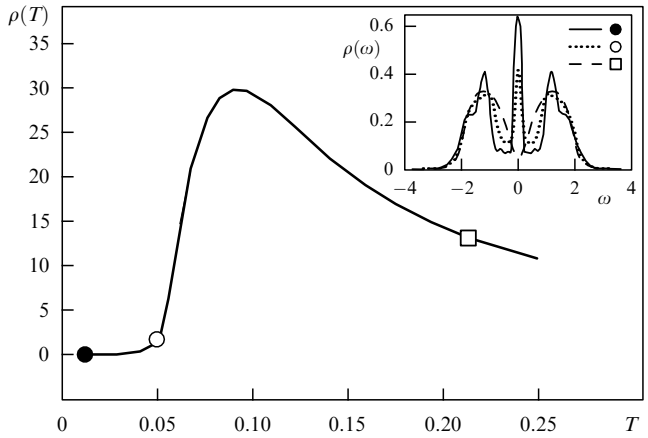

Figure 5. Resistance of the metallic phase near the metal – insulator transition ($U = 2.3W$) as a function of the temperature T according to a Hubbard-model calculation in terms of the DMFT method [9]; the temperature is expressed in units of the matrix element t of hopping between nearest neighbors. The inset shows the spectral density for three temperatures marked on the $\rho(T)$ curve by circles.

this interval of temperatures, the resistance is given by

$$\rho \sim \rho_M \left(\frac{T}{\varepsilon_f^*}\right)^2, \quad \rho_M \sim \frac{ha}{e^2}, \tag{2.13}$$

where ρ_M is the Mott limit for ρ, which corresponds to the mean electron path of the order of interatomic spacing a. A sharp increase in ρ at $T \sim \varepsilon_f^*$ corresponds to a 'bad' ('incoherent') metal, in which the quasiparticle peak is strongly suppressed but still exists. Finally, in the region of $T \gg \varepsilon_f^*$, the quasiparticles are completely absent and a pseudogap manifests itself in the transport properties, which determines the semiconductor nature of conductivity. The inset in Fig. 5 demonstrates the suppression of the quasiparticle peak with increasing temperature; precisely this feature causes the nature of the temperature dependence of resistance in SCSs.

The nature of the quasiparticle peak is completely understandable. This peak is in essence the Suhl – Abrikosov resonance, which was first predicted in connection with the problem of the Kondo effect in metals containing paramagnetic impurities. It is also called the Kondo peak, which is formed near the Fermi level as a result of the multiple scattering of electrons on impurities accompanied by spin flip. In the Hubbard model under consideration, there are initially no localized spins at lattice sites, but there are spin fluctuations, and the electron scattering on them leads to a resonance of electrons on the Fermi surface. This phenomenon is considered in detail in Section 8.

Under deviation from half-filling, the three-peak structure is retained, but with an increasing level of doping $\delta = n - 1$, the lower Hubbard band is displaced toward the chemical potential and the width of the quasiparticle peak increases substantially; however, its height does not change (Fig. 6a). It is seen from Fig. 6b that the maximum value of the imaginary part of the spin dynamic susceptibility substantially decreases with a decreasing level of doping. Electron scattering on spin fluctuations, whose spectral density is determined by $\operatorname{Im}\chi(\omega)$, leads to the quasiparticle peak that represents the Suhl – Abrikosov resonance. Figure 6c shows the calculated temperature dependence of the spin – lattice relaxation time $1/T_1$, which is determined by $\operatorname{Im}\chi(\omega)$.

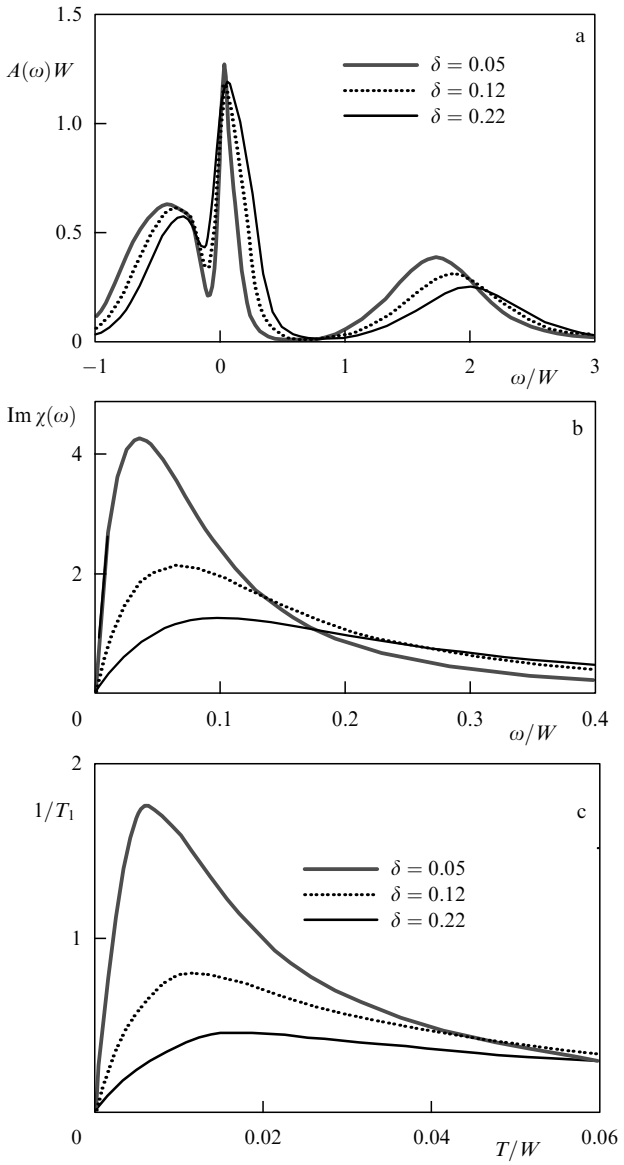

Figure 6. Evolution of the electron (a) and spin spectral density (b) in the Hubbard model with an increasing level of doping. The calculation was performed in the DMFT framework at $T = 0$ and $U/W = 2$. (c) Temperature dependence of the relaxation time $1/T_1$ calculated at the same value of the parameter U/W [33].

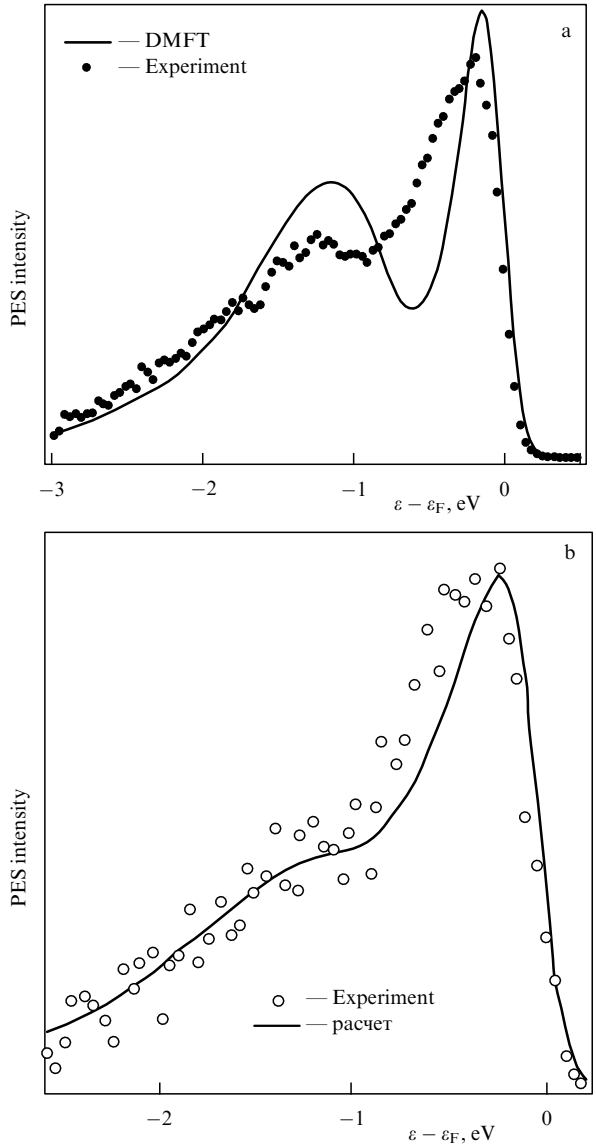

Figure 7. Comparison of the experimental and calculated spectral density of V_2O_3 doped with Cr (in order to transfer the system into the region of the metal–insulator phase transition) [7]: (a) according to the data in [35, 36] and (b) according to the newest data [37].

This quantity changes with an increasing level of doping in the same way as the spin density itself. The results of DMFT calculations presented in Figs 2–6 demonstrate typical behavior of the spin density of SCSs depending on the value of the Coulomb repulsion U, electron concentration n, and temperature T. These dependences can serve as a theoretical basis for the interpretation of the results of experimental studies of SCSs.

3. Experimental tests of the DMFT predictions

3.1 Structure of the electron spectrum

The development of experimental methods of studying the electron structure of solids has allowed confirming many qualitative predictions of the DMFT method. First and foremost, this refers to the three-peak structure of the spectrum of substances in the strongly correlated metallic phase near the Mott transition. The existence of a Hubbard subbahd located deep under the Fermi level, caused by the incoherent processes of transitions at localized atomic levels, was first demonstrated as early as 1992 in [34] on the example of the compound $NiS_{2-x}Se_x$ with the help of photoemission spectroscopy (PES). The observation of a quasiparticle peak in this compound was revealed later.

As an example of the observation of a three-peak structure, we give Fig. 7a, which shows the spectral density for V_2O_3 measured with the help of PES (data points), and the results of calculations using the LDA + DMFT (QMC) method (continuous curve).[3] The theoretical curve has

[3] The abbreviation used for this method means the following: DMFT (QMC) indicates the method for solving the auxiliary problem of the single-impurity Anderson model; LDA indicates the method of calculating the band structure of the compound. In the LDA, the exchange-correlation energy depends only on the electron density of a homogeneous electron gas [38].

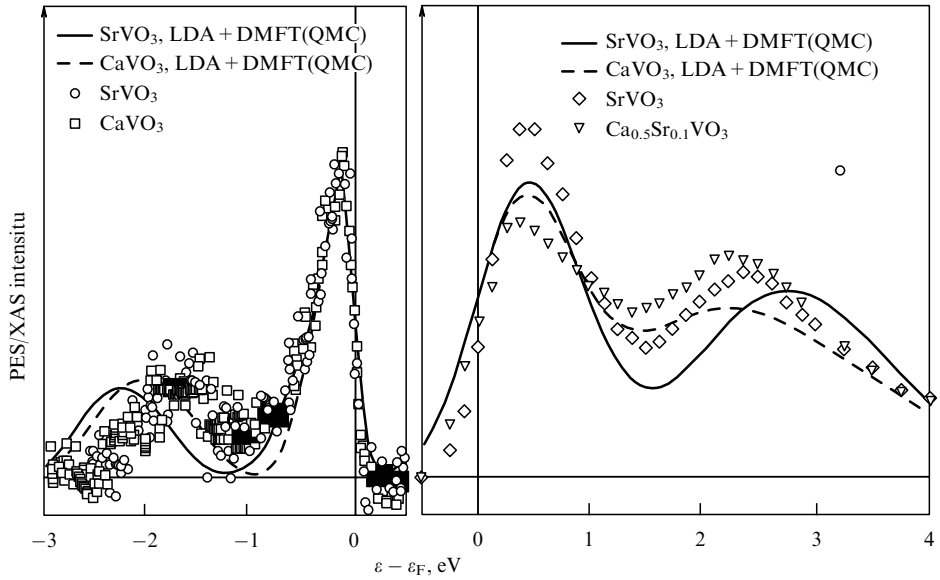

Figure 8. Electron density of $SrVO_3$ and $CaVO_3$ [10]: comparison of the experimental data obtained by the PES and XAS methods (symbols) and data calculated in the DMFT framework (curves).

quasiparticle and noncoherent (Hubbard) peaks, whose positions coincide with the positions of the experimental peaks.

Figure 7b shows recently obtained experimental data and the results of DMFT calculations for the paramagnetic–metal (PM) phase. In Ref. [37], the correct relation between the intensities of the quasiparticle and noncoherent peaks was also obtained. The calculations were carried out for the Coulomb potential $U = 4.2$ eV. It was shown that the intensity of the coherent peak in the PM phase varies by only 10% as the temperature increases from 400 to 1200 K, which also agrees with the experimental results.

Figure 8 shows the spectral density for two compounds, measured by PES (below the Fermi level) and by X-ray absorption spectroscopy (XAS) (above the Fermi level). Both Hubbard subbands and a quasiparticle peak are clearly seen. The results of calculations by the LDA + DMET (QMC) method agree satisfactorily with the experimental data.

Figure 9, which compares the spectral densities of four compounds (with the same crystal structure) calculated using the LDA + DMFT (QMC) method and the LDA method (i.e., without taking correlations into account) is very instructive. It can be seen that the LDA does not give Hubbard subbands. For the $SrVO_3$ and $CaVO_3$ compounds, the entire spectral density is concentrated in the region of the quasiparticle peak; therefore, these compounds, according to the predictions of the standard band theory (with strong correlations taken into account) are metals. The predictions for the other two compounds, $LaTiO_3$ and $YTiO_3$, differ dramatically: the LDA predicts a metallic state, whereas taking strong correlations into account leads to an insulating state with a wide gap in the spectrum, which corresponds to reality.

3.2 Phase diagram

We now consider how the phase diagram prediction in terms of the DMFT method (see Fig. 4) agrees with the real phase diagram. As an example, we use the phase diagrams of two compounds (Fig. 10): V_2O_3 and $NiS_{2-x}Se_x$. In the first case, the metal–insulator phase transition occurs under the effect of pressure or due to doping (see the upper abscissa scale). We see that doping is equivalent to 'chemical pressure,' because the structure of the phase diagram is independent of which pressure is applied, real or 'chemical.' In the second case, the metal–insulator phase transition occurs as a result of doping. The low-temperature regions, which correspond to magnetically ordered phases, differ from each other. In V_2O_3, only an antiferromagnetic insulating (AFI) phase is realized at low temperatures, whereas in $NiS_{2-x}Se_x$, there occurs an alternation of an AFI phase, a weakly ferromagnetic insulating (WFI) phase, and an antiferromagnetic metallic (AFM) phase.

This situation is quite typical of very different SCS materials in which metal–insulator phase transitions occur; the low-temperature phases can strongly differ in the nature of magnetic or other types of ordering. This is related to the differences in the crystal and electron structure of the compounds, in which a significant role belongs to specific magnetic interactions, different in magnitude and type in different materials, which have not been taken into account in constructing the phase diagram presented in Fig. 4. As regards the high-temperature parts of the diagram, which lie outside the region of magnetic ordering, they are very similar and qualitatively correspond to the schematic diagram in Fig. 4, although Fig. 4 presents phases as functions of the Coulomb repulsion U and that shown in Fig. 10, as functions of the pressure and concentration. However, it is necessary to keep in mind that the abscissa axis in Fig. 10 corresponds to the relative value of the Coulomb interaction U/W, which can change as a result of an increase in the matrix elements t_{ij} of electron transitions from site to site. An increase in W is equivalent to a decrease in U; this leads to a similarity in the phase diagrams shown in Figs 4 and 10 (we note that the sequence of metallic and insulating phases is different in these diagrams!). The specific features of the phase diagrams of different classes of SCSs are considered in Sections 6–8. We have not so far touched on the problem of the nature of the paramagnetic state in the insulating and metallic phases, i.e., the problem of the degree of localization of atomic magnetic

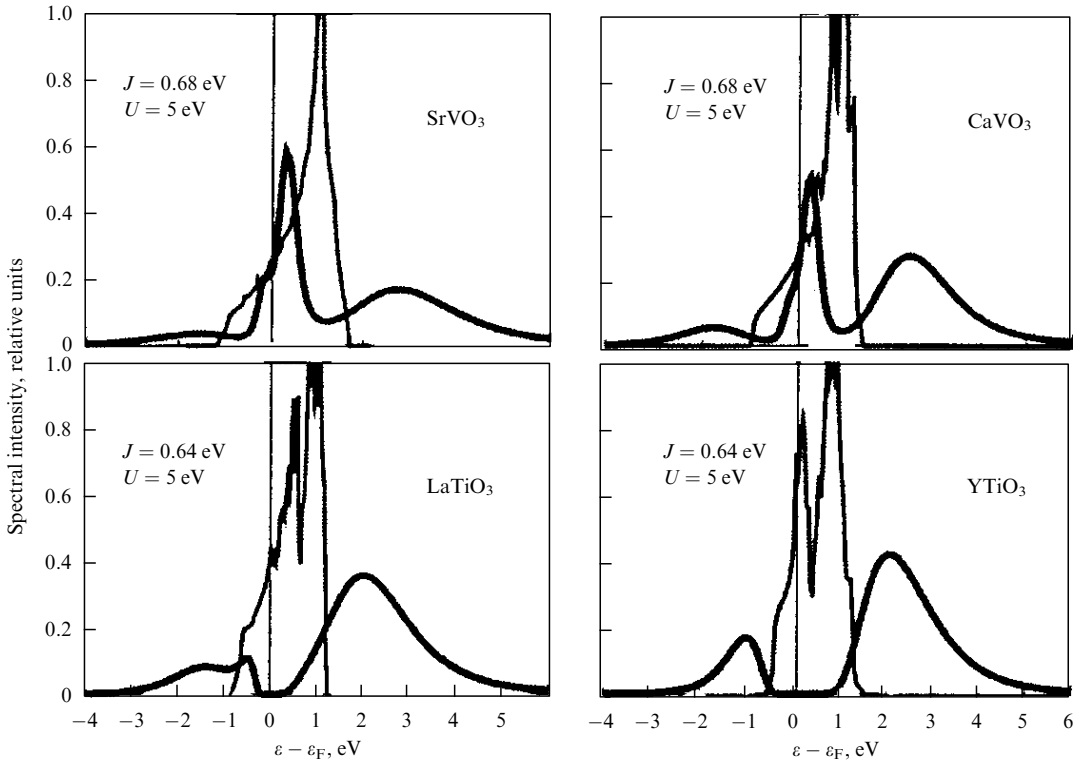

Figure 9. Results of the calculations of the spectral density for four isomorphic compounds with (thick curves) and without (thin curves) taking electron correlations into account [8].

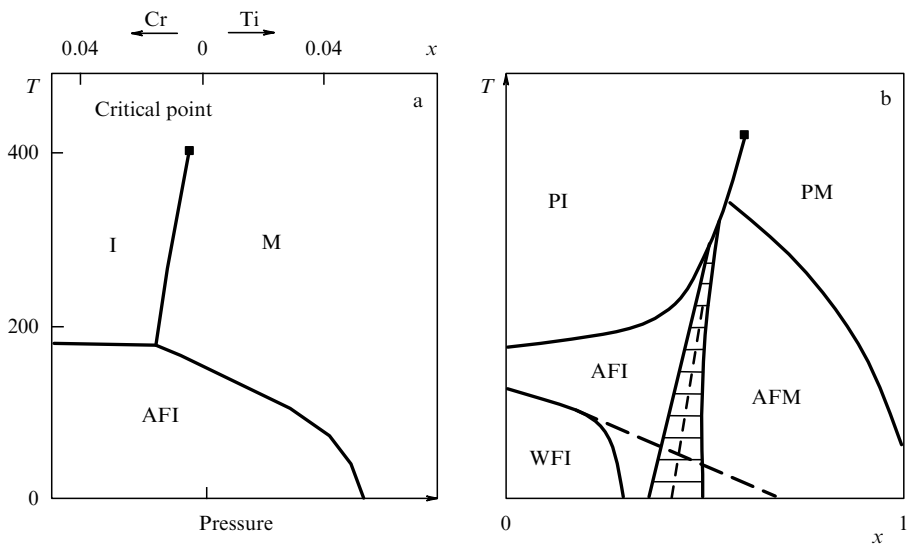

Figure 10. Phase diagrams of V_2O_3 (a) and $NiS_{2-x}Se_x$ (b): I, insulator; M, metal; AFI, antiferromagnetic insulator; AFM, antiferromagnetic metal; WFI, weak ferromagnetic insulator; PI and PM, paramagnetic insulator and paramagnetic metal (borrowed from [7].)

moments in SCSs, which strongly depends on the electron structure of the matter and on the values of the energy parameters. This question is considered when we discuss the specific classes of SCSs.

4. Specific features of the electron structure of d and f systems

4.1 d systems

In pure d and f elements, and even more so in related chemical compounds, there exist various electron states (atomic orbitals) that make contributions to the density of states near the Fermi level. This leads to the question of which electrons must be considered in simplified models, such as Hubbard or any other models of SCSs. Calculations of the band structure of a substance by the LDA method (without taking correlations into account) usually give a complex pattern of dispersion curves ε_k originating from different orbitals. In considering the physical properties of d and f systems, we must, first of all, separate the orbitals related to the electrons of the unfilled shells. These electrons remain strongly localized in the solid state, whereas the s and p outer-shell electrons become collectivized. Because the d and

f electrons are strongly localized near the atomic cores of the corresponding d and f elements, their on-site Coulomb repulsion is especially large; therefore, its magnitude U must be an important parameter of the electron structure.

It is necessary to note that the d or f states emerge onto the Fermi surface, as follows from an analysis of cohesion in the series of transition elements depending on the number of electrons in the unfilled shell. This conclusion also follows from the results of numerous LDA calculations of the band structure of d and f systems. The degree of localization of electrons increases in the sequence of 3d, 4f, and 5f elements, and this should be taken into account in constructing simplified (basic) models of the corresponding systems.

In the case of 3d elements, a significant delocalization (collectivization) of these electron states occurs and we can restrict ourselves to taking only them into account in the description of the physical properties of these substances, such as the magnetic susceptibility and transport and thermodynamic characteristics. In this situation, we can use the Hubbard model with Hamiltonian (2.3) if we ignore the degeneracy of electron states in the azimuthal quantum number.

4.2 f systems

In the 4f and 5f elements (lanthanides and actinides), the localization of electrons in the unfilled shells is stronger; therefore, it is necessary to account for the collectivized electron states originating from the outer shells. We arbitrarily call them s electrons. Then, we come to one of the two basic models. The first is the periodic Anderson model (PAM), which is specified by the Hamiltonian

$$H = \sum_{ij\sigma} t_{ij} c_{i\sigma}^{+} c_{j\sigma} + \varepsilon_{\mathrm{f}} \sum_{i\sigma} n_{i\sigma}^{\mathrm{f}} + U \sum_{i} n_{i\uparrow}^{\mathrm{f}} n_{i\downarrow}^{\mathrm{f}} + \sum_{ij\sigma} (V_{ij} c_{i\sigma}^{+} f_{j\sigma} + V_{ij}^{*} f_{j\sigma}^{+} c_{i\sigma}) , \tag{4.1}$$

where $c_{i\sigma}^{+}(c_{i\sigma})$ and $f_{j\sigma}^{+}(f_{j\sigma})$ are the respective operators of creation (annihilation) of s and f electrons, $n_{i\sigma}^{\mathrm{f}} = f_{i\sigma}^{+} f_{i\sigma}$ is the operator of the number of f electrons at a site i with a spin σ, ε_{f} is the atomic level of the f electron, and V_{ij} is the hybridization matrix element of s and f electrons.

Thus, the PAM takes the completely localized f electrons, collectivized s electrons, and their hybridization into account, but ignores the interaction between s electrons and takes the strong Coulomb interaction of f electrons into account. Besides the parameters W and U (the same as in the Hubbard model), this model involves the hybridization parameter V. The f electrons are initially considered completely localized, but their motion over the lattice becomes possible because of the hybridization with the collectivized electrons.

The second model, which accentuates the interaction of spin and charge degrees of freedom in the f and d systems through the exchange interaction, is defined by the Hamiltonian

$$H = \sum_{ij\sigma} t_{ij} c_{i\sigma}^{+} c_{j\sigma} - J \sum_{i\sigma\sigma'} (\mathbf{S}_i \, \mathbf{s}_{\sigma\sigma'}) \, c_{i\sigma}^{+} c_{i\sigma} , \tag{4.2}$$

where $\mathbf{S}_i$ is the spin operator of the unfilled electron shell of a d or f atom localized at a site i, $\mathbf{s}$ is the spin of a collectivized electron, and J is the so-called sd exchange (or sf exchange) integral. Model (4.2) is called the sd model or, in recent years, the Kondo lattice model (KLM).

If the Coulomb parameter U in Hamiltonian (4.1) or the exchange parameter J in Hamiltonian (4.2) is large, this is called the regime of strong electron correlations; then, when dealing with these models, the same difficulties as in the case of the simpler Hubbard model described by Hamiltonian (2.3) appear. These difficulties can be overcome with the help of the DMFT method. The corresponding results are considered in what follows when we discuss those classes of SCSs that are described in terms of the PAM or KLM. Anticipating these results, we note that the strong correlations in both models also lead to the appearance near the Fermi level of a sharp quasiparticle peak, which determines the entire low-energy physics in the corresponding domain of the model parameters. This confirms the previously expressed assertion that the DMFT is the most universal adequate method for describing various classes of SCSs.

We now consider what is neglected in the three basic models represented by their Hamiltonians. We mean the degeneracy of the electron states of the d or f type. The d-type states are fivefold degenerate, but this degeneracy is lifted in solids due to the effect of the crystalline field that acts from the adjacent atoms. The character of splitting of a degenerate level of a discrete atom is determined by the symmetry of its environment. Many compounds of transition metals, e.g., oxides, have a cubic symmetry. The atoms of nontransition elements (ligands, e.g., oxygen) frequently form octahedra or tetrahedra around the transition-element atom. In a field of cubic symmetry, the fivefold degenerate d level is split into two levels, which belong to two groups of states: $\mathrm{t}_{2\mathrm{g}}(\mathrm{d}_{xy}, \mathrm{d}_{yz}, \mathrm{d}_{zx})$ and $\mathrm{e}_{\mathrm{g}}(\mathrm{d}_{x^2-y^2}, \mathrm{d}_{3z^2-r^2})$. In the octahedral environment, the triplet states $\mathrm{t}_{2\mathrm{g}}$ have a lower energy than the doublet states e_{g}. In the tetrahedral environment, the positions of these levels are reversed. Thus, depending on the environment, levels of either the $\mathrm{t}_{2\mathrm{g}}$ or e_{g} symmetry are filled, and we deal with actual electrons (lying near the Fermi surface) that are either triply or doubly degenerate. This group of levels spreads to form a band, and precisely this band should be associated with the electrons considered in the Hubbard model. In calculating the electron structure of a specific d compound according to the LDA + DMFT method, we must consider precisely these electronic states.

In f systems containing lanthanides or actinides, the situation is different: the 4f states and, moreover, the 5f states in the solid state are localized more strongly than the 3d states; therefore, for describing their properties (primarily, transport properties), it is also necessary to consider the group of collectivized electrons and the interaction with them via hybridization or exchange. We should therefore use models that are more complex than the Hubbard model, namely, the PAM or the sd model [28]. It should immediately be noted that the PAM is a more general model and can be reduced to the sd model under certain conditions [39].

5. Compounds of 3d transition metals

5.1 Metal – insulator phase transitions

For many years, the central problem in the study of compounds of 3d elements was the nature of the metal – insulator (MI) phase transition. It was not clear how a metal with an incompletely filled electron band can become an insulator. It was Mott who first gave a physical explanation to this phenomenon [40 – 43]. According to his intuitive idea, the

strong electron–electron interaction (which is ignored in the band theory) can be responsible for this phenomenon. Indeed, we imagine a substance that consists of atoms, each contributing one electron to the band of collectivized states. Without the Coulomb interactions, this substance is metallic. But if the strong Coulomb interaction U of two electrons that fall onto the same atom is taken into account, then a high energy is required to transfer electrons from site to site. In the case of half-filling, each atom has one electron, and hence the transfer of electrons over the lattice becomes impossible at large U. In other words, the band of single-particle states is split into two subbands such that the lower includes the system with one electron per site, the upper includes the system with two electrons per site, and the Fermi level lies in the gap between these subbands. Thus, upon half-filling of the initial band, the substance becomes insulating. The metal–insulator phase transition at $n = 1$ is called the Mott transition.

Later, Hubbard confirmed Mott's idea by calculations in the framework of the model that bears his name; the bands split as a result of the electron correlations are therefore called the lower and upper Hubbard subbands. The results of DMFT studies presented in Section 3 confirm this picture of the electron spectrum of the Hubbard model and determine the fine structure of the spectrum of the metallic phase near the phase transition. However, the insulating state of the system at $U > U_c$ and $n = 1$ has an effect on the metallic phase at concentrations n different from unity but close to it, which can lead to the extension of the insulating-phase field into the range of electron concentrations $n \neq 1$. Thus, the occurrence of the metal–insulator phase transition is expected at $n = 1$ and at a certain critical value of the ratio U/W, but also in some vicinity of the line $n = 1$. Hence, it follows that there are at least two ways of realizing the phase transition in experiments on real SCSs: one is connected with a change in the band width W (and therefore with an increase in the parameter U/W), e.g., by the application of an external or internal (chemical) pressure, and the second is connected with a doping of the initial system. The first way is referred to as BC-MIT (from Bandwidth-Control Metal–Insulator Transition), and the second, as FC-MIT (from Filling-Control MIT).

We briefly discuss how the problem of the metal–insulator phase transition can be considered on the basis of the Fermi-liquid theory, in which each state of an electron in the lattice with a given momentum is associated with a state corresponding to noninteracting electrons in the same lattice; in the framework of this theory, it seems impossible to approach the insulating phase. We recall, however, that in the Fermi-liquid theory, the spectral weight of a quasiparticle state is determined by the quantity

$$Z < 1\,, \quad Z \sim \frac{m}{m^*}\,, \tag{5.1}$$

which depends on the ratio of the electron mass m to the quasiparticle effective mass m^*. If m^* increases as the Coulomb interaction increases, then the intensity of the quasiparticle peak decreases and we have $Z \to 0$ as $m^* \to \infty$. Thus, the divergence of the effective mass of charge carriers as a result of the electron–electron interaction indicates a transition of the metal into the insulating state, although a direct description of the insulating phase in the framework of the Fermi-liquid theory is impossible. An approach to the description of the insulating phase was theoretically developed in [44]. An increase in the effective mass of carriers in the vicinity of the metal–insulator phase transition is observed in many SCS calculations. An increase in m^* leads to many anomalies in the behavior of the metallic phase of real SCSs near the phase transition, and the nearer the phase transition to the second-order phase transition, the more distinct these anomalies are. We have already seen from the results of calculations of the electron structure by the DMFT method that the first-order transition can occur in a simple model, e.g., the Hubbard model, as a result of taking correlations into account. However, as a result of interaction of the electron system, for instance, with an atomic disorder or with lattice degrees of freedom, a first-order transition is usually developed instead of a continuous phase transition.

The metal–insulator phase transition caused by electron correlations is usually called the Mott or Mott–Hubbard phase transition. We emphasize its difference from the phase transitions caused by the appearance of any long-range order, for example, magnetic, in which case an energy gap appears at the boundary of the new Brillouin zone (and disappears at $T > T_N$). We note one more (non-Mott) type of metal–insulator phase transition, under which a certain superstructure appears in a stoichiometric compound at $T < T_N$ and the substance is insulating, but pockets of carriers appear at the boundaries of the new Brillouin zone and the substance becomes conducting with a deviation from stoichiometry. This situation is frequently observed in cuprates in which high-temperature superconductivity is realized.

Along with the Hubbard model, the so-called pd model is used for an analysis of the compounds of 3d elements; in this model, d states at the transition-element atoms and p states at the atoms of ligands are taken into account. The Hamiltonian describing the pd hybridization can be represented as

$$H = \varepsilon_d \sum_{i\sigma} n^d_{i\sigma} + U_{dd} \sum_i n^d_{i\uparrow} n^d_{i\downarrow} + \varepsilon_p \sum_{j\sigma} n^p_{j\sigma} + V_{pd} \sum_{ij\sigma} (d^+_{i\sigma} p_{j\sigma} + p^+_{j\sigma} d_{i\sigma})\,, \tag{5.2}$$

where i is the order number of an atom of the transition element and j is the order number of an atom of the ligand. This model takes only the atomic levels of d and p electrons into account and ignores electron motion over the lattice. However, the pd hybridization allows the electrons to pass from the d sublattice into the p sublattice with an effective hopping matrix element between the nearest sites in the d sublattice

$$t \sim \frac{V^2_{pd}}{\varepsilon_d - \varepsilon_p}\,, \tag{5.3}$$

which determines the width of the carrier band.

In this situation, an important role is played by the charge transfer energy $\Delta = \varepsilon_d - \varepsilon_p$ (in the compounds of 3d elements, the d level lies above the p level of ligands). When $\Delta \gg U_{dd}$, the width of the hybridized band is $V^2_{pd}/\Delta \ll U_{dd}$ and the system is a Mott insulator. When $\Delta \ll U_{dd}$, two energies should be compared: the band width V^2_{pd}/Δ and the energy gap Δ that separates the energies of the d and p states. At a sufficiently large value of Δ and with the condition $V^2_{pd}/\Delta \ll \Delta \ll U_{dd}$ satisfied, a charge-transfer metal–insulator phase transition (CT-MIT) occurs [45].

Direct information on the electron structure of real substances can be obtained using spectroscopic methods. A comparison of experimental data with the results of model calculations allows determining the basic parameters of the Hamiltonian; the necessary a priori estimates of these parameters can be made, for example, via LDA calculations.

5.2 Various types of chemical compounds

An analysis of experimental and theoretical data on the electron structure and metal – insulator phase transitions in various compounds of transition 3d elements can be found in the fundamental review by Imada, Fudjimori, and Tokura [46] published in 1998 (see also [47]). The list of the compounds investigated is presented in Table 1. As is seen, oxides predominate in the list, but sulfides and selenides are also present.

The list begins with four BC-MIT compounds: V_2O_3, NiS, $NiS_{2-x}Se_x$, and $RNiO_3$. The first two have long been known as prototypes of compounds in which a metal – insulator phase transition can occur under the external or chemical pressure. The V_2O_3 compound is regarded as a Mott insulator, whereas NiS and $NiS_{2-x}Se_x$ are regarded as insulators with a charge transfer between the 3d states of Ni and np states of the chalcogen. In this case, the band of np states is filled, and the Hubbard subband of Ni is empty. The relation between the width of the filled band and the energy gap between the np and 3d bands can be changed by applying pressure or by doping. An analogous situation occurs in $RNiO_3$ compounds, where R is a rare-earth element in the range from La to Lu.

The V_2O_3 compound is the most thoroughly studied of the compounds in which the metal – insulator phase transition occurs. This compound has a corundum structure, in which

Table 1. Compounds of 3d elements in which metal – insulator transitions were revealed (according to [46]).

Compound	Type of transition*	Néel temperature** T_N, K	Parameter***	Transition****	Structure, dimension*****
V_2O_{3-y}	MH	~ 180	FC, BC	1	3
$NiS_{2-x}Se_x$	CT	40 – 80	BC	1	Corundum, 3
$R\,NiO_3$	CT	130 – 240	T, BC	1	Rutile, 3
$NiS_{1-x}Se_x$	CT	260	T, FC, BC	1	Perovskite, 3
$Ca_{1-x}Sr_xVO_3$	—	—	—	—	3
$La_{1-x}Sr_xTiO_3$	MH	140	FC	C	Perovskite, 3
$La_{1-x}Sr_xCuO_{2.5}$******	CT	110	FC	C	1 or 3
HTSC cuprates					
$Sr_{14-x}Ca_xCu_{24}O_{41}$	CT	—	FC	C	1 or 2
$BaVS_3$	MH	~ 35	T	C	1
Fe_3O_4	—	—	T	1	Spinel, 3
$La_{1-x}Sr_xFeO_3$	CT	740 ($x = 0$) 134 ($x = 1$)	FC T		Perovskite, 3
$La_{2-x}Sr_xNiO_{4+y}$	CT	~ 500 ($x = y = 0$)	FC	C	2, K_2NiF_4
$La_{1-x}Sr_{1+x}MnO_4$	CT	120	—	—	2, K_2NiF_4
$La_{1-x}Sr_xMnO_3$	CT	140	FC	C	Perovskite, 3
$La_{2-2x}Sr_{1+2x}Mn_2O_7$	CT		FC	C	2
Manganites	See Section 7				
FeSi			T	CR	Perovskite, 3
VO_2	(MH)		T	1	1 or 3
Ti_2O_3	MH		FC, T $T = 400 - 600$ K		Rutile, 3 Corundum
$LaCoO_3$	CT		T	CR	Perovskite, 3
$La_{1.17-x}A_xVS_{3.17}$	(MH)		FC ($x_c \sim 0.35$) $T = 280$ K	CR	2

* MH — MH, Mott – Hubbard phase transition; CT, phase transition with charge transfer;
** Néel temperature of stoichiometric compounds;
*** Control parameter responsible for the phase transition: BC, bandwidth; FC, band filling; T, temperature;
**** Type of phase transition: 1, first-order phase transition; C, continuous (second-order) transition; CR, crossover;
***** Type of crystal lattice and (or) effective dimension;
****** See Table 2.

the V atoms form chains along the c axis and a honeycomb structure in the basal plane. Each V atom is surrounded by an octahedron consisting of trigonally distorted atoms; as a result, the triply degenerate t_{2g} level is split into two sublevels (one nondegenerate and one doubly degenerate) and, according to band-structure calculations, the nondegenerate level should be related to electrons with a strong correlation, which prevail on the Fermi surface.

Therefore, the nondegenerate Hubbard model can be adequate for the description of the V_2O_3 compound with the parameters W and U that satisfy the condition for the metal–insulator phase transition, i.e., the relation $U \sim W$.

The photoemission spectra (see Fig. 7) indicate the existence of a wide region of noncoherent states under the Fermi surface, which correspond to the lower Hubbard subband, and of a quasiparticle peak at the Fermi level. The DMFT calculations well confirm these experimental data. From the phase diagram in Fig. 10, it is apparent that the metal–insulator phase transition that occurs under the external or chemical pressure applied to the compound is of the BC-MIT type. The experiments also show that the electron specific heat (the coefficient γ in the relation $C = \gamma T$) increases in approaching the phase transition from the side of the metallic phase due to a decrease in pressure, which corresponds to an increase in the effective mass by a factor of 3–5. The total body of experimental data indicates that V_2O_3 exhibits the Mott phase transition described by the nondegenerate Hubbard model. The results of investigations of the electron structure by the DMFT method have already been discussed in Section 3, where some other compounds were also considered that are given in Table 1 before the cuprates. The DMFT gives a satisfactory description of these representatives of SCSs. The cuprates, which are high-temperature superconductors, are considered in Section 6.

Moving further down Table 1, we come to a group of compounds including Fe_3O_4 and strontium-doped compounds $LaFeO_3$, La_2NiO_4, and $LaMnO_4$, in which the metal–insulator phase transition is caused by an ordering of the different-valence ions of the transition element. The clearest and best-known representative of such compounds is Fe_3O_4.

The magnetite Fe_3O_4 has a spinel structure in which one-third of the Fe ions are located at sites that have a tetrahedral environment and two thirds at sites with an octahedral environment. The tetrahedral and octahedral sites are respectively called A and B sites. At a temperature $T_V \approx 120$ K, there occurs a change in the resistance reaching two orders of magnitude, which is caused by the ordering of Fe^{2+} and Fe^{3+} ions — a phenomenon known as a Verwey phase transition. At the A sites, only Fe^{3+} ions are found, whereas at the B sites, one-half of the ions are Fe^{3+} ions and the other half are Fe^{2+} ions, which have the respective spins $S = 5/2$ and $S = 3/2$. At the point T_V, an ordering of these ions in the B sublattice begins, such that the low-temperature ordered phase becomes almost insulating. This ordering occurs as a result of the Coulomb repulsion of ions located on adjacent sites in the B sublattice, because this process minimizes the Coulomb energy of the crystal. Magnetite is a ferrimagnet in which the spins in the A and B sublattices are antiparallel; the magnetic ordering appears at the Curie temperature $T_C = 858$ K, and hence the magnetic and charge ordering are well separated.

Charge ordering of another type, which was revealed in $La_{1-x}Sr_xFeO_3$ at a temperature below 210 K and $x \approx 2/3$, is accompanied by the development of an antiferromagnetic order. One of the initial compounds, $LaFeO_3$, is an antiferromagnetic insulator with $T_N = 134$ K. In the $La_{1-x}Sr_xFeO_3$ solid solution, the Néel temperature monotonically decreases as x increases. When x reaches approximately 2/3, the resistance at $T = 207$ K increases sharply; upon cooling, a narrow thermal hysteresis is observed, which indicates a first-order transition in the phase with two types of long-range order: insulating and antiferromagnetic.

The compound La_2NiO_4, which has the structure of the layered compound K_2NiO_4, exhibits a cooperative ordering of holes upon doping by strontium, and a simultaneous ordering of spins of Ni ions. Depending on the Sr concentration, either charge ordering of the spin-density-wave type can arise or charged diagonal domain walls can appear in $La_{2-x}Sr_xNiO_4$. Charge ordering manifests itself in anomalies in the transport and optical properties at Sr concentrations $x = 1/3$ and 1/2.

We mention one more compound, $La_{1-x}Sr_{1+x}MnO_4$, which also exhibits charge ordering near $x = 1/2$. The stoichiometric compound $LaSrMnO_4$ ($x = 0$) can be considered a Mott insulator with an antiferromagnetic ordering.

The group of manganites with a perovskite structure (see Table 1), which belongs to a wide class of compounds with a ferromagnetic ordering exhibiting a 'colossal' magnetoelectric effect, is considered in Section 7.

6. Cuprates as high-temperature superconductors

6.1 Basic experimental data

High-temperature superconductivity was discovered in the group of doped copper oxides whose structure is based on the perovskite structure (Table 2). The most important structural elements in these oxides are CuO_2 planes separated by planes consisting of La or Nd, Y, and Bi atoms. Each Cu atom is

Table 2. HTSC cuprates.

Compound	Type of transition	T_N, K	Parameter	Transition	T_c^{max}, K	Range of doping in which $T_c \neq 0$
$La_{2-x}Sr_xCuO_4$	CT	300	FC	C	40	$x = 0.06-0.25$
$Nd_{2-x}Ce_xCuO_4$	CT	~ 240	FC	C	24	$x = 0.15-0.17$
$YBa_2Cu_3O_{7-y}$ (YBCO–Y123)	CT	~ 400	FC	C	94	$y = 0.1-0.7$
$Bi_2Sr_2Ca_{1-x}R_xCu_2O_{8+\delta}$ (Bi2212)	CT	260	FC	C	90	$\delta = 0.11-0.18$
$HgBa_2Ca_{n-1}Cu_nO_{2n+2+\delta}$ ($n = 1-3$)	CT		FC	C	97–135 164 ($P = 31$ GPa)	$\delta = 0.08-0.12$

surrounded by six atoms that form an octahedron. This structure is characteristic of the initial stoichiometric compounds, which are antiferromagnetic insulators. High-temperature superconductivity appears in the doped compounds upon the substitution of a nontransition element by atoms of an element with a different valence.

We first consider the initial compound La_2CuO_4 in more detail. Because it contains trivalent La ions and divalent Cu^{2+} ions with a d^9 configuration, the t_{2g} states are completely filled. In the crystalline field of a distorted octahedron, of the two e_g-symmetry states, the $d_{3z^2-r^2}$ state is also filled and the $d_{x^2-y^2}$ state is only half-filled (because there is also a degeneracy in spin). The strong on-site Coulomb repulsion leads to the formation of a gap, and the compound becomes insulating. On the energy scale, the $2p_\sigma$ orbitals of oxygen lie near the $d_{x^2-y^2}$ orbitals of copper; therefore, a pd hybridization of adjacent atoms of Cu and O occurs, and La_2CuO_4 is an example of compounds of the CT type, according to the arguments given in Section 5. The stoichiometric compound La_2CuO_4 is an antiferromagnetic insulator with the Néel temperature $T_N \approx 300$ K and remains insulating at temperatures slightly exceeding T_N due to strong correlation effects.

The doped compound $La_{2-x}M_xCuO_4$, where $M =$ Sr, Ba, Sr, is an insulator at $x \leqslant 0.05$ but becomes metallic at large x; the antiferromagnetic long-range order is destroyed in this case, but a short-range magnetic order is retained in the entire metallic region. The magnetic-order correlation length ξ changes with increasing x in accordance with the law $\xi \sim a/\sqrt{x}$, where a is the lattice constant. Because of the large crystalline anisotropy, the fluctuations in magnetic order are strong in the CuO_2 plane; therefore, the correlation length ξ in fact coincides with the average spacing between the dopant atoms. The electric properties, most of all conductivity, also manifest strong anisotropy; therefore, the compound is quasi-two-dimensional from the standpoint of electric and magnetic properties. Upon doping, the dopant atoms replace only La and do not fall into the CuO_2 planes. The divalent Sr, Ba, and Ca ions, replacing the trivalent La ions, produce holes in the CuO_2 planes, which are charge carriers.

The antiferromagnetic exchange interaction is very large: $J \approx 1600$ K, although $T_N \approx 300$ K. This large difference between J and T_N confirms the idea that this compound is a quasi-two-dimensional magnetic material. If this compound were exactly two-dimensional, no magnetic long-range order could exist in it. However, owing to the existence of a certain exchange coupling between the planes, a three-dimensional magnetic order with T_N that is substantially smaller than J is established in the compound, as must be the case for quasi-two-dimensional systems. It is believed that La_2CuO_4 is a quasi-two-dimensional Heisenberg antiferromagnet with the magnetic moment at the Cu ions equal to $0.4\,\mu_B$. The deviation in the value of the magnetic moment from $0.5\,\mu_B$ is caused by quantum fluctuations, which are always present in any antiferromagnetic structure.

The phase diagrams of HTSC cuprates are similar; therefore, in Fig. 11, we give only a schematic phase diagram characteristic of different groups of HTSC materials in their general features. On the (T, x) plane, for example, for $La_{2-x}Sr_xCuO_4$, the diagram looks as follows. For $0 \leqslant x < 0.05$, there exists an insulating antiferromagnetic phase with T_N that rapidly decreases from the maximum value at the stoichiometric composition to zero. With a further increase in x, a normal metallic phase with a magnetic

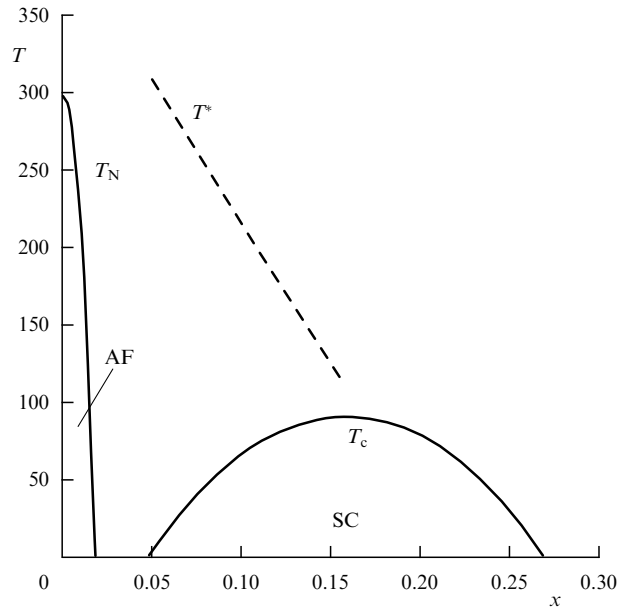

Figure 11. Phase diagram of HTSC cuprates (schematic).

state of the spin-liquid type arises, and then a superconducting phase appears. The temperature of the superconducting transition T_c passes through a maximum at $x \approx 0.15$ and again becomes zero at $x \approx 0.3$. A normal metallic phase is realized outside the interval $0.05 \leqslant x < 0.3$. The maximum values of T_c at $x_m \approx 0.15$ are approximately 40 K; this x_m is usually called the optimum concentration. The range $x < x_m$, in which the superconducting state is observed, corresponds to a regime called underdoped, and the range $x > x_m$ corresponds to the regime called overdoped. In Fig. 11, a dashed line that goes through the region of the normal metallic phase, where the nature of the normal state changes and a crossover from the usual state of the metallic system (above the T^* line) to a special metallic state is observed (see Section 6.2).

We have described the basic properties of the $La_{2-x}Sr_xCuO_4$ system in detail. Another family of cuprates, $Nd_{2-x}Ce_xCuO_4$, is remarkable because the doping with cerium introduces electrons rather than holes into the CuO_2 planes; however, the general features of the phase diagram remains as before, although the dimensions of the phase fields on the (T, x) plane change noticeably: the antiferromagnetic insulating phase exists for $0 \leqslant x < 0.13$ and is immediately followed by a metallic superconducting phase whose existence interval in the neodymium system is narrower than in the lanthanum system.

6.2 Pseudogap state

We now return to the phase diagram in Fig. 11 and focus on the line denoted by T^*. It was already long ago noted that the properties of the normal metallic phase differ strongly for underdoped and overdoped cuprates. In the latter case, the metallic phase is described sufficiently well in terms of the Fermi-liquid approach, i.e., there is a definite Fermi surface and the damping of quasiparticles tends to zero upon approaching this surface. In the case of underdoped systems, at sufficiently low temperatures ($T < T^*$), anomalies in all the electron properties of the system are observed. The change in the properties upon intersection of the T^* line is not sharp and represents not a phase transition but a crossover from the

usual Fermi-liquid state to a pseudogap state. The concept of a pseudogap state means, first and foremost, a reduction in the density of states at the Fermi surface. This follows, in particular, from a very noticeable decrease in the linear coefficient γ in the electronic specific heat and a decrease in the Pauli magnetic susceptibility χ_0 upon crossing the T^* line and especially from the data of tunneling experiments and of angle-resolved photoelectron spectroscopy (ARPES).

The ARPES method allows directly measuring the spectral density of quasiparticles in the vicinity of the Fermi surface and reconstructing the Fermi surface itself. It turned out that a characteristic phenomenon was observed in all classes of HTSC cuprates that were investigated, namely, the destruction of part of the Fermi surface along the directions $(0, k_y)$ and $(0, k_x)$ of the Brillouin zone, whereas in the diagonal directions (k_x, k_y), the Fermi surface remained in the usual sense: the intensity of the ARPES spectrum decreases sharply upon crossing it. In the $(0, k_y)$ and $(k_x, 0)$ directions, the change in $A(k, \omega)$ occurs in a wide interval; moreover, at a fixed quasimomentum, the density $A(k, \omega)$ has a two-humped structure with a minimum at the 'former' Fermi surface, which could exist in the absence of a pseudogap state, for example, at $T > T^*$. A detailed discussion of this phenomenon can be found in the fundamental reviews [48, 49], and recent data can be found in review [50] devoted to an ARPES study of $La_{2-x}Sr_xCuO_4$, and in [51] devoted to studying the Bi2212 system (see also the references given in these works). Thus, in HTSC cuprates, the Fermi surface has an 'arched' nature, i.e., is preserved only on the arcs that adjoin the diagonal directions of the Brillouin zone.

These unusual properties of the normal phase of underdoped cuprates undoubtedly must influence the HTSC formation mechanisms and, therefore, they immediately drew considerable attention of theorists. There are two scenarios for the appearance of a pseudogap state. In one of them, the appearance of a pseudogap is connected with fluctuations of Cooper pairs at $T > T_c$, which lead to a coherent superconducting state at T_c. Another scenario is based on fluctuations of the spin or charge order parameters, which in the metallic phase of all cuprates are very large, although both the magnetic and insulating long-range orders are absent in the range of existence of the superconducting phase. The first mechanism is apparently less probable because the pseudogap state manifests itself most strongly as the level of doping decreases to $x \approx 0.05$, in proportion to moving away from the superconductivity region. However, the fluctuations in spin order grow upon approaching the stoichiometric composition, at which the system becomes an antiferromagnetic insulator.

We now consider the dynamic magnetic susceptibility of the metallic system that is in a state close to the antiferromagnetic ordering [52]:

$$\chi(\mathbf{q}, \omega) \approx \frac{\xi^2}{1 + \xi^2(\mathbf{q} - \mathbf{Q})^2 - \mathrm{i}\omega/\omega_s}\,, \tag{6.1}$$

where $\mathbf{Q} = (\pm\pi, \mp\pi)$ is the wave vector of the antiferromagnetic structure in the insulating phase, ω_s is the characteristic frequency of fluctuations, and ξ is the correlation length of spin fluctuations. The interaction of electrons with spin fluctuations is proportional to $\chi(\mathbf{q}, \omega)$; therefore, it must sharply increase for those electrons at the Fermi surface whose wave vectors are close to the boundaries of the magnetic Brillouin zone, or for electrons located on the flat segments of the Fermi surface (if they exist) separated by the vector $\mathbf{Q}$. Two models thus appear in which the pseudogap state can manifest itself: the model of 'hot' spots and the model of 'hot' regions near the Fermi surface [48]. Underdoped systems exist near the band half-filling, and hence the Fermi surface undisturbed by band correlations lies near the magnetic Brillouin zone, and one of the two models can be realized in this case.

Near the 'hot' spots in the k-space region of the width ξ^{-1}, electrons are strongly scattered with a change in the momentum by the vector $\mathbf{Q}$, which leads to the opening of a pseudogap in the vicinity of these points, similarly to how a gap opens on the entire Fermi surface due to the appearance of an antiferromagnetic phase if the bare Fermi surface involves nesting. If we disregard the dynamics of spin fluctuations and consider the static fluctuations to be Gaussian, then the problem of the interaction of electrons with such fluctuations can be solved exactly in the one-dimensional case [48], and its solution can be used for a qualitative study of the situation in the two-dimensional case. The results of calculations indicate the pseudogap character of electron states in the hot regions of the Fermi surface; in particular, they reflect the two-hump structure of the spectral density of states (Fig. 12).

In the above approach, the strong electron correlations inherent in all HTSC cuprates were ignored. The Coulomb interaction was not taken into account explicitly at all, although implicitly it is present in the expressions for the correlation length ξ and for the force of interaction of electrons with spin fluctuations Δ, which were introduced phenomenologically, but their microscopic nature was based on the (Coulomb) interaction of electrons. The strong Coulomb correlations, as we saw above, are taken into account most effectively in the DMFT. Keeping in mind the application of the theory to cuprates, the authors of [53, 55–57] suggested a hybrid approach by combining a microscopic DMFT method and the above-described method based on including static spin fluctuations [48] through the phenomenological parameters ξ and Δ. The Coulomb correlations in the framework of the single-band Hubbard model can be taken into account in the standard DMFT scheme under the assumption that the self-energy part of the electron GF $\Sigma(\omega)$ depends only on frequency. The presence of inhomogeneities in the system, which are taken into account through the correlation length ξ, leads to a contribution to the self-energy $\Sigma_k(\omega)$ that depends on the quasimomentum. The $\Sigma(\omega)$ and $\Sigma_k(\omega)$ contributions are assumed to be additive. With this approach, which was called DMFT + Σ_k, and the parameters of model $U = 4\,t$ and $n = 0.8$, the density of states $\rho(\omega)$ and the spectral density $A(k, \omega)$ were calculated; the two-hump structure of the spectral density indicated the formation of a pseudogap state. The calculation of dispersion curves showed that the Fermi surface has a hole structure; for momenta with the directions close to $(0, 0) - (\pi, \pi)$, well-specified quasiparticles exist, whereas in the direction toward the points $(0, \pi)$ and $(\pi, 0)$, a typical two-hump structure of $A(k, \omega)$ appears such that we can speak of the destruction of the Fermi surface near these points (Fig. 12a).

Figure 12b shows the real part of the optical conductivity calculated for the same values of the parameters at two temperatures and two values of the intensity of the pseudogap fluctuations Δ. It is seen that at nonzero Δ, a dip appears in the $\mathrm{Re}\,\sigma(\omega)$ curve in the metallic phase at low frequencies, which gradually disappears with increasing the temperature.

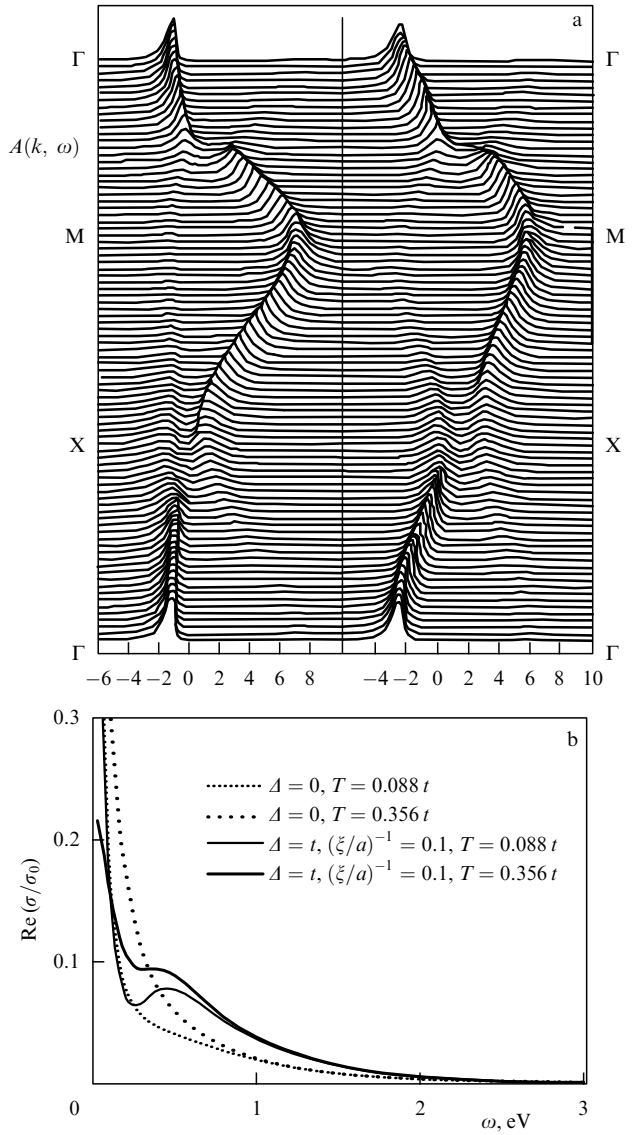

Figure 12. Effects of the pseudogap state in the Hubbard model obtained on the basis of DMFT + Σ_k calculations using the parameters $U = -4t$, $t' = -4t$, and $n = 0.8$: (a) the spectral density $A(\mathbf{k}, \omega)$ along symmetry directions in the first Brillouin zone $\mathrm{F}(0,0) \to \mathrm{X}(\pi,0) \to \mathrm{M}(\pi,\pi) \to \Gamma(0,0)$ at $\Delta = 2t$ and $T = 0.0088t$ [53]; and (b) the real part of the optical conductivity at two temperatures, $t = 0.25$ eV, $(\xi/a)^{-1} = 0.1$ [54].

At high frequencies (of the order of $\omega \sim U$), together with a Drude peak, a wide maximum appears caused by the electron excitations and by transition of electrons into the upper Hubbard subband. In the insulating phase, the Drude peak disappears, and the conductivity at $\omega = 0$ decreases rapidly with decreasing the correlation length ξ of static fluctuations. This picture of the behavior of $\mathrm{Re}\,\sigma(\omega)$ corresponds to that observed in cuprates.

This approach meets with certain difficulties, most of all in the substantiation of the additivity of $\Sigma(\omega)$ and $\Sigma_k(\omega)$; but this approach is attractive because it allows studying the phenomenon while changing the parameters ξ and Δ that characterize fluctuations in the system, although these parameters themselves are only implicitly determined by the chosen values of the basic model parameters U and n. We note in connection with the above that the DMFT + Σ_k method, which takes spatial fluctuations into account, is a heuristic approach rather than a systematic method of expansion in terms of the parameter $1/d$. In recent years, various proposals have appeared for the introduction of spatial fluctuations into the DMFT scheme, mainly by passing from the lattice problem to the problem for a certain local cluster (rather than a single site) embedded into an effective medium that creates a dynamic mean field acting on this cluster [12]. The question of going beyond the limit $d \to \infty$ and, thereby, of including spatial fluctuations into the DMFT scheme is considered in a number of serious theoretical studies [58, 59], although there is still no complete clarity in this problem. The various new approaches proposed, including those that are entirely microscopic (do not use the phenomenological quantities ξ and Δ), are discussed in [48, 51, 54]. We also mention paper [53] devoted to the extension of the DMFT + Σ_k method to the case where the real band structure of a substance calculated on the LDA basis is taken into account instead of a model Hubbard Hamiltonian being used. This approach was called LDA + DMFT + Σ_k.

In [53], this approach was applied to the compound $Bi_2Ca_2SrCu_2O_8$, which was selected because numerous ARPES data are available for such systems. In [53], the authors considered the specific structure of the $d_{x^2-y^2}$ electron states for Cu ions, which were calculated within the LDA method. The LDA data were used to calculate the basic parameters that determine the low-energy physics of the system, i.e., the matrix elements t, t', ... of the transitions between the nearest and next-to-nearest neighbors, the local Coulomb potential U, and the value of the spin – electron interaction Δ. The calculations were performed for an underdoped compound with $\delta = 0.15$, $\Delta = 0.21$ eV, $\xi = 5\,a$, and $T = 255$ K. The results of calculations of $\rho(\omega)$, $A(k, \omega)$, the Fermi surface, and ARPES spectra confirm the general picture of the pseudogap state and agree well with the experimental data.

The majority of ARPES investigations of cuprates were performed on the Bi2212 system [60]; the results of the first successful studies of LSCO are given in [61]; the results of recent studies are given in [50], where the ARPES spectra of $La_{2-x}Sr_xCuO_4$ were studied in detail in the concentration range $0.03 < x < 0.30$. These experimental results confirmed the evolution of the electron properties with a change in the level of doping described above on the basis of theoretical studies. In the overdoped regime, the system behaves like a Fermi liquid, but in the underdoped regime, all signs of the pseudogap state are revealed at hole concentrations down to $x = 0.03$. The Fermi surface manifests itself on the arcs lying in the direction toward the point (π, π), but a pseudogap state is revealed in the directions toward the points $(0, \pi)$ and $(\pi, 0)$. In a wide range of x, a 'large' Fermi surface (rather than pockets at the boundaries of the magnetic Brillouin zone) is observed; with an increase in the level of doping, it changes from the hole to the electron type. We also note that the ARPES spectra allowed restoring the dispersion curves for the quasiparticle states and determining the transition matrix elements t and t', which agree well with the data of LDA calculations.

The ARPES studies of HTSC cuprates and other SCSs revealed characteristic kinks in the dispersion curves at energies several hundred meV away from the Fermi level. The appearance of kinks is a very common phenomenon in systems with d and f elements. Initially, the kinks were discovered at energies 40 – 70 meV and their appearance was ascribed to the interaction of electrons with collective modes

in the system. Phonons, magnons, and other branches of Bose excitations can serve as such modes. In a recent work [62], it is shown that a strong electron–electron interaction can also generate kinks when a three-peak structure with well-separated Hubbard subbands is formed in the system. These kinks lie inside the quasiparticle spectral peak and separate the region of the Fermi-liquid behavior of the system from the deeper regions (with respect to the Fermi level) located inside the central peak, where the behavior of quasiparticle states differs from the Fermi-liquid behavior. The position of these high-energy kinks thus determines the applicability limits of the Fermi-liquid state for SCSs, which cannot be determined in the framework of the Fermi-liquid theory. The existence of such kinks, which was theoretically predicted in the Hubbard model, must be a characteristic property of SCSs. A detailed bibliography on the ARPES studies of various SCSs in which both low-energy kinks caused by electron interaction with bosons and high-energy kinks appearing due to Coulomb interaction between the electrons is given in [62].

We note that apart from the two above methods (phenomenological and microscopic) of investigation of the pseudogap state, which are based on the DMFT, there is one additional microscopic approach based on Hubbard's idea to include a large Coulomb energy in the zero-approximation Hamiltonian and regard hopping (a specific mode of electron transfer over the lattice) as a perturbation. In the framework of the self-consistent Born approximation (SCBA), this approach allows obtaining an integral equation for the self-energy part of the electron GF $\Sigma(\mathbf{k},\omega)$, which describes the interaction of the strongly correlated (Hubbard) electrons with spin fluctuations in the system [63].

In the SCBA approach, in contrast to the DMFT method, the dependence of self-energy not only on the frequency but also on the momentum is taken into account; however, the SCBA involves an unknown quantity, the dynamic spin susceptibility, for which an equation relating it to the electron GF should be written in order to determine both these quantities self-consistently. This is a very difficult problem, which explains the large popularity of the DMFT, where only the electron GF has to be calculated, although this advantage comes at the expense of ignoring spatial correlations in the system. Therefore, the SCBA method is a very useful supplement to the DMFT method.

In practical work with the SCBA approach, some approximation for the dynamic susceptibilities must be chosen. In [63], the SCBA equations were solved numerically using the following values of the parameters, which, according to the estimates of the authors of that work, correspond to the parameters of real cuprates: $U = 8t$ and $4t$, $t = 0.4$ eV, $t = -0.3t'$, and $\omega_s = 0.4\,t$ (ω_s is the width of the spectrum of spin fluctuations). The calculation was performed for two values of the level of doping ($\delta = 0.05$ and 0.3) and two temperatures ($T = 0.03\,t \approx 140$ K and $T = 0.31t$). The calculated characteristics of the quasiparticle spectrum agree well with the DMFT results for cuprates discussed above. Thus, in the underdoped regime, there arise a pseudogap state in the vicinity of points $(0,\pi)$ and $(\pi,0)$ and quasiparticle states that adjoin the diagonal direction. In the overdoped regime and at high temperatures, quasiparticle peaks in all directions of the Brillouin zone are observed and the system is close to the Fermi-liquid state. The Fermi surface changes its topology with a change in the level of doping.

We note that cuprates are described not by the Hubbard model but by the pd model, and an important parameter of the pd model is the energy of charge transfer $\Delta = \varepsilon_p - \varepsilon_d$ from oxygen to copper. Specifically, Δ plays the role of the effective Coulomb repulsion U at a copper site. In cuprates, Δ is assumed to be of the order of W, which corresponds to the strong-coupling condition $U \approx W$ [63].

6.3 Specific features of the superconducting state

We now consider specific features of the superconducting state in cuprates. Numerous experiments show that in these compounds, the usual Cooper pairing of electrons (holes) in the singlet state is realized, but with a specific spatial symmetry of the wave function of the pair, the so-called d symmetry (see, e.g., [20]). The coordinate and momentum dependence of a Cooper pair in this case are given by

$$\psi(x,y) \sim x^2 - y^2\,, \quad \psi(\mathbf{k}) \sim \cos k_x - \cos k_y\,. \tag{6.2}$$

We note that the d symmetry of pairing in cuprates has no relation to the symmetry of the 3d orbitals of Cu described by the wave function of electrons with the $d_{x^2-y^2}$ symmetry. The d symmetry of pairing in cuprates is determined by the specific nature of the pairing mechanism caused by strong electron correlations. The idea of the correlation mechanism of superconductivity in cuprates was first suggested by Anderson [64], who noted that the HTSC in cuprates occurs near the metal–insulator transition (i.e., at a low level of doping) and is therefore caused not by the electron–phonon mechanism realized in the usual superconductors but by the strong electron–electron interaction.

If we accept the Hubbard model with Hamiltonian (2.3) as a working electron model for cuprates, then we must take into consideration that we must deal with an intermediate case where $U \approx W$, which is most difficult for theoretical analysis. However, we can attempt to approach this case from the side of weak ($U \ll W$) and strong ($U \gg W$) Coulomb interactions, use a perturbation theory in an appropriate small parameter, and then interpolate the results to $U \sim W$. In the case of weak interaction ($U \ll W$), it is possible to use the standard perturbation theory and to derive the Eliashberg equations for a superconductor, in which the kernel is determined by two contributions to the effective interaction of electrons, V_s (through spin fluctuations) and V_c (through charge fluctuations), which can be written as

$$V_s(\mathbf{k},\omega) \sim U^2\chi_s(\mathbf{k},\omega)\,, \quad V_c(\mathbf{k},\omega) \sim U^2\chi_c(\mathbf{k},\omega)\,, \tag{6.3}$$

where $\chi_s(\mathbf{k},\omega)$ and $\chi_c(\mathbf{k},\omega)$ are the dynamic magnetic and dielectric susceptibilities, respectively. A numerical study of the Eliashberg equations shows that they have solutions in the case of the d symmetry of the superconducting gap and the superconducting transition temperature $T_c \sim 10$ K.

In the other limit, $U \gg W$, it is useful to pass from the initial Hamiltonian (2.3) to an effective Hamiltonian, using W/U as a small parameter. Then, we come to the tJ model, which is given by the Hamiltonian

$$H = t\sum_{ij\sigma} \tilde{c}^{+}_{i\sigma}\tilde{c}_{i\sigma} + J\sum_{ij}\left(\mathbf{S}_i\mathbf{S}_j - \frac{n_i n_j}{4}\right), \tag{6.4}$$

where $\mathbf{S}_i$ is the spin operator at a site i, $\tilde{c}^{+}_{i\sigma}$ is the operator of creation of electron with a spin σ at a site i when there is no electron at this site, n_i is the number of electrons at a site i, and $J = 4t^2/U$ is the effective exchange integral for the neighboring sites. Thus, in the limit $U \gg W$, the Hubbard

model reduces to model (6.4), which describes the motion of correlated electrons on a lattice, interacting with each other by means of exchange forces of an antiferromagnetic nature.

To investigate the tJ model, the so-called extended DMFT scheme (EDMFT) was developed in [65]. The extension is needed because in contrast to the Hubbard model, where the Coulomb interaction is local, the tJ model involves the exchange interaction between nearest neighbors. This reduces the problem of motion of a strongly interacting electron on a lattice to the single-impurity Anderson problem, which, besides the interaction of the localized electron with the 'sea' of noninteracting fermions (as in the standard DMFT for the Hubbard model), must also include the interaction of the localized spin with the 'sea' of spin fluctuations. In other words, it is necessary to introduce an auxiliary single-impurity Anderson model in which the localized electron interacts with the fermion and boson degrees of freedom that imitate the dynamic mean field acting on a given d electron from other d electrons strongly interacting with it.

This means that we must simultaneously calculate the electron GF $G(\mathbf{k},\omega)$ and the spin GF $\chi(\mathbf{k},\omega)$, i.e., the dynamic spin susceptibility, and consider them on a general basis. In accordance with the basic idea of the DMFT, when considering the self-energy part of the electron GF $\Sigma(\mathbf{k},\omega)$ and the spin GF $M(\mathbf{k},\omega)$, we should ignore their dependence on the momentum, i.e., proceed from the representations

$$G(\mathbf{k},\omega)=\frac{1}{\omega-\varepsilon_{\mathbf{k}}+\Sigma(\omega)}\,,\quad \chi(\mathbf{q},\omega)=\frac{1}{J_{\mathbf{q}}+M(\omega)}\,, \quad (6.5)$$

where $J_{\mathbf{q}}$ is the Fourier component of the exchange interaction; we recall that $\varepsilon_{\mathbf{k}}$ is the Fourier component of the hopping matrix element. In [65], an intricate EDMFT scheme was developed, which allowed simultaneously calculating $\Sigma(\omega)$ and $M(\omega)$.

We give some results of calculations in [65]. Figure 13 depicts the spectral density of the electron states $A(\omega)$ and the evolution of $A(\omega)$ with the level of doping δ. At all values of δ, a wide incoherent region is observed, which corresponds to the lower Hubbard subband, and a quasiparticle peak on its upper edge, onto which the Fermi level falls. As δ increases, the integrated intensity of the quasiparticle peak increases due to a decrease in the incoherent states, and the system approaches the Fermi-liquid regime. With decreasing δ, traces of the pseudogap state manifest themselves. The width of the pseudogap determines the temperature T^*, which is shown in the inset in Fig. 13 as a function of δ. It is also shown in [65] that the pseudogap in the spin density of states appears at the line $(0,0)-(\pi,\pi)$ as we move away from the point (π,π). A similar behavior of the dynamic magnetic susceptibility is also revealed in cuprates according to the neutron spectroscopy data. The study of the dynamic spin susceptibility [65] in the framework of the tJ model supplements the DMFT results of the study of the electron states of the Hubbard model and explains the low-energy physics of cuprates. The tJ model was recently investigated in the framework of another version of the EDMFT method in [66], where the optical conductivity was studied depending on the temperature and the level of doping.

In [19, 20], the possibility of the appearance of the superconducting state was studied in the framework of the tJ model. The solution of the Eliashberg equations derived for

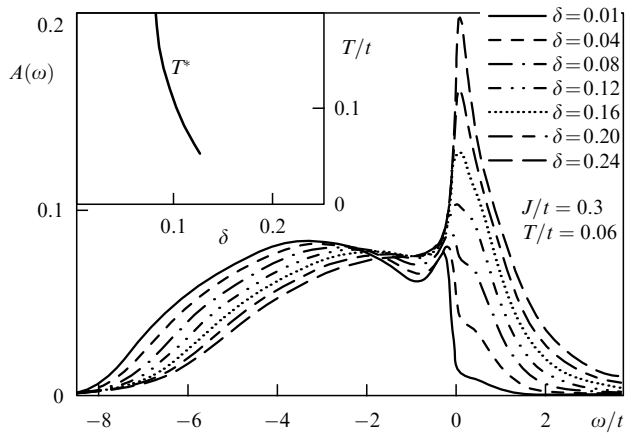

Figure 13. Local spectral density of electrons $A(\omega)$ in the tJ model calculated using the extended DMFT method [65]. The inset displays the dependence of the T^* temperature on the doping level.

Hamiltonian (6.4) showed the possibility of electron pairing with the d symmetry at T_c equal to several dozen degrees kelvin. Thus, the Hubbard model in the two limit cases $U \ll W$ and $U \gg W$ showed the possibility of the appearance of the d-type superconductivity as a result of the action of a spin-fluctuation mechanism caused by the on-site Coulomb repulsion. We also note that T_c depends on the level of doping in approximately the same way as in the experiment. The problem, however, lies in the fact that the values of T_c reaching several dozen degrees kelvins are possible only if $U \sim W$, i.e., in the intermediate case, which is beyond the limits of weak and strong coupling. This means that it is most expedient to proceed from the Hamiltonian of the complete Hubbard model, without assuming the presence of any small parameter.

6.4 Competition between the superconducting and antiferromagnetic states

The microscopic theory of HTSC is not yet completed, and the central issue on the path of its development is the problem of the competition of antiferromagnetic (AF) and superconducting (with the d symmetry) (dSC) order parameters in the Hubbard model with strong electron correlations. The early approaches to this problem are presented in review [67]. In Ref. [68], it was shown using the method of functional renormalization group that for the Hubbard model under the conditions of weak coupling, the leading instabilities are those related to the formation of the AF and dSC order parameters. In Refs [69 – 71], devoted to studying the competition of these parameters under conditions of strong coupling, the authors used the DMFT scheme with one complication: instead of a monatomic impurity center in which strong Coulomb interaction is included, they used a minimum cluster of four neighboring atoms of a square lattice. A necessary condition for the construction of an adequate DMFT when a superconducting state with the d symmetry is considered is the extension of the impurity cluster, because the corresponding order parameter must allow pairing of electrons on neighboring sites as a result of spatial extension of the wave function with the d symmetry. This means that into the initial (one-impurity) version of the DMFT scheme, which ignores spatial fluctuations, we should introduce such fluctuations, although limited by the size of the chosen cluster.

Lichtenstein and Katsnelson [69] derived DMFT equations that involved either the AF or the dSC order parameter. The solution of these equations in the case of a moderate Coulomb repulsion, $U/W = 0.6$, showed that either one order parameter or another can be realized in the Hubbard model; the dependences of these order parameters on the doping level (deviation from $n = 1$) were calculated. The antiferromagnetic order parameter has a maximum at $x = 0$ and vanishes at $x \approx 0.05$. The superconducting order parameter with the d symmetry becomes different from zero immediately at $x > 0$ (i.e., from the beginning of doping) and attains a maximum at $x \approx 0.15$. Such behavior, as well as the maximum values of T_N and T_c, are close to those observed in cuprates, for example, in $La_{2-x}Sr_xCuO_4$; however, the result obtained cannot be considered the resolution of the problem of the competition of these two order parameters, because the case of the coexistence of both order parameters in the same volume has not yet been investigated. This problem was further developed on the basis of the method proposed in [69] in the recent work by Capone and Kotliar [71], who showed that a change in U leads to a sharp change in the nature of the AF and dSC phases. In the limit of strong correlations ($U \geqslant W$), the AF and dSC phases do not mix (there are no solutions of the DMFT equations with both nontrivial order parameters) and a first-order transition between these phases occurs with a change in the level of doping. It thus becomes possible to extend the metastable SC phase to the region of small x. In the region of weak correlations ($U \lesssim W$), a phase of coexistence of both order parameters appears, with the relative weights of the order parameters changing with a change in the level of doping, and the AF component prevails at small U in the mixed state. Recently, analogous results were obtained using the functional renormalization group method [72].

Studying the chemical potential μ as a function of x in the case of strong correlations showed that in the region of the first-order transition between the AF and dSC phases, phase separation can occur, which agrees with the data obtained by other methods. The results in [71] in many respects agree well with the results in [70] obtained by a special variational method.

The authors of fundamental review [73] detail various theoretical approaches to research on the low-energy physics of cuprates. They conclude that the two-dimensional single-band Hubbard model with a moderate Coulomb repulsion U is capable of explaining the basic totality of the properties of these compounds: the specific features of the phase diagram on the (T, n) plane, the dependence of the Néel temperature T_N and the temperature T_c of the superconducting transition with the d symmetry of the order parameter on the doping level, and also the behavior of the spectral density $A(\mathbf{k}, \omega)$ of quasiparticle states, the type of the Fermi surface, and the structure of the pseudogap state. The entire low-energy physics of HTSC compounds is caused by the proximity of the system to the Mott–Hubbard transition into the insulating state; in this case, the electron properties of the system in both the normal and superconducting phase are caused by the interaction of quasiparticles with spin fluctuations, which are well developed in the vicinity of the antiferromagnetic phase. Nonperturbative calculations with the parameter values chosen as $U = 8\,t$, $t = 0.35$ eV, $t' = -0.3\,t$, and $t'' = 0.2\,t$ lead to results that agree well with the experimental data. We note that the above properties are retained in the model upon doping of the system, which corresponds to the band half-filled with both holes and electrons. These successes of the theory became possible due to the creation of nonperturbative methods, of which the most important is the DMFT scheme. Further development of this method is leading to new unexpected results, which reveal the fine special features of the physics of SCSs. One important example is the detection of the fine structure of the spectral density in the Hubbard model at $n = 1$ in the vicinity of the metal–insulator phase transition [73].

Beginning with moderate values $U \approx 6\,t$, two sharp peaks located far from the Hubbard subbands centered at the energies $\mp U/2$ appear in the density of states for the paramagnetic phase at the boundaries of the Mott–Hubbard gap. These peaks lie sufficiently close to those peaks that would appear in the case of an antiferromagnetic long-range order; therefore, the appearance of peaks in the paramagnetic phase should be interpreted as an effect caused by a short-range magnetic order. In this DMFT version, the short-range order is effectively taken into account by the choice of a suitable finite-size cluster, which consists of several atoms embedded in a medium of noninteracting fermions that imitate the dynamic mean field acting on the cluster. The fine structure of the spectrum revealed near the Fermi level leads to the formation of a pseudogap in the weakly doped system in the vicinity of points $(0, \pi)$ and $(\pi, 0)$. The standard DMFT scheme with a monatomic impurity center cannot reproduce the pseudogap state. In Ref. [73], the pseudogap state is obtained within a microscopic model without the phenomenological introduction of the correlation length of spin fluctuations used in [48, 51, 53].

In spite of the significant success of the theory, the problem of the HTSC mechanism in cuprates remains unsolved, because, for example, the role of the phonon pairing mechanism in them is unclear [74, 75]. This mechanism must be investigated under conditions of strong electron–electron interaction. For usual superconductors with their well-known phonon mechanism, the Coulomb repulsion tends to weaken superconductivity: T_c decreases with increasing the Coulomb pseudopotential. In the metallic phase of an SCS near the metal–insulator phase transition, the Coulomb repulsion leads to a strong renormalization of the initial electron band, as we saw from the DMFT data; near the Fermi level, a quasiparticle band with the width ZW appears, where $Z \ll 1$. The small width of the band leads to an increase in the quasiparticle density of states $\rho = \rho_0/Z$ at the Fermi surface, which, it seems, must in turn lead to an increase in the attraction parameter ρV (V is the electron pairing potential). In the Fermi liquid, this potential is renormalized as a result of the decreasing intensity of the quasiparticle peak proportional to the factor Z^2; therefore, the pairing parameter ρV becomes equal to $Z\rho_0 V$, i.e., decreases considerably. However, in the case of strong Coulomb correlation, the character of its influence on pairing through the electron–phonon coupling, as DMFT calculations showed [76], changes radically. This question requires further study.

Although no complete quantitative theory of HTSC cuprates has been constructed so far, the attempts to explain this unique phenomenon, which began already twenty years ago, have strongly advanced the theory of SCSs on the whole and allowed understanding the electronic physics of different materials containing d and f electrons, as we can easily see from examining other classes of SCSs.

7. Manganites

7.1 Crystal and electron structure

Following intensive studies of the HTSC materials of the group of metal-oxide compounds of copper, a true boom arose around the manganites — another class of oxides of transition elements. Of greatest interest here are the compounds of the $La_{1-x}A_xMnO_3$ type, where A is a divalent element (Ca, Ba, Sr, ...). The concentration x of A can be varied within wide limits ($0 \leqslant x \leqslant 1$); the physical properties of manganites change sharply as x changes; the system passes through a chain of phase transitions with various types of ordering: magnetic, structural, electronic.

Great interest in the manganites arose due to the so-called 'colossal' magnetoresistance (CMR). The CMR effect is observed in the range of concentrations where a metallic ferromagnetic phase exists, and it lies in the fact that the resistivity ρ decreases upon the application of a magnetic field. The ratio $\Delta\rho/\rho$ in fields of the order of 1 T can reach about ten percent. The effect reaches a maximum value in the vicinity of the Curie temperature T_C (Fig. 14). This phenomenon is accompanied by various anomalies of physical properties, which have been considered in detail in many reviews (e.g., [77–79]).

One of the remarkable properties of manganites consists in the appearance in them of a metallic ferromagnetic phase in a certain vicinity of the concentration $x \approx 0.3$ (Fig. 15). At smaller concentrations, an insulating phase appears, which is denoted in Fig. 15 as FI (ferromagnetic insulator), or CI (canted antiferromagnetic phase). At high concentrations, an antiferromagnetic insulating (AFI) phase can appear. Thus, the metallic phase is ferromagnetic, and the explanation of the connection between the magnetic and electric states is one of the primary problems of the theory. As can be seen from Fig. 15, with increasing the temperature, the ferromagnetic metallic phase becomes insulating in a certain range of the existence of ferromagnetism; in any case, its conductivity decreases sharply in the vicinity of T_C.

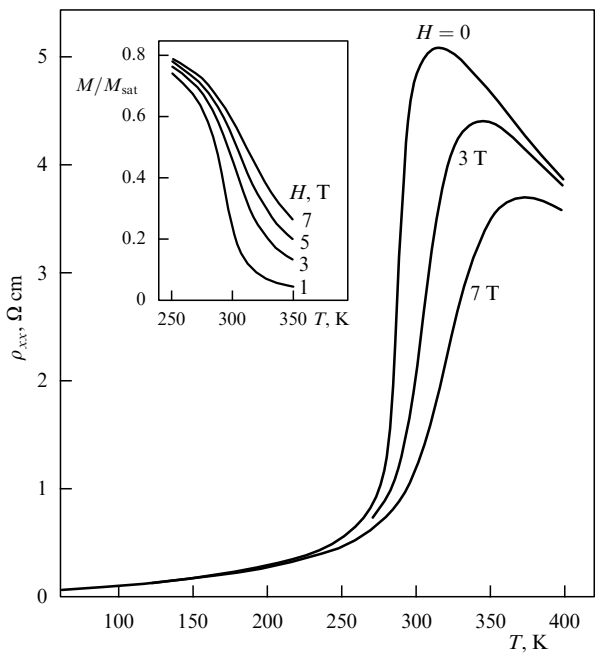

Figure 14. Temperature dependence of the resistance of a single crystal of $La_{2/3}(Pb, Ca)_{1/3}MnO_3$ in different fields H. The inset shows the magnetization in the transitional temperature range [80].

To understand the physical properties of manganites, we should consider their electron structure. The oxides of the $La_{1-x}Ca_xMnO_3$ type can be regarded as mixed-valence compounds, which are solid solutions from the range between $LaMnO_3$ and $CaMnO_3$ with the valence states of the $La^{3+}Mn^{3+}O_3^{2-}$ and $Ca^{2+}Mn^{4+}O_3^{2-}$ ions. The valence structure of the intermediate compound is written as $(La^{3+}_{1-x}Ca^{2+}_x)(Mn^{3+}_{1-x}Mn^{4+}_x)O_3$. Thus, when doping the initial compound $LaMnO_3$ by a divalent element with a concentration $x < 0.5$, holes arise in the 3d band with the same concentration x. At $x > 0.5$, the compound can be regarded as the initial compound $CaMnO_3$ doped with electrons with the electron concentration $1 - x$. Hence, in a mixed-valence manganites, the charge carriers are either holes or electrons in the 3d band [81].

The Mn ions surrounded by octahedra of atoms have the t_{2g} level lying lower than the e_g level; therefore, the Mn^{4+} ion has the configuration t_{2g}^3, and the Mn^{3+} ion has the configuration $t_{2g}^3 e_g^1$. In view of the strong intraatomic Hund coupling, the three electrons at the t_{2g} level produce a localized spin $S = 3/2$; the e_g electron of the Mn^{3+} ion, in view of the same Hund rule, aligns its spin parallel to the localized spin of the ion on which it is located at a given moment; but the e_g electrons are collectivized; therefore, during motion of the e_g electron through the lattice, it is energetically favorable that all localized spins are parallel to each other, i.e., that a ferromagnetic ordering occur. According to this idea, which was suggested many years ago by Zener [82], the kinetic mechanism of magnetic ordering is caused not by the exchange interaction but by electron motion. The ferromagnetic ordering minimizes the kinetic energy.

The above considerations lead us to the sd model specified by Hamiltonian (4.2). In considering manganites, the Hamiltonian should be interpreted as follows: the operators $c_{i\sigma}$ and $c_{i\sigma}^+$ correspond to the collectivized e_g electrons and the matrix element t_{ij} describes hops over the lattice occupied by Mn ions that have a localized spin $S = 3/2$. The intraatomic exchange integral $J \gg W$ must be positive in order to ensure the parallelism of the electron and ion spins. The sd exchange model in which the condition $J \gg W$ is satisfied was called the double exchange (DE) model (not very appropriate but a widespread name).

The physics of manganites is mainly developed on the basis of the DE model. Because of the small parameter W/J, it is possible to pass from Hamiltonian (4.2) to an effective Hamiltonian, which in the limit as $J \to \infty$ describes the motion of spinless fermions on a lattice [83, 84]:

$$H = \sum_{ij} t_{ij}(\theta_{ij})\, \tilde{c}_i^+ \tilde{c}_j\,, \tag{7.1}$$

with an effective hopping matrix element that depends on the angle between the spins located at sites i and j. For the nearest neighbors, we have

$$t(\theta) = t \cos\frac{\theta}{2}\,. \tag{7.2}$$

Results (7.1) and (7.2) were obtained in the limit of the classical spin S, although $S = 3/2$ for manganites. In the ferromagnetic case, $\theta = 0$ and expression (7.1) ensures the

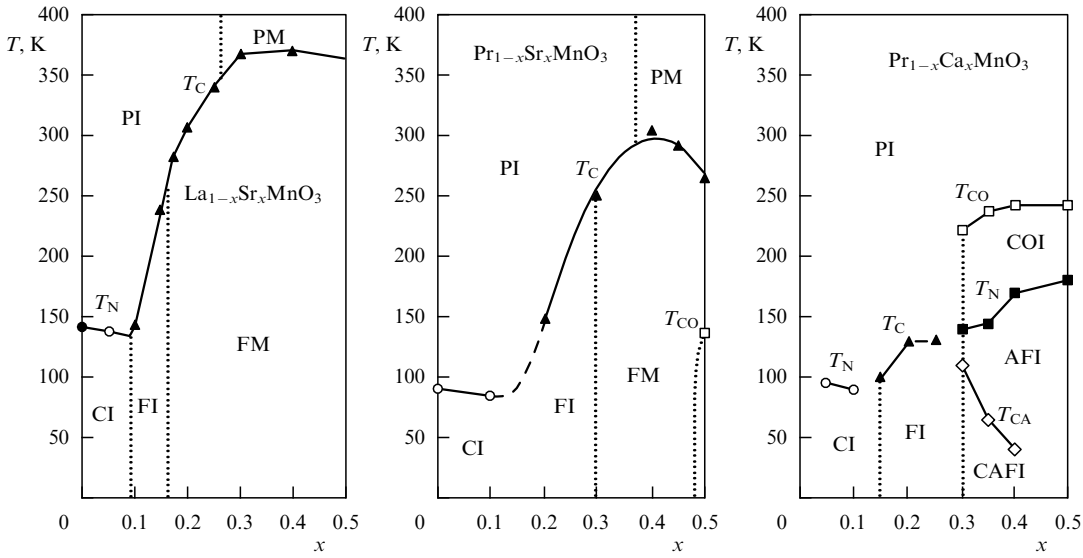

Figure 15. Phase diagrams of materials with the colossal magnetoelectric effect: CI, canted spin state; COT, insulator with charge ordering; PI and FI, paramagnetic and ferromagnetic insulators; FM and PM, ferromagnetic and paramagnetic metals; AFI, antiferromagnetic insulator; CAFI, canted spin insulating state; T_C, T_N, and T_{CO}, temperatures of the ferromagnetic, antiferromagnetic, and charge ordering, respectively; and T_{CA}, temperature of transition to the canted spin state [78].

minimum energy. Hence, it follows that in the paramagnetic state, the electron band must become narrower because the average value of $\cos\theta/2 < 1$ is less than unity.

7.2 Calculation of the electron spectrum in the dynamic mean-field theory

The DE model has become the basic working model for the description of the properties of manganites. To ensure the possibility of a quantitative comparison of the results of theory and experiment, it was necessary to develop methods of dealing with Hamiltonian (4.2) under the conditions of not only the maximally strong but also an intermediate sd exchange coupling ($J \sim W$). Furukawa developed the DMFT method for the sd model with Hamiltonian (4.2), but only for classical spin; the details of the method were presented in a series of works [85–88]. For the classical spin ($S = \infty$), the solution of the auxiliary problem of the single-site center is strongly simplified; therefore, the transport and magnetic characteristics of manganites were already calculated in the first works [85, 86]. It turned out that the resistance implicitly depends on the temperature through the magnetization. The results of numerical calculations at temperatures close to the Curie point corresponded to a quadratic dependence $\rho(M)/\rho(0) = 1 - CM^2$ with the coefficient $C < 4$ for $J \gg W$ and $C = 1$ in the weak-coupling limit ($J \ll W$). The results of calculations of the optical conductivity [86] showed good agreement with the experimental data.

Figure 16 displays the phase diagram of manganites in the (J, n) plane calculated in terms of the Furukawa method at $S = \infty$ [88]. A large region is occupied by the ferromagnetic phase F; at $n = 1$, in a small region that adjoins the straight line $n = 1$, an antiferromagnetic phase (AF) is located; at greater n, a paramagnetic phase P appears. Between the P and F phases, a region PS of phase separation is located, which expands with decreasing J. The existence of this phase is established from the presence of a jump in the dependence of the electron concentration n on the chemical potential μ. This phase diagram was calculated under the assumption that an

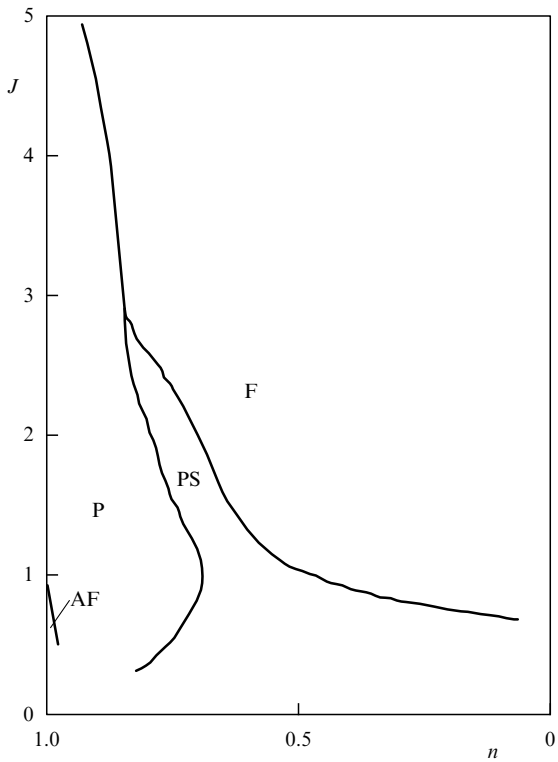

Figure 16. Low-temperature phase diagram of manganites in the plane (J, n) calculated in terms of the DMFT for the classical spin $S = \infty$ [88]. PS stands for the region of phase separation.

AF structure with only two sublattices can be realized in the system. In reality, as n deviates from unity, phases with incommensurate magnetic structures are also realized.

In Ref. [88], the authors also calculated phase diagrams in the quantum case, although for the localized spin $S = 1/2$ (in manganites, $S = 3/2$), which simplifies the calculations. The quantum corrections, which proved to be essential, mani-

fested themselves mainly in a contraction of the ferromagnetic phase region as a result of the increasing regions of the paramagnetic and antiferromagnetic phases. The inhomogeneous PS phase remains within the limits of the boundaries established in the calculation with $S = \infty$. At $S = 3/2$, the role of quantum corrections decreases; therefore, the phase diagram for classical spin can be regarded as a guideline for the phase diagrams of manganites.

The existence of the PS phase in the model with classical spins was also shown in Ref. [89] based on a study of the instability of DMFT solutions under large-amplitude local fluctuations.

The DE model augmented by Coulomb interactions at the same site and at the nearest neighbors was studied in terms of the DMFT [90] in the approximation of the Ising localized spin, where only its S^z component is taken into account. The calculation of transport and thermodynamic properties showed the importance of electron correlations for manganites, in particular, in the range of concentrations $0 \lesssim x \lesssim 0.5$, where the DE model with a quantum spin gives an inadequate behavior of the Curie temperature with decreasing x.

The simplified DE model in which the localized spin is replaced by the Ising spin was used in [21, 90–92] for the investigation of the thermodynamic and transport properties of manganites using the DMFT technique. In this model, it is possible to easily include additional interactions, for example, a diagonal disorder [90–92]. We also note papers [93–95] devoted to theoretical studies of some models of manganites.

A remarkable property of manganites discovered recently is the charge ordering of the Mn^{3+} and Mn^{4+} ions, which occurs in doped systems in the range of the existence of the ferromagnetic phase [96, 97]. The DE model cannot explain this phenomenon, and therefore additional terms must be introduced into the Hamiltonian of the model to account for the chaotic distribution of the Mn^{3+} and Mn^{4+} ions over the lattice sites caused by the chaotic distribution of divalent ions of the doping element. This leads to a chaotic distribution of the Coulomb potential that acts on the collectivized e_g electrons from Mn ions. To describe the ferromagnetic and charge ordering, the following model, at least, must be used [91]:

$$H = t \sum_{ij\sigma} c^{+}_{i\sigma} c_{j\sigma} - J \sum_{i} S^z_i s^z_i + E_w \sum_{i} w_i + V \sum_{i\sigma} n_{i\sigma} w_i \,. \tag{7.3}$$

Here, the first two terms correspond to a simplified DE model in which the exchange interaction of the localized spin with the spin of the e_g electron is approximated by the Ising term with the electron spin $s^z_i = 1/2(n_{i\uparrow} - n_{i\downarrow})$. The third term describes the local variation in the energy upon doping; w_i is a classical variable that takes two values: $w_i = 1$ if a substitution occurs at the site i and $w_i = 0$ for other sites occupied by Mn ions. The last term accounts for the difference between the Coulomb potential at the site occupied by a doping atom and the Coulomb potential at this site occupied by an Mn atom.

The first two terms in the Hamiltonian can be responsible, as we know, for the ferromagnetic ordering in the system; and the last two terms, which depend on the chaotic distribution of dopants over the lattice sites, can be responsible for the charge ordering, which minimizes the Coulomb energy. The total Hamiltonian in (7.3) realizes both tendencies, the magnetic and the charge ordering. This Hamiltonian is very complex, but it allows performing part of the calculations analytically, which leads to the exact solution of the well-known Falicov–Kimball model. Based on passing from the complete DE model to a simplified model, this fact allows an effective application of the DMFT method to model (7.3). The result of the study in [91] was the calculation of the temperatures of charge (T_{CO}) and ferromagnetic (T_C) ordering depending on the electron concentration n. The curves $T_{CO}(n)$ and $T_C(n)$ are similar to each other and have a maximum at $n = 0.5$, but the first curve lies below the second. This means that with decreasing the temperature, the ferromagnetic ordering appears first, to be followed by charge ordering.

7.3 Charge and orbital ordering

It should be kept in mind that some other mechanisms of charge ordering have been suggested, e.g., due to the interaction of e_g electrons with the Jahn–Teller distortions of the octahedral environment of chaotically distributed ions. Among the various types of charge ordering, we first mention the stripe structures initially discovered in HTSC compounds (see review [98]); in manganites, they exist in the insulating phase. The stripe structures represent alternating chains of Mn^{3+} and Mn^{4+} ions consisting of identical ions arranged into the sequence $Mn^{3+} - Mn^{4+} - Mn^{3+}$. Their formation is apparently due to elastic interactions caused by the Jahn–Teller distortions of the environments of the Mn^{3+} ions. Repulsive forces apparently exist between such stripes formed by three chains, preventing them from adhering to each other.

In manganites, orbital ordering is also observed in addition to the spin and charge ordering; all these three forms of ordering are usually closely related. They are shown schematically in Fig. 17, which displays such structures observed in many manganites at $x \approx 0.5$. Figure 17 depicts ordering of e_g orbitals of the $d_{3z^2-r^2}$ type.

Until now, in describing the fundamental features of the physics of manganites, we ignored the orbital degeneracy of Mn ions in them. But the importance of the orbital degeneracy of ions in the magnetic insulating compounds of

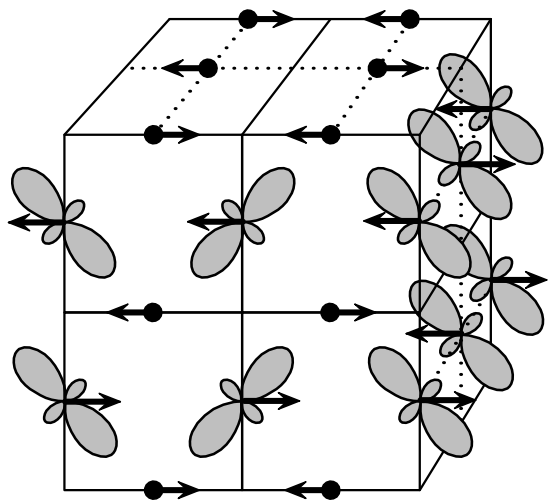

Figure 17. Spin, charge, and orbital ordering observed in the majority of manganites at $x = 1/2$ [81].

transition elements has already long been recognized. Anderson [99] first showed that the kinetic exchange between magnetic ions depends on the symmetry of the trivalent degenerate orbitals and the crystal lattice geometry. The complete theory of kinetic exchange in insulating crystals with Jahn–Teller ions was developed by Kugel' and Khomskii [100], who proceeded from the Hubbard model with the intraatomic exchange interactions additionally taken into account. It turned out that in such crystals, the spin and orbital degrees of freedom closely interact with each other even in the absence of the spin–orbit interaction in the ions, which is primarily manifested precisely in the orbital ordering. The two types of ordering substantially influence each other, and the theory allows predicting the type of one ordering if the type of the other is known.

Because insulators of this type are parent substances for metallic (doped) manganites, these ideas were extended to the double exchange model, which in the general case describes metallic systems [101]. Taking the orbital degeneracy into account allows, for example, explaining the asymmetry of the phase diagram for the $La_{1-x}Sr_xMnO_3$ system, which looks different for of $x \leqslant 0.5$ and $x > 0.5$, although it should be symmetric from the standpoint of the electron–hole symmetry of the Hamiltonian of the non-degenerate DE model.

We note in conclusion that although the DE model qualitatively correctly describes many properties of manganites, it does not ensure quantitative agreement with the results of experiments. The authors of [102] therefore concluded that the DE model must be augmented by lattice degrees of freedom in order to be considered a base model for this class of compounds. Various aspects of the role of lattices in the formation of the electric and magnetic properties of manganites can be found in reviews [21, 103].

It is instructive to compare two oxide classes of SCSs, cuprates and manganites. These two classes have much in common. The compounds of both classes have a perovskite structure. The initial compounds in both cases are antiferromagnetic insulators. The physics of electrons in them is determined by Mn or Cu ions surrounded by oxygen ligands. The substitution of a trivalent element by a divalent one leads to the appearance of holes in the system of Mn ions in the manganites or in the system of Cu ions in the cuprates. These holes are charge carriers in both cases. Here, however, the similarity of these two oxide classes ends, because the interactions in these systems are different: a strong sd exchange in the first case and a strong on-site Coulomb interaction in the second. Because of this difference, different phenomena occur in these compounds: CMR in the manganites and HTSC in the cuprates, which are not connected with each other.

Although the main interactions in manganites and cuprates are different, they frequently exhibit common physical phenomena, for example, phase separation and the appearance of special types of charge ordering in the form of a striped structure. Apparently, this is a general manifestation of strong electron correlations in both systems.

7.4 Ferromagnetic half-metals

One more question to be discussed in relation to the physics of manganites is the structure of the electron spectrum of metallic ferromagnetic phases depending on the electron spin σ. In the case of a classical localized spin and the extremely large sd exchange parameter $J \gg W$, an analytic expression for the electron GF can be obtained as [86],

$$G_\sigma(\mathbf{k},\omega) = \frac{P_\sigma^+}{\omega + J + \mu - P_\sigma^+ \varepsilon_k + \mathrm{i} P_\sigma^- W} + \frac{P_\sigma^-}{\omega - J + \mu - P_\sigma^- \varepsilon_k + \mathrm{i} P_\sigma^+ W}, \tag{7.4}$$

where $P_\sigma^\pm = (1 \pm M\sigma)/2$ and M is the spontaneous magnetic moment in the system of localized spins. Expression (7.4) describes two bands of single-particle states with a given spin σ, which are centered at the energies $\omega + \mu = \mp J$ and are characterized by the damping $P_\sigma^\mp W$. The relative weights $P_\sigma^\pm$ of these bands depend on the orientation of the electron spin with respect to the spontaneous moment. In the ground state ($M = 1$) for the spin $\sigma = \uparrow$, we have $P_\uparrow^+ = 1$ and $P_\uparrow^- = 0$; therefore, the spin states fill the lower band, while the upper band is empty. At the other spin orientation ($\sigma = \downarrow$), the lower band is empty. This means that in the ground state, all electrons are polarized in the direction of the spontaneous magnetic moment, and no electrons with the opposite spin are present. This substance was called a ferromagnetic half-metal. With increasing the temperature, states with the opposite spin in each of the bands appear, and the system ceases to be a saturated ferromagnet.

The half-metallic ferromagnets can arise not only in systems described by the sd model but also in systems with strong Coulomb correlations, which are described, for example, by the Hubbard model [104]. Such systems are exemplified by CrO_{2r}, or Heusler alloys such as Co_2MnZ, RMnSb, in which the half-metallic state can be experimentally established with the help of photoemission spectroscopy or tunneling microscopy with polarized electrons. The ferromagnetic half-metals are promising materials for spintronics, which deals with spin-dependent electron transport.

8. Compounds based on f elements

8.1 Heavy fermions

Among the extensive classes of systems that contain 4f and 5f elements, of special interest are systems with heavy fermions (HFs), which have unique physical properties (see reviews [105–109]). The low-temperature electron heat capacity and magnetic susceptibility in many of them is several hundred times greater than the appropriate values for usual metals; because in the simplest models of metals with weakly interacting electrons, both quantities are proportional to the effective mass of charge carriers, these anomalous substances were called HF systems. Among the first systems of this type, alloys that contain U and Ce, such as $CeAl_3$, CeCu6, UBe_{13}, and UPt_3, were studied. Later, the class of HF materials broadened rapidly and other unique properties were discovered in them, drawing the attention of many researchers, both experimenters and theorists.

It turned out that at high temperatures, these substances behave as systems with weakly interacting localized magnetic moments of f electron shells and conduction electrons with ordinary masses. At low temperatures, the magnetic moments of f electrons begin strongly interacting with conduction electrons and with themselves. Just in this case the phenomenon of heavy fermions occurs. To this remarkable phenomenon, another one is frequently added: a transition from the metallic into the insulating state is possible at low temperatures. Such substances were called 'Kondo insulators' for the reason that is to become clear in what follows. Typical

representatives of the compounds of this class are $Ce_3Bi_4Pt_3$, CeNiSn, SmB_6, TmSe, $YbBi_2$, and UNiSn.

The most important question that relates to the entire extensive class of heavy-fermion compounds is whether they are usual Fermi liquids with properties predicted by the Landau theory. For some HF systems, such as UPt_3, the totality of the experimental measurements of heat capacity, electric resistance, and the de Haas – van Alphen effect indicates that they can be described by the Landau theory with renormalized Fermi-liquid parameters. The Fermi-liquid picture implies the existence of a well-defined Fermi surface and a steplike electron-momentum distribution function $f(\varepsilon_{\mathbf{k}})$, as well as the existence of quasiparticle damping described by the relation $\gamma(\omega) \sim \omega^2 + T^2$ at low energies ω (referenced to the Fermi level) and low temperatures (much lower than the Fermi energy ε_F).

But this picture of quasiparticle excitations was found to be violated in many HF systems discovered later (see review [108] and the references therein), such as $UCu_{5-x}Pd_x$ ($x = 1$ and 1.5), $CeCu_{5.9}Au_{0.1}$, $Th_{1-x}U_xRu_2Si_2$ ($x < 0.07$), and $U_{1-x}Th_xPd_2Al_3$ ($x > 0.4$). These systems exhibit $C_v(T)$, $\chi(T)$, and $\rho(T)$ temperature dependences that differ from those predicted by the Fermi-liquid theory. A typically non-Fermi-liquid behavior in HF systems is manifested in the divergence of the linear coefficient in heat capacity $C_v(T)$, a strong temperature dependence of $\chi(T)$ as $T \to 0$, and a specific temperature dependence of the electric resistivity $\rho(T)$.

The magnetic properties of these systems are very uncommon and diverse, which is expressed, most of all, in how the localized magnetic moments themselves are revealed in them. In a number of systems, the atomic magnetic moments of f shells are conserved in the alloy or in the compound; in such systems, some features of the Kondo effect frequently manifest themselves, in particular, as is well known, in dilute alloys of magnetic atoms in a usual metal. In other cases, the magnetic moments of f shells strongly differ from integer values as a result of a hybridization of f electrons with conduction electrons. Such systems were called mixed-valence systems. The complete suppression of localized magnetic moments is also possible. At low temperatures, different types of magnetic ordering frequently appear.

Remarkably, the electric and magnetic properties of HF systems, including the appearance of a long-range magnetic order in them, are closely related to each other, and it is frequently difficult to identify the basic mechanism responsible for the formation of the totality of their physical properties: either the formation of a narrow quasiparticle peak near the Fermi surface corresponding to charge carriers with large effective masses and, as a result, the appearance of anomalies in the magnetic properties, in particular, the appearance of a magnetic order; or, on the contrary, the appearance of a magnetic order and, as a result, a change in the electron states of the system, including alterations in the Fermi-liquid picture. Examples of HF compounds whose properties are connected with the appearance of magnetic ordering are given by U_2Zn_{17} and UCu_5, which are antiferromagnets with the respective Néel temperatures $T_N = 9.7$ and 15 K.

8.2 The Kondo effect and the single-impurity Anderson model

We have seen that the physics of HF systems is very rich in anomalies of different physical properties, but two questions are apparently crucial for the understanding of the entire picture of the phenomena observed. The first is: What factors are responsible for the formation of a quasiparticle spectrum near the Fermi surface with large effective masses of charge carriers? And the second is: Due to what factors is a small energy scale (temperature T_0) formed that separates the high-temperature metallic region with the usual properties of charge carriers from the low-temperature region where the strong interaction of the localized moments with the conduction electrons manifests itself and signatures of an insulating state appear? It became clear quite soon after the discovery of HF systems that the answers to these questions should be sought on the basis of two well-known phenomena: the hybridization of localized f electrons with conduction electrons and the Kondo effect, i.e., the appearance of a resonance peak in the density of states at the Fermi level as a result of electron scattering on the localized moments of impurity centers, which is accompanied by spin flip. Both phenomena are described well in the framework of the sd exchange model [Hamiltonian (4.2)] and the single-impurity Anderson model, which were proposed and studied in detail long before the discovery of HF systems. In connection with the discovery of such systems, the periodic Anderson model (PAM) became topical, which is the basic model for the HF systems [Hamiltonian (4.1)].

We first examine the single-impurity sf model and the single-impurity Anderson model; their Hamiltonians can be written as

$$H = \sum_{k\sigma} \varepsilon_k f^+_{k\sigma} f_{k\sigma} - J \sum_{kk'\sigma_1\sigma_2} (\mathbf{S}\mathbf{s}_{\sigma_1\sigma_2}) f^+_{k\sigma_1} f_{k'\sigma_2}\,, \tag{8.1}$$

$$H = \sum_{k\sigma} \varepsilon_k c^+_{k\sigma} c_{k\sigma} + \varepsilon_f \sum_{\sigma} f^+_{\sigma} f_{\sigma} + U n_{f\uparrow} n_{f\downarrow} + V \sum_{k\sigma} (c^+_{k\sigma} f_{\sigma} + f^+_{\sigma} c_{k\sigma})\,. \tag{8.2}$$

The single-impurity sf model deals with a single localized spin embedded in the 'sea' of collectivized noninteracting electrons with a dispersion law $\varepsilon_{\mathbf{k}}$. In the single-impurity Anderson model, we consider a single localized f level imbedded in the 'sea' of s electrons (which do not interact between themselves but allow hybridization with f-level electrons) and of f electrons (which interact with each other if they are at the same site).

The most dramatic phenomenon described in the framework of the single-impurity sf model is the Kondo effect, i.e., the appearance of a narrow resonance peak in the density of states at the Fermi surface (Suhl – Abrikosov resonance) in the case of an antiferromagnetic exchange coupling ($J < 0$). The width of this peak is determined by the so-called Kondo temperature (see, e.g., [110])

$$T_K = W \exp\left(-\frac{1}{|J|\rho}\right), \tag{8.3}$$

where ρ is the density of states at the Fermi level. The quantity T_K is the only energy scale that characterizes the entire low-energy physics of the sf model. The main thermodynamic and dynamic properties of the model (the heat capacity, magnetic susceptibility, etc.) depend on the ratio T/T_K; the system therefore has scaling properties. The T_K temperature divides the temperature interval into two regions: at $T < T_K$, the impurity spin is screened by the electron spin cloud such that

if the value of the localized spin is $S = 1/2$, then the effective spin at the impurity site is equal to zero. This phenomenon (Kondo screening) amounts to the formation of a bound state of the impurity spin with the spin cloud of conduction electrons; the value of T_K is the measure of the binding energy of this state.

Because the Hamiltonian of the Anderson model depends on several parameters (W, ε_f, U, V), the behavior of the model is much more complex than that of the single-impurity sf model. Two basic regimes should be distinguished: that of a localized magnetic moment and the intermediate-valence regime. Figure 18 depicts both these regimes, which differ in the position of the f level relative to the Fermi level and the conduction band. In the first case, the atomic level ε_f is below the conduction band and the second atomic level $\varepsilon_f + U$ is above it. Thus, the lower level is always filled and the upper level is empty, and therefore the atom carries a localized moment. In the second case, part of the f states are above the Fermi level because of the strong hybridization of f electrons with the conduction electrons, and the impurity site carries a noninteger magnetic moment (intermediate valence).

Furthermore, one more special case should be noted, the symmetric Anderson model characterized by the following relation between the energies of two f levels: $\varepsilon_F - \varepsilon_f = (\varepsilon_f + U) - \varepsilon_F$; both levels are therefore separated by identical energy intervals from the Fermi level. In this case, the excitation of a hole in f states requires the same energy as the excitation of a particle. If the energy is referenced to the Fermi level ($\varepsilon_F = 0$), the last relation becomes $2\varepsilon_f + U = 0$. In the case of the symmetric model, all the expressions are simplified.

Shrieffer and Wolff [39] showed that under certain conditions, the Anderson model is equivalent to the sf model in which the charge degrees of freedom in the f-electron system are absent (frozen), but there are on-site localized moments. These conditions are apparently realized when the Fermi level lies between two split levels $\varepsilon_\alpha = \varepsilon_f$ ($\alpha = 1$) and $\varepsilon_\alpha = \varepsilon_f + U$ ($\alpha = 2$) of the atomic f states corresponding to the presence of one and two electrons at the impurity site. In this situation, if the average number of f electrons is $\langle n_{f\sigma} \rangle \approx 1$, Hamiltonian (8.2) can be reduced by a canonical transformation to form (8.1) with the effective exchange integral [39]

$$J = -2\,|\,V\,|^2 \frac{U}{|\,\varepsilon_f\,||\,\varepsilon_f + U\,|} < 0\,. \tag{8.4}$$

In the Kondo regime, the Anderson model therefore reduces to the sf model, and a common energy parameter T_K appears, determined by formula (8.3) if we substitute expression (8.4) for the sf exchange integral into it. Consequently, the energy parameters ε_f, U, V, and W are 'absorbed' into a single parameter T_K, which then determines the low-energy physics of the Anderson model, similar to the Kondo temperature in the sf model.

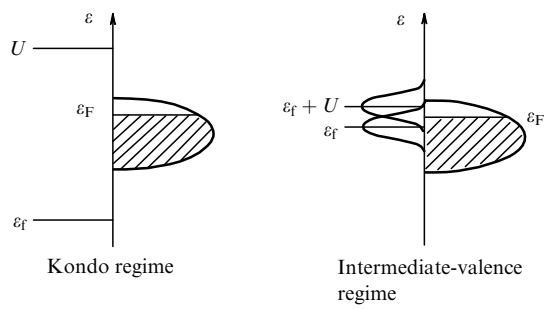

Figure 18. Localized-magnetic-moment regime (Kondo regime) and the intermediate-valence regime in the Anderson model.

8.3 The Kondo lattice and the periodic Anderson model

We now consider the lattice models [the sd model, or the Kondo lattice model (KLM), and the periodic Anderson model (PAM)]. The most reliable information about the structure of the electron spectra in these models was recently obtained in the DMFT framework. We begin with the simpler (KLM) model. When considering manganites, we already mentioned the application of the DMFT scheme to the KLM, in which the localized spins were considered classical unit-length vectors. These studies, in particular, allowed obtaining a phase diagram in the (J, n) plane in this model. Now, we discuss the results of a detailed study of the quasiparticle spectrum in the KLM with a quantum localized spin $S = 1/2$. The DMFT calculations performed at a fixed value $J/W = 0.15$ and different electron concentrations n from the range $0.9 > n > 0.4$ showed that two energy scales, T_0 and T^*, exist in the system [111]. The high-temperature scale T^* is close to the Kondo temperature T_K for the single-impurity model and is independent of n, but the low-temperature scale T_0 is substantially lower than T^* if n deviates from the value $n = 1$ at which T_0 and T^* have an identical scale. As n decreases, the temperature T_0 decreases sharply, with $T_0 \approx 10^{-3}\,W/k$ at $n = 0.9$ and $T_0 \approx 10^{-5}\,W/k$ at $n \sim 0.4$. The parameter T_0 is determined from the position of the narrow Suhl–Abrikosov quasiparticle resonance near the Fermi level, and T^* from the width of the pseudogap in the electron spectrum.

The quantities T_0 and T^* characterize the bounds within which the physical properties of the system vary with a change in the temperature. At $T > T^*$, the system behaves as an ensemble of independent impurities described by the single-impurity Anderson model; in this case, $T^* \approx T_K$ corresponds to the beginning of the formation of Kondo singlets. For temperatures $T < T^*$, a coherent state appears, a Fermi liquid with no localized magnetic moments. In a sense, this situation resembles the one that is characteristic of superconductors, where the Cooper pairs can be formed locally at temperatures exceeding T_c, but a coherent state of Cooper pairs, which manifests itself in the appearance of superconductivity, occurs only at $T < T_c$.

We note that at low temperatures, the properties of the KLM are scaled, i.e., depend on temperature through the ratio T/T_0 as the temperature changes up to $T \approx 10T_0$. For example, such a behavior is characteristic of the intensity of the quasiparticle peak as the temperature increases from 0 to $\approx 10T_0$. These two energy scales manifest themselves also in the presence of two maxima in the temperature dependence of the spectral density of the calculated spin fluctuations, and also in the calculated intensities of the ARPES spectra for two KLM lattices, $YbInCu_4$ and $YbAgCu_4$; we note that good agreement with the experimental data is observed in this case. We note that the conclusion about the existence of two energy scales at low electron concentrations in the KLM was made earlier in [112, 113].

We next turn to a more complex model, the PAM. The physics of the PAM, naturally, must rest on the results of the investigation of the single-impurity Anderson model (frequently called SIAM, a term convenient for comparing

single-impurity and periodic models). In spite of the great progress in studying the SIAM, the study of the PAM encountered significant difficulties, which were partly overcome only in the last decade due to the use of powerful computational methods, first and foremost, the DMFT methods. The 'analytic' period of the study of the PAM is characterized by the use of perturbation-theory methods of various types. Initially, intensive PAM studies were conducted with the help of the perturbation theory through the second order in U. In the Kondo regime with the small parameters such as T/U and $T/|\varepsilon_{\rm d}|$, effective Hamiltonians were obtained in which the sf hybridization was excluded and, as a result, terms that describe the indirect interaction of the localized spins appeared. This allowed investigating the possible magnetically ordered phases. In the intermediate-valence regime, effects of interaction of spin and charge degrees of freedom were studied. Studies of the structure of the quasiparticle spectrum and its evolution with a change in the parameters of the Hamiltonian required the use of nonperturbative methods.

The fundamental feature of the PAM — the existence of a characteristic energy scale similar to the Kondo temperature $T_{\rm K}$ in the SIAM — was revealed by Rice and Ueda [114], who used one such nonperturbative approach, the variational Gutzwiller method. In the Anderson model (in both the SIAM and the PAM), the number of f electrons is not conserved because of their mixing with the conduction electrons. This leads to the appearance of two variational parameters, the average number $\langle n_{\rm f}\rangle$ of f electrons at a site and the average number of doubly filled f states $D = \langle n_\uparrow n_\downarrow\rangle$. Obtaining the effective Hamiltonian of the PAM at large Coulomb interactions requires using Gutzwiller's idea (initially used in the Hubbard model) that the PAM Hamiltonian is to be projected onto the space of states that contain no doubly filled f states on the sites. This leads to the effective Hamiltonian

$$H_{\rm eff} = \sum_{\mathbf{k}\sigma} \varepsilon_{\mathbf{k}} c^+_{\mathbf{k}\sigma} c_{\mathbf{k}\sigma} + \varepsilon_{\rm d} \sum_{i\sigma} n^{\rm d}_{i\sigma} + \sum_{i\sigma} \widetilde{V}_\sigma (c^+_{i\sigma} f_{i\sigma} + c_{i\sigma} f^+_{i\sigma}) , \tag{8.5}$$

which does not involve the on-site Coulomb interaction of f electrons but contains a renormalized hybridization parameter depending on the average filling of sites by one-electron states:

$$\widetilde{V}_\sigma = \sqrt{q_\sigma}\, V . \tag{8.6}$$

The normalization parameter q_σ in the limit as $U \to \infty$ depends on the filling of f states; in the paramagnetic case, we have

$$q_\sigma = q \sim \left(1 - \langle n^{\rm f}\rangle\right) . \tag{8.7}$$

In the symmetric case $\left(2\varepsilon_{\rm f} + U = 0,\, n = 2,\, \langle n^{\rm f}\rangle = 1\right)$, the Fermi level falls into the hybridization gap and the system is insulating at $T = 0$ (a Kondo insulator). The hybridization-induced reduction in the energy per lattice site relative to the energy of the metallic phase is $\delta E = -kT^*$, where

$$kT^* = W \exp\left(-\frac{1}{4J\rho}\right) . \tag{8.8}$$

Thus, the reduction of energy caused by hybridization in the PAM has the same Kondo form as that in the SIAM but involves the factor 1/2 in the exponent. We see that the energy scale for the Anderson lattice is substantially greater than that for the single-impurity model. This analytic result is to be refined in the numerical approaches to the PAM theory presented below.

It follows from effective Hamiltonian (8.5) that in the second-order perturbation in hybridization, the transfer of f electrons through the lattice can occur, which leads to the appearance of an effective band of carriers with the width

$$W^{\rm f}_{\rm eff} \sim |\widetilde{V}_\sigma|^2 \sim q_\sigma \sim \left(1 - \langle n^{\rm f}\rangle\right) . \tag{8.9}$$

The narrow band arising in the system of strongly correlated f electrons near the half filling of the localized f states corresponds to charge carriers with the large effective mass

$$\frac{m^*}{m} \sim (W^{\rm f}_{\rm eff})^{-1} \sim \frac{T_{\rm F}}{T^*} , \tag{8.10}$$

where $T_{\rm F}$ is the Fermi temperature. These carriers correspond to heavy fermions revealed in a number of rare-earth and actinide compounds. Together with relation (8.10), there is a relation between the density of f states at the Fermi level $\rho_{\rm f}(\varepsilon_{\rm F})$ and the density of states $\rho(\varepsilon_{\rm F})$ in the conduction band,

$$\rho_{\rm f}(\varepsilon_{\rm F}) \approx \rho(\varepsilon_{\rm F})\, \frac{T_{\rm F}}{T^*} . \tag{8.11}$$

Relation (8.11) reflects the presence of a very sharp and high peak of quasiparticle states near the Fermi level.

The simplest explanation of the appearance of such carriers is that at $\langle n^{\rm f}\rangle \approx 1$, there are only a few holes (and twos, i.e., doubly occupied states) to (or from) which an f electron can pass while 'wandering' over the lattice. Because the band of f carriers arises near the Fermi level, which is formed by all conduction electrons and f electrons, and because it is characterized by a high density of states, it is clear that the f electrons prevail on the Fermi surface. The structure of the electron states in the PAM in the Kondo regime revealed on the basis of analytic calculations is responsible for the heavy-fermion physics [114]. On scales that considerably exceed kT^*, there exist wider peaks of quasiparticle states, which lie near the atomic levels $\varepsilon_{\rm f}$ and $\varepsilon_{\rm f} + U$. Such quasiparticle states correspond to the generation of a hole at the lower level and an electron – hole pair on the upper level.

These conclusions were confirmed in other analytic approaches to the Kondo and Anderson lattices, most of all in the approach with the use of the method of slave bosons (auxiliary bosons) and of the $1/N$-expansion method, where N is the number of degenerate orbitals for f electrons. These approaches are of great interest because they allow obtaining systematic corrections to the zeroth approximation, which is the mean-field approximation.

8.4 Investigation of the periodic Anderson model using the dynamic mean-field theory

A detailed study of the PAM using the DMFT and QMC methods for calculating the auxiliary single-impurity Anderson model was carried out by Jarrel [115] for the symmetric PAM, where

$$\varepsilon_{\rm F} = -\frac{U}{2} , \quad \langle n^{\rm f}\rangle = 1 , \quad \langle n^{\rm s}\rangle = 1 . \tag{8.12}$$

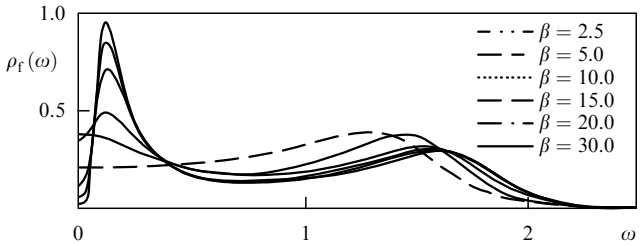

Figure 19. Temperature dependence of the density of states of f electrons $\rho_f(\omega)$ calculated in the DMFT terms at the parameter values $V = 0.5$, $U = 2$, $T^* = 0.23$, and $\beta = 1/kT$ [115].

This means that the Fermi level falls into the middle of the bare s band and that there is one electron per site. Then, at $T = 0$, gaps appear in the quasiparticle spectrum and in the spectra of collective charge and spin excitations. Figure 19 shows the variation in the density of quasiparticle states as a function of temperature. At high temperatures greater than a certain characteristic value T^*, $\rho_f(\omega)$ is a relatively smooth function of frequency. As the temperature decreases ($T < T^*$), a distinct maximum is formed, and $\rho_f(\omega)$ at small ω rapidly decreases to zero as $T \to 0$; i.e., a gap in the spectrum appears at $T = 0$. Because the energy is referenced to the value of the chemical potential, the system becomes insulating at $T = 0$ (a Kondo insulator). The appearance of a peak in $\rho_f(\omega)$ is caused by the resonance Kondo scattering of electrons by localized moments, and the position of this peak should be connected with the Kondo temperature in the PAM. In Fig. 19, $T^* = 0.23$ (in W units); in this case, the width of the gap in the spectrum is $\Delta \approx 0.5\,T^*$. The calculation of the dynamic magnetic (χ_s) and charge (χ_c) susceptibilities shows that they also have gaps, which are twice as wide in magnitude as those in the single-particle spectrum, $\Delta_s = \Delta_c \approx 2\Delta \sim T^*$.

Thus, an energy scale T^* analogous to the Kondo temperature T_K in the single-impurity Anderson model appears in the PAM. A comparison of the calculated values of T^* and T_K shows that T_K is less than T^*, in accordance with the prediction in [114].

The above results were obtained using the QMC method for the numerical calculation of the single-impurity model. In another fundamental work [116], the authors used the NFG method in the DMFT approach for the numerical calculation of the single-impurity model.

The calculations of the frequency dependence of the self-energy $\Sigma(\omega)$ allow obtaining the density of quasiparticle f states in the vicinity of the Fermi level $\Sigma(\omega)$:

$$Z_f^{-1} = 1 - \left.\frac{\mathrm{d}\,\mathrm{Re}\,\Sigma_f(\omega)}{\mathrm{d}\omega}\right|_{\omega=0} \equiv \frac{m^*}{m}\,, \tag{8.13}$$

where the effective quasiparticle mass m^* is introduced, which turns out to be considerably greater than the electron mass m. A comparison of the effective masses m^* calculated with the same values of the parameters ($U = 2$, $V^2 = 0.2$) in the symmetric case for the two models, the PAM and the SIAM, shows that m^*_{PAM} is considerably less than m^*_{SIAM}. The results of numerical calculations are in good agreement with the analytic dependence $m^*_{\mathrm{PAM}}/m^*_{\mathrm{SIAM}} \sim \exp(-1/|J|\rho)$. This indicates an exponential increase in the energy scale T^* in the PAM relative to the scale T_K for the SIAM, which was revealed by analytic methods in [114].

In Ref. [116], the authors investigated the electron spectrum of the PAM not only near the half filling of the conduction band ($n_s = 1$) but also at small electron concentrations. At $n_s = 1$, the energy scale T_0 is of the order of the Kondo temperature T_K, although T_0 exceeds T_K; with a decrease in n_s, T_0 decreases strongly, and at $n_s = 0.2$ the ratio T_0/T_K decreases by two orders of magnitude relative to that observed at $n_s = 0.8$. This result agrees with the results of earlier studies of the PAM [117] and with the result of the study of the KLM [111, 113] presented in Section 8.3. We note that the appearance of two energy scales in the PAM and the KLM at small concentrations of conduction electrons was predicted in [112]. The results of DMFT calculations [111, 113] agree with these predictions only qualitatively, thus confirming the physics of the PAM and KLM systems with a low electron density, which is responsible for these phenomena. According to the arguments in [112], at low concentrations $n_s \ll 1$, the number of electrons is insufficient to screen all magnetic moments localized at the lattice sites; therefore, the behavior of the system is expected to be completely different from its behavior in the case of $n_s \approx 1$, when all the moments can be screened.

The last basic research of the electron structure of the PAM was performed by the DMFT + NRG method in [118] in connection with the study of the transport properties of the f system. We consider the formulation of DMFT equations for the PAM described by Hamiltonian (4.1) in more detail. The Green's functions of conduction electrons $G(\mathbf{k},\omega)$ and the Green's function of f electrons $F(\mathbf{k},\omega)$ are expressed through the self-energy part of $\Sigma(\mathbf{k},\omega)$ for correlated f electrons by the exact equations [118]

$$G(\mathbf{k},\omega) = \left[\omega - \varepsilon_{\mathbf{k}} - \frac{|V|^2}{\omega - \varepsilon_{\mathbf{k}} - \Sigma(\mathbf{k},\omega)}\right]^{-1}, \tag{8.14}$$

$$F(\mathbf{k},\omega) = \left[\omega - \varepsilon_{\mathbf{f}} - \Sigma(\mathbf{k},\omega) - \frac{|V|^2}{\omega - \varepsilon_{\mathbf{k}}}\right]^{-1}. \tag{8.15}$$

In accordance with the general idea of the DMFT, we assume that $\Sigma(\mathbf{k},\omega)$ is independent of the momentum k and is a function of only the frequency $\Sigma(\omega)$. We introduce the diagonal matrix element of GF (8.15) with respect to the site indices,

$$F(\omega) = \sum_{\mathbf{k}} F(\mathbf{k},\omega)\,, \tag{8.16}$$

and assume that $F(\omega)$ coincides with the GF $F_{\mathrm{loc}}(\omega)$ of the single-impurity Anderson model, which can be written as

$$F_{\mathrm{loc}}(\omega) = \frac{1}{\omega - \varepsilon_f - \Delta(\omega) - \Sigma(\omega)}\,, \tag{8.17}$$

where $\Sigma(\omega)$ is the same self-energy part that determines the GF of f electrons in the PAM and $\Delta(\omega)$ is the hybridization function. The GF $F_{\mathrm{loc}}(\omega)$ of f electrons in the single-impurity model is calculated with the help of some numerical procedure (QMC, NRG, or another) as a functional of $\Sigma(\omega)$ and $\Delta(\omega)$, and these two functions are found from the self-consistency condition $F(\omega) = F_{\mathrm{loc}}(\omega)$.

Thus, the calculation of the local GF of the PAM is reduced to the calculation of the GF for the single-impurity Anderson model with specially chosen parameters. An analogous scheme for the Hubbard model is described in Section 2.

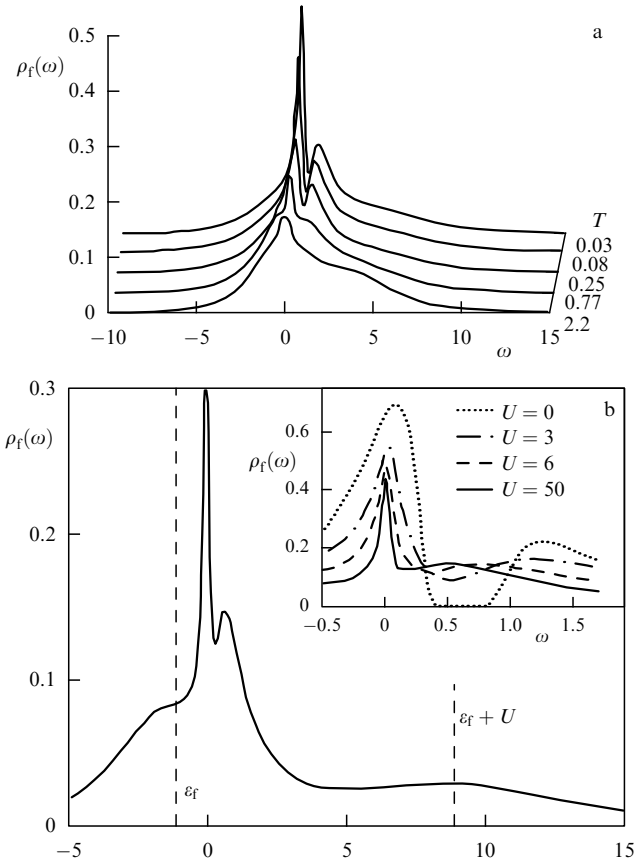

Figure 20. Local spectral density $\rho_f(\omega)$ for the PAM calculated in terms of the DMFT + NRG method [117]: (a) depending on temperature at the parameters $U/\Gamma_0 = 5$, $\varepsilon_f - \varepsilon_c = -2.5\,\Gamma_0$; and (b) at a fixed temperature $T = 0.0003\ \Gamma_0$. The chemical potential is $\mu = 0$, $n = 1.6$, and all the energies are given in the units of $\Gamma_0 = \pi V^2 \rho_0(0)$ (Anderson's width of the f level).

Equations (8.14)–(8.17) are to be supplemented by two additional equations that determine the local densities of f and s electrons at a site:

$$\langle n_f \rangle = -\frac{2}{\pi} \int d\omega f(\omega) \operatorname{Im} F(\omega)\,, \tag{8.18}$$

$$\langle n_s \rangle = -\frac{2}{\pi} \int d\omega f(\omega) \operatorname{Im} G(\omega)\,. \tag{8.19}$$

The expression for the total electron density

$$n = \langle n_f \rangle + \langle n_s \rangle \tag{8.20}$$

is an equation for the chemical potential μ.

Figure 20 displays the calculated spectral electron density of f electrons $\rho_f(\omega) = -1/\pi \operatorname{Im} F(\omega)$ depending on the temperature and the Coulomb potential. Figure 20a shows how the intensity of the central peak varies with temperature at fixed U: as T decreases, the quasiparticle peak increases strongly; moreover, in the vicinity of the chemical potential, a pseudogap caused by the hybridization of the localized and collectivized electrons appears. In Fig. 20b, it is shown how the spectral density of f states changes at a fixed temperature with increasing U. At $U = 0$, there exists a hybridization gap, which gradually disappears with increasing U, forming a quasiparticle Kondo peak characteristic of the Hubbard model. It is seen from Fig. 20b that incoherent maxima analogous to atom-like Hubbard bands of the Hubbard model appear.

The authors of Ref. [118] calculated many transport properties of the PAM and showed that the totality of various thermodynamic and transport properties of f systems with HFs is described well in terms of the PAM calculated by the DMFT + NRG method. Thus, the calculations showed that in the metallic state at low temperatures ($T < T_0$), the electric resistivity behaves as $\rho(T) \sim T^2$, as in the theory of the Fermi liquid. At $T \sim T_0$, a sharp increase in $\rho(T)$ is first observed; then, after passing through a maximum ($T_{\max} \sim 10-200$ K), $\rho(T)$ decreases logarithmically. This behavior of $\rho(T)$ is typical of many real HF systems. The optical conductivity $\sigma(\omega)$ at low T demonstrates a Drude peak. The calculations in the Kondo-insulator regime show an activational behavior of $\rho(T)$ and the absence of a Drude peak, which agrees with experimental data. The results of calculations of the thermo-emf and thermal conductivity also agree satisfactorily with the experimental data. Thus, paper [118], as well as [116, 117, 119] in which the DMFT methods are used, show that the PAM is an adequate model for describing the low-energy physics of f systems with HFs.

The formation of HFs in SCSs is a more common phenomenon, not restricted to systems with 4f and 5f elements. There are numerous systems based on 3d elements with very high values of the linear coefficient γ in the heat capacity and the static magnetic susceptibility χ_0 of the Pauli type (Table 3). These 3d systems also exhibit a Fermi-liquid behavior; in particular, their electric resistance changes according to the law $\rho \sim T^2$. But the mechanisms of the formation of heavy effective masses in these systems can differ from those in the f systems. Table 3 [33] lists some of these mechanisms associated with specific compounds. Thus, MIT denotes the most common mass enhancement mechanism in f systems caused by the proximity to the metal–insulator transition. Other mechanisms are denoted by KL (Kondo lattice), F (frustration), and QCP (proximity to the quantum critical point). The frustration mechanism occurs in systems with a mixed exchange interaction between ferromagnetic and antiferromagnetic ions or in systems with antiferromagnetic coupling, in which the character of the geometric arrangement of ions in the lattice does not allow establishing a long-range magnetic order that minimizes the exchange energy. The various scenarios of the formation of HFs are discussed in [120].

Table 3. Heavy-fermion compounds of transition metals [33].

Compound	γ, mJ mol^{-1} K^{-2}	Mechanisms
LiV_2O_4	350–490	F/KL
$Y(Sc)Mn_2$	160	F
$CaRuO_3$	77	QCP/MIT
β-Mn	70	F
$Gd_{0.8}Sr_{0.2}TiO_3$	50	MIT
Sr_2RuO_4	39	MIT/QCP

8.5 Phase diagram

We now turn to an analysis of magnetically ordered phases in terms of the PAM. In the Kondo lattice, just as in the single-

impurity Anderson model, by eliminating the hybridization term, we can obtain an effective Hamiltonian of the sf exchange for the PAM and then, with the help of an additional canonical transformation, reduce it to an effective Hamiltonian in which the initially localized f electrons can hop over the lattice, and an indirect exchange interaction of an oscillating nature, similar to the Ruderman–Kittel–Kasuya–Yosida (RKKY) interaction arises between the localized spins that are formed on the lattice sites. Thus, in the Kondo regime of the PAM at low temperatures ($T < T_K$), there is a competition between two opposite phenomena, the Kondo screening (formation of a Kondo singlet at each lattice site with a localized f electron) and the exchange interaction between localized moments on the lattice. Kondo screening tends to make the entire lattice nonmagnetic, whereas the RKKY interaction tends to create a magnetic order. Which of the phases is realized as a result of the competition between these two tendencies depends on the relation between kT_K and the indirect interaction $\sim J^2/W$.

The corresponding theoretical problem is very complex. In the framework of the mean-field approximation in the method of auxiliary bosons [121, 122], a phase diagram was constructed in terms of the PAM for the Kondo regime with the average number of f electrons $\langle n^f \rangle \approx 1$. It turned out that at any degree of hybridization V, the magnetic state strongly depends on the total number $n = \langle n^f \rangle + \langle n^s \rangle$ of electrons at a site. At $n = 1$ and 2 and in small vicinities of these values, an antiferromagnetic insulating phase arises, similar to what occurs in the Hubbard model at half-filling. For $n < 2$ and $n < 1$, a ferromagnetic metallic phase appears in a wide interval of concentrations. These results, however, can be significantly refined by using the DMFT.

The problem of the competition of the Kondo screening and RKKY interaction was recently thoroughly studied in a series of works [123–126] in the DMFT framework. Taking the long-range RKKY interaction into account in the DMFT framework requires an extension in order to include nonlocal terms together with the local self-energy of electrons, which is taken into account in the standard scheme. Several versions of such an extension were proposed in [123–125]. In [124], a phase diagram in the (T, V) plane was constructed. The ordered antiferromagnetic phase prevails at small V and low temperatures, while the phase with the formation of Kondo singlets dominates at large V. The Néel temperature T_N and the Kondo temperature T_K decrease in approaching the point $V_c \approx 0.25$ at low T, but their curves do not intersect each other, at least down to the lowest temperature $T = 0.01W$ that was attained. Apparently, the point V_c is the quantum critical point of the PAM.

The PAM depends on so many parameters (including the densities of f and s electrons $\langle n_f \rangle$ and $\langle n_s \rangle$) that the Kondo regime already involves many possibilities for the realization of different phases with a long-range order, including antiferromagnetic and superconducting ones; therefore, the determination of phase diagrams on the (T, V), (T, U), and (T, n) planes requires significant effort. Experiments show that in the weak-coupling regime (in which the localized magnetic moments are conserved), the local moments of f electrons have a tendency toward antiferromagnetic ordering, whereas in the Kondo regime (in which the localized moments are screened by conduction electrons), itinerant-electron magnetism with incommensurate wave vectors **Q** and small magnetic moments is realized. The crossover from the localized moment to the collectivized one, which is observed in $CeCu_{(1-x)2}Ge_2$ with a change in the coupling constant upon doping, was studied in [127]. The phase transitions between the Kondo insulator and the paramagnetic metal in a magnetic field in the DMFT framework were investigated in [126].

8.6 Nonstandard superconductivity

In the HF systems, two phases with a long-range order — antiferromagnetic and superconducting — compete at low temperatures. The superconductivity in these compounds was first discovered in $CeCu_2Si_2$ [128] in 1979, then in UBe_{13} [129] in 1983, and in UPt_3 [130] in 1984 (at present, about twenty superconducting HF compounds are known). At the very beginning, an idea was suggested that a nonstandard superconductivity caused by the nonphonon mechanism of pairing is realized in the HF compounds. This was an extremely bold hypothesis, expressed even before the discovery of HTSC in cuprates. One of the bases for this hypothesis was a consideration that the pairing mechanism via a virtual exchange of excitations (phonons) was connected with the same electron–phonon interaction that is responsible for the electric resistance of metals as a result of the real scattering of electrons by phonons. In the HF compounds at low temperatures, the resistance behaves as $\rho(T) \sim T^2$. In the usual Fermi systems, the same law of variation of $\rho(T)$ corresponds to the electron–electron interaction. This can serve as an indication that in the systems where a quadratic temperature dependence of resistance is observed, precisely the electron–electron interaction is responsible for the pairing mechanism [131]. Furthermore, because of the narrowness of the quasiparticle peak in HF systems, the Fermi energy in them is small in comparison with the energy that corresponds to the characteristic frequency of the phonon spectrum.

Experimental studies of the superconductivity of HF systems showed that the superconducting order parameter (the gap in the electron spectrum) takes zero values at some points or even on certain lines on the Fermi surface. This indicates a special symmetry of the wave functions of Cooper pairs [132], for example, a d symmetry, as in cuprates. This type of symmetry leads, in the case of a local character of the Coulomb potential, to a minimization of the repulsive energy in the anisotropic Cooper pair. As in cuprates, attraction arises in the HF systems as a result of antiferromagnetic fluctuations. Neither of the phenomena observed in these systems — antiferromagnetic and superconducting ordering — excludes the other but they compete with one another. For example, in UPt_3 at temperatures below $T_c \sim 0.33$ K, superconductivity coexists with an antiferromagnetic ordering.

An unexpected event proved to be the discovery of superconductivity in the compound Sr_2RuO_4, in which the pairing is assumed to have a triplet nature (and the order parameter has a p symmetry, correspondingly) [133]. This type of pairing can arise due to ferromagnetic fluctuations, similar to those observed in ^{3}He. We have no possibility to consider the problems of superconductivity in HF systems in much detail here and refer the reader to reviews [134, 135].

Some examples of f systems that exhibit various phenomena caused by the strong electron correlation are given in Table 4 [136].

Table 4. Examples of f systems with strong electronic correlation

Type of system	Compound
Concentrated Kondo systems	Ce, $La_{1-x}Ce_x$, $La_{1-x}Ce_xAl_3$, $La_{1-x}Ce_xCu_6$, $Ce_{1-x}La_xPb_3$
Heavy fermions	$CeCu_6$, $CeAl_3$, UCu_5, $CeRu_2Si_2$, UAl_2, UIr, U_2Zn_{17}, UPt_3, UCd_{11}
Kondo insulators	$Ce_3Bi_4Pt_3$, CeNiSn, SmB_6, $YbBi_2$, CeRhSb, $Ce_3Sb_4Pt_3$, YbB_{12}, $Ce_3Au_3Sb_4$
Intermediate-valence systems	$CeSn_3$, $CePd_3$, (Sm, Y)S, $CeFe_2Al_8$, $CeCu_2Ge_2$
Non-Fermi-liquid systems	U_2Pt_2In, $UCu_{5-x}Pd_x$, $YbCu_{5-x}Al_x$, $U_{1-x}Ni_3Sn_{4-y}$, $CeCoIn_5$
Antiferromagnets	$UAgCu_4$, URu_2Si_2, UCu_5, U_2Zn_{17}, UGd_{11}
HF superconductors	UPt_3, UBe_{13}, $CeCu_2Si_2$, $CePd_2Si_2$, URu_2Si_2
Reentrant superconductors	(La, Ce)Al_2, (La, Th)Ce, UGe_2, $CeRu_2$, LaCe

9. Conclusion

9.1 General properties of materials with strong electron correlations

Chemical compounds based on transition metals, rare-earth elements, and actinides, in spite of their different crystal–chemical structure and composition, have much in common in the behavior of their physical properties. When being stoichiometric, many of these compounds are insulators or 'bad' metals. Upon substitution of atoms of some elements (in no way necessarily of the d or f type) by atoms with a different valence, these initially insulating compounds can become metals. The classical example is given by the HTSC cuprates, for instance, La_2CuO_4, in which La is replaced by Sr, or the manganite $LaMnO_3$, in which La is replaced by Ca. A typical feature is that even at relatively small levels of doping, the physical properties of these compounds can change quite substantially. The passage from the insulating to metallic state occurs as a second-order phase transition. Such electron transitions are usually accompanied by strong changes in the magnetic and transport properties.

The metal–insulator transitions, as we have seen, can also occur in stoichiometric compounds under the effect of some external factors, e.g., pressure, temperature, or substitution by elements with the same valence (which imitates external pressure). The metal–insulator transitions represent a very common manifestation of strong electron correlations in d and f systems.

Another general property of strongly correlated systems (SCSs) is a complex structure of quasiparticle states, which manifests itself in spectroscopic experiments (PES and ARPES) and in optical conductivity. These experiments frequently reveal a narrow quasiparticle peak of coherent states in the vicinity of the Fermi energy and two wide maxima located on the opposite sides of the Fermi level at distances equal to the characteristic local (intraatomic) energies: the Coulomb potential U at the atoms of either the d or f element, or the intraatomic Hund exchange J. These high-energy excitations are a consequence of incoherent transitions of an electron or a hole onto a localized atomic level. The existence of such incoherent excitations is a sufficiently general property of SCSs, which seems to have been first found in [44] many years ago.

The existence of a narrow quasiparticle peak near the Fermi level implies a strong renormalization of the charge-carrier effective masses, by one or two orders of magnitude (heavy fermions). The intensity of the quasiparticle peak usually changes substantially with changes in the concentration and decreases sharply with increasing the temperature. This behavior is especially characteristic of the heavy-fermion (HF) systems, in which the magnetic and structural properties strongly change in passing from high to low temperatures. The crossover from one regime to another occurs at a representative temperature T_0, which is of the order of the Kondo temperature T_K.

A characteristic feature of many SCSs is a strong dependence of their magnetic properties on the control parameters, one of the most important of these being the level of doping, i.e., the concentration of the substituting element. At a zero level of doping (stoichiometric composition), the compound with d and f elements is usually an antiferromagnetic insulator. With an increasing level of doping, the long-range magnetic order disappears, but the strong fluctuations of short-range order are retained. In this situation, states with a different long-range order occur. In particular, a superconducting state appears in cuprates and HF systems. Their phase diagrams on the (T, n) plane are quite diverse, but there is the following regularity: at low temperatures, with a deviation in the composition of the compound from stoichiometric (which frequently corresponds to band half-filling), a metallic phase appears in which different types of long-range order can compete. At high temperatures, the phase diagram is simplified; in the paramagnetic state, insulating and metallic phases usually compete. In the cases where doping leads to the appearance of a ferromagnetic ordering, as in manganites, the phase diagrams become more diverse. For example, the ferromagnetism can be replaced by magnetic ordering of other types.

In strongly correlated systems, the heterogeneous state of phase separation is frequently realized. Examples of this state are encountered in cuprates in the form of ferromagnetic inclusions in an antiferromagnetic matrix. The energy gain of the heterogeneous state relative to the homogeneous state is caused by the competition of the kinetic energy of electrons and the interactions that are responsible for some long-range order (e.g., antiferromagnetic). The appearance of islands of a ferromagnetic phase inside the ordered antiferromagnetic phase decreases the kinetic energy of electrons. Theoretical arguments in favor of the possible existence of such heterogeneous phases in compounds such as cuprates or manganites can be found in reviews [93, 137].

9.2 Theoretical description of d and f systems in terms of the basic models and DMFT

A remarkable fact is that the basic physical properties of SCSs with d or f elements can be described with the help of three simple models: the Hubbard model, the sd model, and the periodic Anderson model. This is just what we intended show in this review. Moreover, it typically suffices to use the simplest version of the model, in which only nondegenerate electron states corresponding to atoms of the d and f elements are taken into account. In the Hubbard model, only one electron band is considered, which imitates d electrons with a strong interaction between themselves. In the sd model, which

is frequently called the Kondo lattice model (KLM), a band of electrons is considered that interact not directly between themselves but by means of the exchange forces with localized magnetic moments belonging to the electron shells of atoms of d or f elements. In the most complex model — the periodic Anderson model (PAM) — two groups of electrons are considered: f electrons, which strongly interact among themselves, and noninteracting s electrons; their hybridization is also taken into account.

In these three basic models, only maximally localized interactions of electrons are taken into consideration: they interact only if they are located at the same lattice site. This refers to both the Coulomb interaction, which is considered in the Hubbard model and the PAM, and the exchange interaction considered in the sd model. The local nature of these interactions allows developing an effective method for the calculation of the electron structure, the dynamic mean-field approximation. The DMFT allows calculating the quasiparticle spectrum of electron states at an arbitrary value of the Coulomb parameter U or the exchange parameter J, i.e., solving the problem of strong correlations in the case where $U \gtrsim W$ or $J \gtrsim W$. The relevant investigations show that in the Hubbard model at $U \sim W$ and band half-filling ($n = 1$), a three-peak structure of the quasiparticle spectrum arises; in this case, the height of the quasiparticle peak strongly depends on the temperature and the level of doping (deviation of n from 1): it decreases with increasing T and $|n - 1|$. As U approaches a certain critical value $U_c \sim W$, the quasiparticle peak disappears and a phase transition from the metallic to the insulating state occurs. The three-peak structure of the spectrum and its change with a change in the temperature and in the level of doping, which follow from the DMFT approach to the Hubbard model, are just those features that are observed in many SCSs considered in this review.

However, if we want to calculate the dynamic response functions, such as the conductivity or magnetic susceptibility, then we should introduce spatial fluctuations into the DMFT scheme. In this review, we considered several versions of the corresponding extension of the DMFT scheme: the use of a multiimpurity cluster (instead of the single-impurity auxiliary problem) or the phenomenological introduction of static short-wavelength fluctuations. This is one of the main areas in which the DMFT is developing now. With spatial correlations taken into account in the DMFT framework, it is possible, for example, to solve the problem of pseudogap states in HTSC materials.

The low-energy physics of f systems is described by the PAM at least as successfully as the Hubbard model describes d systems. The most important new element in the PAM is the hybridization of the collectivized and localized electrons. The PAM can be used especially effectively for the description of systems with heavy electrons and of Kondo insulators. These systems are realized in a certain range of parameters of the Hamiltonian that correspond to the Kondo regime. In this regime, a single energy scale T_0 exists in the system above the Kondo temperature T_K — the energy scale of the single-impurity Anderson model. The scale T_0 divides the temperature scale into two regions: the high-temperature region, in which the localized magnetic moments are conserved in the system rather weakly interact with the collectivized electrons, and the low-temperature region, in which this interaction is very strong and Kondo singlets (coupled states of the localized spin and the screening cloud of the spin polarization of electrons) are formed. In the Kondo regime, a three-peak structure is realized in the spectral density of the metallic phase in the PAM (just as in the Hubbard model), with a very narrow central peak at the Fermi level. In this case, a strong renormalization of the electron mass occurs: $m^*/m \sim T_F/T_0 \gg 1$, i.e., heavy electrons appear.

The results of the DMFT calculations of the PAM correspond to the picture presented above and adequately describe the transport properties of f systems. Of special importance is the problem of constructing the phase diagram of the model allowing competition of two opposite phenomena, Kondo screening and long-range indirect exchange of the RKKY interaction type. To solve it, it is necessary to extend the DMFT to allow spatial correlations in the system. The passage from the single-impurity auxiliary problem to the problem of a multiimpurity cluster has already allowed considering the competition of two forms of ordering in the PAM, antiferromagnetic and superconducting, similarly to how this was done in the framework of the extended DMFT method for the Hubbard model.

9.3 Newest results of studies in the DMFT

Thus, the basic physical properties of virtually all classes of compounds of d and f elements are described within the DMFT framework by three basic models. To obtain a quantitative agreement with the experimental data, an LDA + DMFT method (described in reviews [7 – 12]) was developed, which allows considering the real crystal structure of specific chemical compounds. One of the basic factors is taking the degeneracy of d and f states of electrons in atoms into account. The introduction of orbital degrees of freedom together with spin and charge ones allows obtaining various types of ordering in the crystal, including orbital ordering, and the interaction between them. A general discussion of this question can be found in review [136]. The orbital degeneracy of electrons is especially important in considering the LDA + DMFT scheme for describing pure metals with 4f and 5f incompletely filled shells. Detailed calculations are presently in progress for cerium and plutonium (see [7, 8, 138]). Detailed calculations of the electron structure were carried out for the compounds NiO [139, 140] and Sr_2RuO_4 [141]. We also note paper [142], in which the DMFT method was applied to the calculation of the band structure and ARPES spectra of ferromagnetic nickel; the results obtained agree very well with the experimental data.

We now turn to some important results obtained in the DMFT most recently. DMFT calculations for the Hubbard model allow obtaining inhomogeneous states of the phase-separation type together with uniform phases. In [143], the authors constructed a phase diagram for the paramagnetic state on the (μ, U) plane for the Bethe lattice with electron transitions between the nearest neighbors taken into account (Fig. 21a). At $T = 0$ and half-filling (at which $\mu = U/2$), the system is insulating at $U > U_{c2}$, where $U_{c2} \approx 5.84t$ (cf. Fig. 4). Upon deviating from the half-filling, the ground state of the system is metallic, and the chemical potential varies jumpwise from $\mu = \mu_{c2}^-$ to μ_{c2}^+ as the electron concentration n approaches unity from below or from above. Thus, for $\mu_{c2}^- < \mu < \mu_{c2}^+$, the system is insulating at half-filling. In the regions where $\mu_{c1}^- < \mu < \mu_{c2}^-$ or $\mu_{c1}^+ > \mu > \mu_{c2}^+$, the metallic and insulating phases coexist, whereas a stable metallic phase is realized beyond these regions. The appearance of a metallic phase at the points $\mu = \mu_{c2}^\pm$ is caused by the appearance of states inside the Mott gap, and the disappearance of the

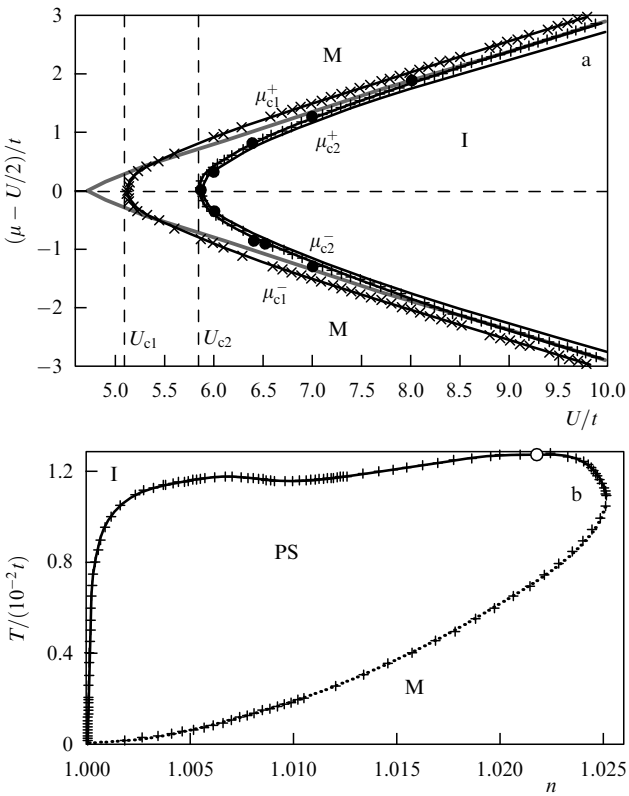

Figure 21. Phase diagrams for the Hubbard model [143]: (a) on the (μ, U) plane at $T = 0$ and (b) on the (T, n) plane near the half-filling at $U = 6t$.

insulating phase at the points $\mu = \mu_{c1}^{\pm}$ is related to the fact that μ reaches the boundary of the gap.

At a finite temperature, a phase separation region arises in a small vicinity of $n = 1$ (Fig. 21b). This region is substantially enlarged with increasing the temperature if we take the electron hopping to next-to-nearest sites into consideration. This hopping causes frustration in the system and breaks the electron – hole symmetry, and the phase diagram therefore becomes asymmetric with respect to the point $n = 1$, which is typical of SCSs based on d elements.

We note that the majority of works concerning the Hubbard model in the DMFT framework were performed on a square lattice. However, in [144, 145], the DMFT (QMC) method was applied to a two-dimensional triangular lattice at half-filling [144] and at a deviation from half-filling [145]. The motivation for these calculations was the discovery of superconductivity in $Na_xCoO_2 \times y\,H_2O$ and the exotic phase diagram of the compound Na_xCoO_2. At $n = 1$ on the triangular lattice, a metal – insulator transition occurs at $U_c = 12\,t$ [144] and $U_c = 15\,t$ [145]. As was shown in [145], at a deviation from the half-filling, the phase diagram strongly depends on the sign of the hopping matrix element. At $t > 0$ and $n \neq 1$, the system is metallic but has different properties in different regions of the (U, n) phase plane. At large U, approximately in the middle of the concentration interval $1 < n < 2$, a ferromagnetic phase with signatures of itinerant-electron magnetism appears. Outside this interval, in the metallic paramagnetic phase, localized magnetic moments appear, which manifest themselves in the Curie – Weiss behavior of the magnetic susceptibility. At $t < 0$ and $U \gtrsim W$, signatures of the weakly correlated paramagnetic metal with a Pauli susceptibility appear in the periodic lattice. The studies in [144, 145] show an important role of frustrations in the system with strong correlations. At the same time, the DMFT results in [145] satisfactorily describe the basic properties of the exotic compound Na_xCoO_2.

We note in conclusion that the DMFT method is an approximate theory in application to real systems with a finite spatial dimension; however, in comparison with other approaches, it has a number of advantages in describing strongly correlated systems. The equations of this theory have two exact limits: at $U = 0$ (the free-electron limit) and $t = 0$ (the atomic limit). Hence, at finite U, an interpolation between these limits occurs, which takes the collectivized and local aspects of the electronic states of SCSs into account. It is important to note that the necessary sum rules for the Green's functions of electrons are satisfied in this approach and their analytic properties are not violated. We also recall that, as applied to the basic model of SCS — the Hubbard model — the DMFT method connects two conflicting regimes at the band half filling: the insulating state with a gap in the electron spectrum and the metallic state with a quasiparticle peak at the Fermi level. Earlier, completely different theoretical approaches were used for describing these regimes, the decoupling of Green's functions (the so-called Hubbard III approximation [2]) for describing the dielectric state, and the Gutzwiller approximation for describing the quasiparticle state. The DMFT method linked together both these regimes and showed that the transition between them occurs as a result of a change in the Coulomb repulsion parameter U. This single advantage is already a motivation strong enough to discard spatial correlations in describing real strongly correlated systems. Nevertheless, there are several extended versions of the DMFT scheme, which were described above; they allow taking these correlations into account.

We now compare the situation with the description of the electron state of simple (nontransition) metals and d and f metals and related chemical compounds. Fifty years divides the periods of the construction of detailed theories for these groups of metals. The description of simple metals is based on the standard band theory and Landau Fermi-liquid theory. The combination of these two fundamental concepts allowed creating the science of fermiology in the 1950s, whose predictions were confirmed using many experimental techniques that existed at that time. This was the period of the predominance of analytic approaches to the theory of condensed state, which was caused by two factors: the relevant physical objects were relatively simple and the computational possibilities were very limited.

After fifty years, the situation changed radically: the objects of studies — d and f metals and their compounds — became substantially more complex. Models have become necessary that are capable of providing one approximate description or another; moreover, in the case of strongly correlated systems, the theory no longer contained a small parameter, and therefore solving the equations of even simple (basic) models required powerful computational facilities, which had already appeared by this time and became accessible. Thus, owing to an appropriate physical idea (to formally consider the models in the limit of a large spatial dimension) and to the development of effective computational programs, the DMFT scheme is becoming the basic tool in the theory of strongly correlated systems.

Acknowledgments. This work was supported in part by the Council for Grants of the President of the Russian Federation

for Leading Scientific Schools (project nos. NSh-4640.2006.2 and NSh-4192.2006.2).

References

1. Hubbard J J *Proc. R. Soc. London Ser. A* **276** 238 (1963)
2. Hubbard J J *Proc. R. Soc. London Ser. A* **281** 401 (1964)
3. Metzner W, Vollhardt D *Phys. Rev. Lett.* **62** 324 (1989)
4. Georges A, Kotliar G *Phys. Rev. B* **45** 6479 (1992)
5. Zhang X Y, Rozenberg M J, Kotliar G *Phys. Rev. Lett.* **70** 1666 (1993)
6. Georges A et al. *Rev. Mod. Phys.* **68** 13 (1996)
7. Kotliar G et al. *Rev. Mod. Phys.* **78** 865 (2006)
8. Georges A, in *Lectures on the Physics of Highly Correlated Electron Systems VIII* (AIP Conf. Proc., No. 715, Eds A Avella, F Mancini) (Melville, NY: AIP, 2004) p. 3
9. Georges A, cond-mat/0403123 [4]
10. Held K *Adv. Phys.* **56** 829 (2007)
11. Lichtenstein A I, Katsnelson M I, Kotliar G, in *Electron Correlations and Materials Properties 2* (Eds A Gonis, N Kioussis, M Ciftan) (New York: Kluwer Acad. Plenum Publ., 2003) p. 428
12. Maier T et al. *Rev. Mod. Phys.* **77** 1027 (2005)
13. Freericks J K, Zlatić V *Rev. Mod. Phys.* **75** 1333 (2003)
14. Edelstein A S *J. Magn. Magn. Mater.* **256** 430 (2003)
15. Kotliar G, Vollhardt D *Phys. Today* **57** (3) 53 (2004)
16. Tokura Y *Phys. Today* **56** (7) 50 (2003)
17. Agilent Technologies Europhysics Prize of 2006, http://www.agilent.com/about/newsroom/presrel/2006/08mar-al06001.html
18. Izyumov Yu A *Usp. Fiz. Nauk* **165** 403 (1995) [*Phys. Usp.* **38** 385 (1995)]
19. Izyumov Yu A *Usp. Fiz. Nauk* **167** 465 (1997) [*Phys. Usp.* **40** 445 (1997)]
20. Izyumov Yu A *Usp. Fiz. Nauk* **169** 225 (1999) [*Phys. Usp.* **42** 215 (1999)]
21. Izyumov Yu A, Skryabin Yu N *Usp. Fiz. Nauk* **171** 121 (2001) [*Phys. Usp.* **44** 109 (2001)]
22. Izyumov Yu A, Chashchin N I, Alekseev D S *Teoriya Sil'no Korrelirovannykh Sistem. Metod Proizvodyashchego Funktsionala* (Theory of Strongly Correlated Systems. Method of the Generating Functional) (Moscow – Izhevsk: RKhD, 2006)
23. Izyumov Yu A, Kurmaev É Z *Usp. Fiz. Nauk* **113** 193 (1974) [*Sov. Phys. Usp.* **17** 356 (1974)]
24. Izyumov Yu A, Kurmaev É Z *Usp. Fiz. Nauk* **118** 53 (1976) [*Sov. Phys. Usp.* **19** 26 (1976)]
25. Vonsovsky S V, Izyumov Yu A, Kurmaev E Z *Sverkhprovodimost' Perekhodnykh Metallov, Ikh Splavov i Soedinenii* (Superconductivity of Transition Metals: Their Alloys and Compounds) (Moscow: Nauka, 1977) [Translated into English (Berlin: Springer-Verlag, 1982)]
26. Zubarev D N *Usp. Phys. Nauk* **71** 71 (1960) [*Sov. Phys. Usp.* **3** 320 (I960)]
27. Abrikosov A A, Gor'kov L P, Dzyaloshinskii I E *Metody Kvantovoi Teorii Polya v Statisticheskoi Fizike* (Quantum Field Theoretical Methods in Statistical Physics) (Moscow: Fizmatgiz, 1962) [Translated into English (Oxford: Pergamon Press, 1965)]
28. Anderson P W *Phys. Rev.* **124** 41 (1961)
29. Bulla R, Costi T A , Vollhardt D *Phys. Rev. B* **64** 045103 (2001)
30. Fye R M, Hirsch J E *Phys. Rev. B* **40** 4780 (1989)
31. Werner P et al. *Phys. Rev. Lett.* **97** 076405 (2006)
32. Haule K *Phys. Rev. B* **75** 155113 (2007)
33. Krug von Nidda H-A et al. *Eur. Phys. B* **34** 399 (2003)
34. Fujimori A et al. *Phys. Rev. Lett.* **69** 1796 (1992)
35. Mo S-K et al. *Phys. Rev. Lett.* **90** 186403 (2003)
36. Limelette P et al. *Science* **302** 89 (2003)
37. Panaccione G et al. *Phys. Rev. Lett.* **97** 116401 (2006)
38. Sham L J, Kohn W *Phys. Rev.* **145** 561 (1966)
39. Schrieffer J R, Wolff P A *Phys. Rev.* **149** 491 (1966)
40. Mott N F *Proc. Phys. Soc. London, Sect. A* **62** 416 (1949)
41. Mott N F *Can. J. Phys.* **34** 1356 (1956)
42. Mott N F *Philos. Mag.* **6** 287 (1961)
43. Mott N F *Metal-Insulator Transitions* 2nd ed. (London: Taylor & Francis, 1990) [Translated into Russian (Moscow: Nauka, 1979)]
44. Brinkman W F, Rice T M *Phys. Rev. B* **2** 4302 (1970)
45. Zaanen J, Sawatzky G A, Allen J W *Phys. Rev. Lett.* **55** 418 (1985)
46. Imada M, Fujimori A, Tokura Y *Rev. Mod. Phys.* **70** 1039 (1998)
47. Pavarini E et al. *Phys. Rev. Lett.* **92** 176403 (2004)
48. Sadovskii M V *Usp. Fiz. Nauk* **171** 539 (2001) [*Phys. Usp.* **44** 515 (2001)]
49. Sadovskii M V, cond-mat/0408489
50. Yoshida T et al. *J. Phys.: Condens. Matter* **19** 125209 (2007); cond-mat/0610759
51. Kuchinskii E Z et al. *Zh. Eksp. Teor. Fiz.* **131** 908 (2007) [*JETP* **104** 792 (2007)]; cond-mat/060665
52. Millis A J, Momen H, Pines D *Phys. Rev. B* **42** 167 (1990)
53. Sadovskii M V et al. *Phys. Rev. B* **72** 155105 (2005)
54. Kuchinskii E Z, Nekrasov I A, Sadovskii M V *Phys. Rev. B* **75** 115102 (2007)
55. Kuchinskii E Z, Nekrasov I A, Sadovskii M V *Pis'ma Zh. Eksp. Teor. Fiz.* **82** 217 (2005) [*JETP Lett.* **82** 198 (2005)]
56. Kuchinskii E Z, Nekrasov I A, Sadovskii M V *Fiz. Nizk. Temp.* **32** 528 (2006) [*Low Temp. Phys.* **32** 398 (2006)]
57. Kuchinskii E Z, Sadovskii M V *Zh. Eksp. Teor. Fiz.* **130** 477 (2006) [*JETP* **103** 415 (2006)]
58. Toschi A, Katanin A A, Held K *Phys. Rev. B* **75** 045118 (2007)
59. Smith J L, Si Q *Phys. Rev. B* **61** 5184 (2000)
60. Damascelli A, Hussain Z, Shen Z-X *Rev. Mod. Phys.* **75** 473 (2003)
61. Ino A et al. *J. Phys. Soc. Jpn.* **68** 1496 (1999)
62. Byczuk K et al. *Nature Phys.* **3** 168 (2007)
63. Plakida N M, Oudovenko V S *Zh. Eksp. Teor. Fiz.* **131** 259 (2007) [*JETP* **104** 230 (2007)]
64. Anderson P W *Science* **235** 1196 (1987)
65. Haule K et al. *Phys. Rev. B* **68** 155119 (2003)
66. Haule K, Kotliar G *Europhys. Lett.* **77** 27007 (2007); cond-mat/0601478
67. Demler E, Hanke W, Zhang S-C *Rev. Mod. Phys.* **76** 909 (2004)
68. Halboth C J, Metzner W *Phys. Rev. B* **61** 7364 (2000)
69. Lichtenstein A I, Katsnelson M I *Phys. Rev. B* **62** R9283 (2000)
70. Sénéchal D et al. *Phys. Rev. Lett.* **94** 156404 (2005)
71. Capone M, Kotliar G *Phys. Rev. B* **74** 054513 (2006)
72. Reiss J, Rohe D, Metzner W *Phys. Rev. B* **75** 075110 (2007)
73. Kyung B et al. *Phys. Rev. B* **73** 165114 (2006)
74. Maksimov E G *Usp. Fiz. Nauk* **170** 1033 (2000) [*Phys. Usp.* **43** 965 (2000)]
75. Kulić M L, Dolgov O V, cond-mat/0610549
76. Capone M et al. *Science* **296** 2364 (2002)
77. Coey J M D, Viret M, von Molnar S *Adv. Phys.* **48** 167 (1999)
78. Salamon M B, Jaime M *Rev. Mod. Phys.* **73** 583 (2001)
79. Dörr K *J. Phys D: Appl. Phys.* **39** R125 (2006)
80. Chun S H et al. *Phys. Rev. Lett.* **84** 757 (2000)
81. Tokura Y, Tomioka Y *J. Magn. Magn. Mater.* **200** 1 (1999)
82. Zener C *Phys. Rev.* **82** 403 (1951)
83. Anderson P W, Hasegawa H *Phys. Rev.* **100** 675 (1955)
84. de Gennes P-G *Phys. Rev.* **118** 141 (1960)
85. Furukawa N *J. Phys. Soc. Jpn.* **64** 2754 (1995)
86. Furukawa N, in *Physics of Manganites* (Eds T A Kaplan, S D Mahanti) (New York: Kluwer Acad., Plenum Publ., 1999) pp. 1 – 38
87. Motome Y, Furukawa N *J. Phys. Soc. Jpn.* **69** 3785 (2000)
88. Nagai K, Momoi T, Kubo K *J. Phys. Soc. Jpn.* **69** 1837 (2000)
89. Lin C, Millis A J *Phys. Rev. B* **72** 245112 (2005)
90. Held K, Vollhardt D *Phys. Rev. Lett.* **84** 5168 (2000)
91. Tran Minh-Tien *Phys. Rev. B* **67** 144404 (2003)
92. Phan Van-Nham, Tran Minh-Tien, cond-mat/0310441
93. Chernyshev A L, Fishman R S *Phys. Rev. Lett.* **90** 177202 (2003)
94. Yunoki S et al. *Phys. Rev. Lett.* **80** 845 (1998)
95. Ramakrishnan T V et al. *Phys. Rev. Lett.* **92** 157203 (2004)
96. Uehara M et al. *Nature* **399** 560 (1999)
97. Loudon J C, Mathur N D, Midgley P A *Nature* **420** 797 (2002)
98. Loktev V M, Pogorelov Yu G *Fiz. Nizk. Temp.* **26** 231 (2000) [*Low Temp. Phys.* **26** 171 (2000)]
99. Anderson P W *Phys. Rev.* **115** 2 (1959)
100. Kugel' K I, Khomskiĭ D I *Usp. Fiz. Nauk* **136** 621 (1982) [*Sov. Phys. Usp.* **25** 231 (1982)]

[4] It is the same as Ref. [8].

101. van den Brink J, Khomskii D *Phys. Rev. Lett.* **82** 1016 (1999)
102. Millis A J, Littlewood P B, Shraiman B I *Phys. Rev. Lett.* **74** 5144 (1995)
103. Edwards D M *Adv. Phys.* **51** 1259 (2002)
104. Irkhin V Yu, Katsnel'son M I *Usp. Fiz. Nauk* **164** 705 (1994) [*Phys. Usp.* **37** 659 (1994)]
105. Brandt N B, Moshchalkov V V *Adv. Phys.* **33** 373 (1984)
106. Grewe M, Steglich F, in *Handbook on the Physics and the Chemistry of Rare Earth* Vol. 14 (Amsterdam: Elsevier, 1991) p. 343
107. Fulde P, Keller J, Zwicknagl G, in *Solid State Physics: Advances in Research and Applications* Vol. 41 (Eds H Ehrenreich, D Turnbull) (New York: Academic Press, 1988) p. 1
108. Degiorgi L *Rev. Mod. Phys.* **71** 687 (1999)
109. Stewart G R *Rev. Mod. Phys.* **73** 797 (2001)
110. Hewson A C *The Kondo Problem in Heavy Fermions* (Cambridge: Cambridge Univ. Press, 1993)
111. Costi T A, Manini N *J. Low Temp. Phys.* **126** 835 (2002)
112. Nozières P *Eur. Phys. J. B* **6** 447 (1998)
113. Burdin S, Georges A, Grempel D R *Phys. Rev. Lett.* **85** 1048 (2000)
114. Rice T M, Ueda K *Phys. Rev. B* **34** 6420 (1986)
115. Jarrell M *Phys. Rev. B* **51** 7429 (1995)
116. Pruschke Th, Bulla R, Jarrell M *Phys. Rev. B* **61** 12799 (2000)
117. Tahvildar-Zadeh A N et al. *Phys. Rev. B* **60** 10782 (1999)
118. Grenzebach C et al. *Phys. Rev. B* **74** 195119 (2006)
119. Smith V E, Logan D E, Krishnamurthy H R *Eur. Phys. J. B* **32** 49 (2003)
120. Fulde P *Ann. Phys.* (Berlin) **9** 871 (2000)
121. Möller B, Wölfle P *Phys. Rev. B* **48** 10320 (1993)
122. Doradziński R, Spalek J *Phys. Rev. B* **58** 3293 (1998)
123. Sun P, Kotliar G *Phys. Rev. Lett.* **91** 037209 (2003)
124. Sun P, Kotliar G *Phys. Rev. Lett.* **95** 016402 (2005)
125. de' Medici L et al. *Phys. Rev. Lett.* **95** 066402 (2005)
126. Ohashi T et al. *Phys. Rev. B* **70** 245104 (2004)
127. Anders F B *Phys. Rev. Lett.* **83** 4638 (1999)
128. Steglich F et al. *Phys. Rev. Lett.* **43** 1892 (1979)
129. Ott H R et al. *Phys. Rev. Lett.* **50** 1595 (1983)
130. Stewart G R et al. *Phys. Rev. Lett.* **52** 679 (1984)
131. Varma C M, cond-mat/0510019
132. Volovik G E, Gor'kov L P *Pis'ma Zh. Eksp. Teor. Fiz.* **39** 550 (1984) [*JETP Lett.* **39** 674 (1984)]
133. Luke G M et al. *Nature* **394** 558 (1998)
134. Sigrist M, Ueda K *Rev. Mod. Phys.* **63** 239 (1991)
135. Cox D L, Maple M B *Phys. Today* **48** (2) 32 (1995)
136. Khomskii D I *Phys. Scr.* **72** CC8 (2005)
137. Nagaev E L *Usp. Fiz. Nauk* **165** 529 (1995) [*Phys. Usp.* **38** 497 (1995)]
138. Pourovskii L V et al., arXiv:cond-mat/0702342
139. Ren X et al. *Phys. Rev. B* **74** 195114 (2006)
140. Kuneš J et al. *Phys. Rev. B* **75** 165115 (2007)
141. Pchelkina Z V et al. *Phys. Rev. B* **75** 035122 (2007)
142. Braun J et al. *Phys. Rev. Lett.* **97** 227601 (2006)
143. Eckstein M et al. *Phys. Rev. B* **75** 125103 (2007)
144. Aryanpour K, Pickett W E, Scalettar R T *Phys. Rev. B* **74** 085117 (2006)
145. Merino J, Powell B J, McKenzie R H *Phys. Rev. B* **73** 235107 (2006)